

PHOTOCATALYTIC ANTIMICROBIAL AND SELF-CLEANING
PROPERTIES OF TITANIA-SILICA MIXED OXIDE THIN FILMS

A THESIS SUBMITTED TO
THE GRADUATE SCHOOL OF NATURAL AND APPLIED SCIENCES
OF
MIDDLE EAST TECHNICAL UNIVERSITY

BY

BERİL KORKMAZ ERDURAL

IN PARTIAL FULFILLMENT OF THE REQUIREMENTS
FOR
THE DEGREE OF DOCTOR OF PHILOSOPHY
IN
CHEMICAL ENGINEERING

OCTOBER 2012

Approval of the thesis:

**PHOTOCATALYTIC ANTIMICROBIAL AND SELF-CLEANING
PROPERTIES OF TITANIA-SILICA MIXED OXIDE THIN FILMS**

submitted by **BERİL KORKMAZ ERDURAL** in partial fulfillment for the
degree of **Doctor of Philosophy in Chemical Engineering Department, Middle
East Technical University** by,

Prof. Dr. Canan Özgen
Dean, Graduate School of **Natural and Applied Sciences**

Prof. Dr. Deniz Üner
Head of Department, **Chemical Engineering**

Prof. Dr. Ufuk Bölükbaşı
Supervisor, **Chemical Engineering Dept., METU**

Prof. Dr. Gürkan Karakaş
Co-Supervisor, **Chemical Engineering Dept., METU**

Examining Committee Members:

Prof. Dr. Hayrettin Yücel
Chemical Engineering Dept., METU

Prof. Dr. Ufuk Bölükbaşı
Chemical Engineering Dept., METU

Prof. Dr. Zekiye Suludere
Dept. of Biological Sciences, Gazi University

Prof. Dr. İnci Eroğlu
Chemical Engineering Dept., METU

Prof. Dr. Mehmet Parlak
Dept. of Physics, METU

Date:

I hereby declare that all information in this document has been obtained and presented in accordance with academic rules and ethical conduct. I also declare that, as required by these rules and conduct, I have fully cited and referenced all material and results that are not original to this work.

Name, Last name : BERİL KORKMAZ ERDURAL

Signature :

ABSTRACT

PHOTOCATALYTIC ANTIMICROBIAL AND SELF-CLEANING PROPERTIES OF TITANIA-SILICA MIXED OXIDE THIN FILMS

Korkmaz Erdural, Beril

Ph.D., Department of Chemical Engineering

Supervisor : Prof. Dr. Ufuk Bölükbaşı

Co-Supervisor: Prof. Dr. Gürkan Karakaş

October 2012, 184 pages

In this study photocatalytic antibacterial and self-cleaning activities of TiO₂-SiO₂ thin films as a function of TiO₂/SiO₂ ratios were investigated. TiO₂-SiO₂ mixed oxides were synthesized by sol-gel method and coated over soda-lime glass plates by dip coating technique. *Escherichia coli* was used as a model microorganism for the photocatalytic antibacterial tests. Degradation rate of methylene blue (MB) molecules was used to characterize photocatalytic self-cleaning activities of thin film surfaces.

The maximum antibacterial activity was achieved over 92 wt% SiO₂ containing thin films. However, when the SiO₂ content exceeds 92 wt%, photocatalytic antibacterial activity decreased considerably, which was explained by the dilution of TiO₂ phase and inaccessibility of TiO₂. Increase in photocatalytic antibacterial activity was attributed to increases in the relative surface area, roughness, hydroxyl (OH) groups and bacterial adhesion. The favored bacterial adhesion enhanced direct contact of bacteria with TiO₂ particles and surface reactive oxygen species.

The highest initial decomposition rate of MB was obtained for 60 wt% SiO₂ and the activity decreases as SiO₂ concentration increases. The increase in photocatalytic activity by the SiO₂ addition can be explained by the increase of the amount of MB per unit area of TiO₂-SiO₂ thin films.

Different adsorption capability of thin films against MB molecule and *E. coli* cell was explained as the first reason why the antibacterial and self-cleaning activities reached their maximum values at different SiO₂ ratios. The second reason could be related with the different control mechanisms of self-cleaning and antibacterial activities by different textural and surface properties.

Keywords: TiO₂-SiO₂, self-cleaning, photocatalytic inactivation, *Escherichia coli*, bacterial adhesion

ÖZ

TİTANYUM-SİLİSYUM OKSİT KARIŞIMI İNCE FİMLERİN FOTO-KATALİTİK ANTİMİKROBİYAL VE KENDİ KENDİNİ TEMİZLEME ÖZELLİKLERİ

Korkmaz Erdural, Beril

Doktora, Kimya Mühendisliği Bölümü

Tez Yöneticisi : Prof. Dr. Ufuk Bölükbaşı

Yardımcı Tez Yöneticisi : Prof. Dr. Gürkan Karakaş

Ekim 2012, 184 sayfa

Bu çalışmada farklı oranlarında SiO₂ içeren TiO₂-SiO₂ ince filmlerin foto-katalitik anti-bakteriyel ve kendi kendini temizleme özellikleri araştırılmıştır. İkili TiO₂-SiO₂ oksitler sol-jel yöntemi ile sentezlenmiş ve daldırma kaplama tekniği ile cam plakalar üzerine kaplanmıştır. Anti-bakteriyel testler için *Escherichia coli* örnek mikroorganizma olarak kullanılmıştır. Kendi kendini temizleme özelliğini karakterize etmek için, metilen mavisi (MM) moleküllerinin degradasyon hızı incelenmiştir.

Yapılan deney sonuçlarına göre, maksimum anti-bakteriyel aktivite, ağırlıkça % 92 SiO₂ içeren ince film yüzeyinde tespit edilmiştir. Ancak SiO₂ miktarı ağırlıkça % 92 değerini aştığında, anti-bakteriyel aktivite belirgin bir şekilde düşüş göstermiştir. Bu durum, ince film yüzeylerde yer alan TiO₂ fazının seyrelmesi ve erişilmez hale gelmesi ile açıklanabilir. SiO₂ ilavesi ile artış gösteren anti-bakteriyel aktivite ise, bağıl yüzey alanında, pürüzlülük, hidroksil gruplarında ve yüzeye tutunan bakteri sayısında meydana gelen artış ile açıklanabilir. Yüzeye tutunan bakteri sayısındaki artış, TiO₂ parçacıkları ve yüzeylerinde yer alan reaktif oksijen türleri ile bakteriler arasındaki direkt temasın artmasına sebep olmuştur.

Metilen mavisinin degradasyonu sırasında, ağırlıkça % 60 SiO₂ içeren ince film yüzeyinde en yüksek başlangıç reaksiyon hızı tespit edilmiş ve SiO₂ ilavesi arttıkça bu değerin düştüğü gözlemlenmiştir. SiO₂ ilavesi ile artan foto-katalitik aktivitenin sebebi, artış gösteren birim TiO₂-SiO₂ ince film yüzeyindeki metilen mavisi miktarıdır.

Maksimum anti-bakteriyel aktivite ve kendi kendini temizleme etkinliği farklı SiO₂ oranları içeren ince filmlerde elde edilmiştir. Bu durumun ilk sebebi farklı oranlarda SiO₂ içeren ince filmlerin, MB molekülü ve *E. coli* hücrelerine karşı farklı adsorpsiyon kapasitesine sahip olmasıdır. İkinci sebep ise, kendi kendini temizleme etkinliğinin ve antibakteriyel aktivitenin farklı dokusal ve yüzey özellikleri tarafından denetlenmesi olabilir.

Anahtar Kelimeler: TiO₂-SiO₂, kendi kendini temizleme, fotokatalitik inaktivasyon, *Escherichia coli*, bakteriyel tutunma

To my family

ACKNOWLEDGEMENTS

First of all, I would like to sincerely express my thanks and gratitude to Prof. Dr. Ufuk Bölükbaşı for her valuable guidance, supervision and endless understanding throughout the research.

I am also grateful to Prof. Dr. Gürkan Karakaş for his endless understanding, valuable criticism and suggestions in all phases of this study.

I wish to express my gratitude to my Ph.D. Examining Committee members Prof. Dr. İnci Eroğlu and Prof. Dr. Zekiye Suludere for their enlightening comments and directions. Appreciation is also expressed Assoc. Prof. Dr. Demet Çetin and Prof. Dr. Zekiye Suludere for their support in supplying data, suggestions and their precious help on SEM application which were performed to observe the cells.

I should to thank Department of Biology of Gazi University and METU Central Laboratory for their help with SEM and XRD analysis. I am thankful to my former and present lab mates; Dr. Özlem Ak, Bilal Bayram, Tuğçe İrfan Ersöz, Dr. Alp Yürüm, Dr. Burcu Mirkelamoğlu, Dr. Aytaç Kocabaş, Dr. Didem Sutay, Nazife Işık Haykır, Merve Çınar, Erinç Bahçegül, Gizem Saber, Dr. Serpil Apaydın, Zeynep Eker, Alev Deniz Öztürk and Dr. Esra Uçkun.

I want to express my sincere gratitude to my parents Müjgan and Tuncer Korkmaz for their understanding, help, patience and being a constant source of emotional support.

Finally, I want to express my deepest love to my husband Serkan Erdural and my little daughter Berin Ece Erdural for their heartfelt support, their excellent sense of humor and patience.

TABLE OF CONTENTS

ABSTRACT	iv
ÖZ.....	vi
ACKNOWLEDGEMENTS	ix
TABLE OF CONTENTS	x
LIST OF TABLES	xiv
LIST OF FIGURES.....	xvi
NOMENCLATURE.....	xxi
CHAPTERS	
1. INTRODUCTION.....	1
2. LITERATURE SURVEY	7
2.1. General remarks about semiconductors	7
2.2. TiO ₂	11
2.3. Photocatalytic reactions of TiO ₂	13
2.4. Improving photocatalytic activity of TiO ₂	16
2.4.1. Improving photocatalytic activity of TiO ₂ by addition of SiO ₂	18
2.4.2 Interactions of TiO ₂ with SiO ₂	21
2.5. Application of TiO ₂ for hydrophilicity and self cleaning effect	25
2.6. TiO ₂ photocatalysis for disinfection.....	27
2.6.1. Photocatalytic effects of TiO ₂ suspension for disinfection	31
2.6.2. Photocatalytic effects of TiO ₂ thin films for disinfection	34
2.6.3. Mechanism of cell death	36
2.6.4. Kinetic models of photocatalytic inactivation of microorganisms..	40
2.7. Relationship between bacterial adhesion and antimicrobial activity	44
2.7.1. Bacterial adhesion	45
2.7.1.1. Interactions between bacteria and material surface during the first phase	45

2.7.1.2. Interactions between bacteria and material surface during the second phase.....	46
2.8. Factors affecting the bacterial adhesion.....	46
2.8.1. Surface free energy.....	47
2.8.1.1. Lifshitz-van der Waals-acid/base acid-base approach	48
2.8.1.2. Explanation of bacterial adhesion by theoretical models	51
2.8.2. Influence of surface hydrophobicity and surface free energies on bacterial adhesion	58
2.8.3. Influence of surface roughness on bacterial adhesion	61
2.9. Synthesis of TiO ₂ thin films	63
2.9.1. Sol-gel process	64
2.9.2. Dip-Coating	68
3. MATERIALS AND METHODS	70
3.1. Materials.....	70
3.2. Synthesis of TiO ₂ , and SiO ₂ -TiO ₂ colloidal mixture.....	70
3.3. Characterization of thin films.....	71
3.3.1. X-Ray Diffraction (XRD)	71
3.3.2. SEM Imaging	72
3.3.3. Imaging with atomic force microscopy images (AFM).....	72
3.3.4. Surface area measurement of thin films.....	73
3.3.5. Contact angle measurements.....	74
3.4. Microorganism and growth conditions	74
3.5. Preparation of <i>E. coli</i> cells	74
3.5.1. Surface adhered cell preparation	75
3.5.2. Preparation of <i>E. coli</i> cells for contact angle measurements.....	76
3.5.3. Preparation of <i>E. coli</i> cells for scanning electron microscopy	76
3.6. Determination of photocatalytic antibacterial activity of TiO ₂ -SiO ₂ thin films.....	77
3.6.1. Photocatalytic inactivation of <i>E. coli</i> cells in suspensions.....	77
3.6.2. Photocatalytic inactivation of surface-adhered <i>E. coli</i> cells	78
3.7. Photocatalytic self-cleaning activity of thin films.....	79

3.8. Characterization of photo-induced hydrophilicity of thin films.....	79
4. RESULTS AND DISCUSSION	80
4.1. Structure of TiO ₂ -SiO ₂ thin films.....	80
4.1.1 SEM results	80
4.1.2 AFM results.....	84
4.1.3 XRD results	88
4.2. Surface area measurements of TiO ₂ -SiO ₂ thin films.....	90
4.3. Photocatalytic self-cleaning activity	91
4.4. Photocatalytic antibacterial activity	97
4.4.1. The effect of photocatalysis on <i>E. coli</i> cells by SEM analysis	98
4.4.2. Photocatalytic inactivation of <i>E. coli</i> cells in suspensions.....	102
4.5. Bacterial adhesion test.....	107
4.6. The thermodynamic properties of SiO ₂ -TiO ₂ thin films and <i>E.coli</i> adhesion	109
4.6.1. Contact angle measurements and surface free energy of SiO ₂ TiO ₂ thin film	109
4.6.2. Interfacial free energy of adhesion of <i>E.coli</i> on SiO ₂ -TiO ₂ thin film.....	113
4.7. Antibacterial activity measurements of suspended <i>E. coli</i> cells and Adhered <i>E. coli</i> cells	118
4.8. Reusability test of thin films	121
4.9. Photo-induced hydrophilicity.....	124
5. CONCLUSIONS.....	126
REFERENCES.....	129
APPENDICES	
A. LIGHT SPECTURUM OF THE UV SIMULATOR.....	160
B. XRD RESOURCES	161
C. SURFACE AREA MEASUREMENTS OF SIO ₂ -TIO ₂ THIN FILMS ..	163
D. DATAOF PHOTOCATALYTIC METHYLENE BLUE DEGRADATION REACTIONS	171

E. CALCULATION OF INITIAL REACTION RATE CONSTANTS FOR PHOTOCATALYTIC DEGRADATION OF METHYLENE BLUE	179
CURRICULUM VITAE	183

LIST OF TABLES

TABLES

Table 2.1. Band gap energies and corresponding radiation wavelengths of various semiconductors.....	9
Table 2.2. Various reactions for TiO ₂ -SiO ₂ in powder or thin film form.....	23
Table 4.1. Surface roughness of thin films.....	84
Table 4.2. RSA of the thin films	91
Table 4.3. Effect of surface composition on adsorbed amounts of MB over thin films	92
Table 4.4. Reaction steps of formation of active species and their half life values.....	106
Table 4.5 Test liquids and their surface tension components	110
Table 4.6. Contact angles and surface free energy components of the thin film surfaces and bacterial surfaces	111
Table 4.7 The solid-liquid (γ_{SL}), solid-bacteria (γ_{SB}) and interfacial energy values and work of adhesion of the thin film.....	115
Table B.1. XRD diffractogram of anatase.....	161
Table B.2 XRD diffractogram of rutile	162
Table C.1 Surface area measurement of thin film (SiO ₂ /TiO ₂ = 0).....	165
Table C.2 Surface area measurement of thin film (49 wt % SiO ₂).....	166
Table C.3 Surface area measurement of thin film (60wt % SiO ₂).....	166
Table C.4 Surface area measurement of thin film (74 wt % SiO ₂).....	167
Table C.5 Surface area measurement of thin film (85 wt % SiO ₂).....	168
Table C.6 Surface area measurement of thin film (92 wt % SiO ₂).....	169
Table C.7 Langmiur constants and correlation coefficients of linear regression lines	170

Table D.1 Equilibrium concentration of MB remaining in the solution after adsorption (ppm)	172
Table D.2 The adsorbed MB amount by thin films.....	173
Table D.3 Changes in the absorbance values of methylene blue adsorbed over thin film containing pure TiO ₂	174

LIST OF FIGURES

FIGURES

Figure 2.1. Comparison of the band gaps for a metal, a semiconductor and insulator	8
Figure 2.2. Valence and conduction band positions for various semiconductors	11
Figure 2.3. Forms of TiO ₂	12
Figure 2.4. Mechanism of photo-induced hydrophilicity	25
Figure 2.5. Schematic patterns of cell envelope of G(+) and G(-) bacteria	29
Figure 2.6. Graphical display of proposed kinetic models for photocatalytic inactivation reaction of <i>E. coli</i> ..	41
Figure 2.7. The spread of the liquid droplet on the surface according to Roughness degree (a) on a flat substratum (b) rough substrata Wenzel regime (c) rough substrata Cassie-Baxter regime	62
Figure 3.1. TiO ₂ - SiO ₂ colloid and thin film preparations	72
Figure 3.2. Example image of contact angle measurement performed by contact angle analyzer	75
Figure 3.3. Antibacterial activity test	78
Figure 4.1. SEM image of a thin film surface containing pure TiO ₂	81
Figure 4.2. SEM image of a TiO ₂ -SiO ₂ thin film surface containing 60 wt% SiO ₂	81
Figure 4.3. SEM image of a TiO ₂ -SiO ₂ thin film surface containing 74 wt% SiO ₂	82
Figure 4.4. SEM image of a TiO ₂ -SiO ₂ thin film surface containing 92 wt% SiO ₂	82

Figure 4.5. SEM image of a TiO ₂ -SiO ₂ thin film surface containing 95 wt% SiO ₂ .	83
Figure 4.6. Cross sectional view of TiO ₂ -SiO ₂ thin films	85
Figure 4.7. Top view of the AFM height mode images of the TiO ₂ -SiO ₂ thin films.	86
Figure 4.8. Three-dimensional AFM images of the TiO ₂ -SiO ₂ thin films	87
Figure 4.9. XRD patterns of TiO ₂ -SiO ₂ thin films	89
Figure 4.10. Effect of irradiation time (300 W/m ²) on the degradation of methylene blue over the TiO ₂ -SiO ₂ thin film	94
Figure 4.11. ln (C/C ₀) versus reaction time data of thin film containing TiO ₂ -SiO ₂ thin film	95
Figure 4.12 Effect of surface composition on the initial reaction rate constant for MB degradation under irradiation	97
Figure 4.13. SEM images of <i>E. coli</i> cell suspensions over the bare glass after 1 h under 300 W/m ² irradiation	99
Figure 4.14. SEM images of <i>E. coli</i> suspensions over TiO ₂ -SiO ₂ coated substrate containing 92 wt% SiO ₂ after 1h in dark	100
Figure 4.15. SEM images of <i>E. coli</i> cell suspensions over the TiO ₂ -SiO ₂ coated substrate containing 92 wt% SiO ₂ after 1h under 300 W/m ² irradiation	101
Figure 4.16. Effects of surface composition on the photocatalytic antibacterial activity of TiO ₂ -SiO ₂ thin films at the end of 1 h under 300W/m ² irradiation at 35 °C	103
Figure 4.17. Effect of surface composition on initial reaction rate for MB degradation and antibacterial activity of TiO ₂ -SiO ₂ thin films under 300 W/m ² irradiation.	104
Figure 4.18. Illustration of photocatalytic inactivation of <i>E. coli</i> on SiO ₂ -TiO ₂ film process.	107
Figure 4.19. Effect of surface composition on the bacterial adhesion over TiO ₂ -SiO ₂ thin films.	108

Figure 4.20. Effect surface composition on the bacterial adhesion (♦) and the photocatalytic antibacterial activity (■) of TiO ₂ -SiO ₂ thin films at the end of 1 h under 300 W/m ² irradiation at 35 °C.....	109
Figure 4.21. <i>E. coli</i> adhesion over the TiO ₂ -SiO ₂ thin surface vs the electron donor component of thin films	113
Figure 4.22. The effect of surface composition on work of adhesion (mN/m).....	116
Figure 4.23. Effect of work of adhesion on number of adhered cells	117
Figure 4.24. The effect of work of adhesion on antibacterial activity	118
Figure 4.25. Effect of irradiation time on the survival ratio of ♦; suspended <i>E. coli</i> cells and ■; adhered <i>E. coli</i> cells over the TiO ₂ -SiO ₂ thin film surface containing 92 wt% SiO ₂	120
Figure 4.26. Effect of use on the photocatalytic antibacterial activity of thin films under 1 h irradiation.....	121
Figure 4.27. Effect of use on the photocatalytic antibacterial activity of thin films under 1 h irradiation.....	122
Figure 4.28. Effect of incubation in the dark and UV light irradiation on antibacterial activity of thin film containing 92 wt% SiO ₂ under 1 h irradiation	124
Figure 4.29 Effect of surface composition on the photo-induced change in water contact angle of TiO ₂ /SiO ₂ thin films.	125
Figure A.1 Light specturum of The UV simulator.....	160
Figure C.1 Adsorption isotherm of thin film contain pure TiO ₂	165
Figure C.2 Adsorption isotherm of thin film contain SiO ₂ and TiO ₂ (49 wt % SiO ₂).....	166
Figure C.3 Adsorption isotherm of thin film contain SiO ₂ and TiO ₂ (60wt % SiO ₂).....	167
Figure C.4 Adsorption isotherm of thin film contain SiO ₂ and TiO ₂ (74 wt % SiO ₂)	168
Figure C.5 Adsorption isotherm of thin film contain SiO ₂ and TiO ₂ (85 wt % SiO ₂).....	169

Figure C.6 Adsorption isotherm of thin film contain SiO ₂ and TiO ₂ (92 wt % SiO ₂).....	170
Figure D.1 Adsorbed MB over per unit area of thin film vs changes in the absorbance values of MB over thin film surface containing pure TiO ₂	175
Figure D.2 Adsorbed MB over per unit area of thin film vs changes in the absorbance values of MB over thin film surface containing 49 wt% SiO ₂	175
Figure D.3 Adsorbed MB over per unit area of thin film vs changes in the absorbance values of MB over thin film surface containing 60 wt% SiO ₂	176
Figure D.4 Adsorbed MB over per unit area of thin film vs changes in the absorbance values of MB over thin film surface containing 74 wt% SiO ₂	176
Figure D.5 Adsorbed MB over per unit area of thin film vs changes in the absorbance values of MB over thin film surface containing 85 wt% SiO ₂	177
Figure D.6 Adsorbed MB over per unit area of thin film vs changes in the absorbance values of MB over thin film surface containing 92 wt% SiO ₂	177
Figure D.7 Adsorbed MB over per unit area of thin film vs changes in the absorbance values of MB over thin film surface containing 95 wt% SiO ₂	178
Figure E.1 ln (C/C ₀) versus reaction time data of thin film containing pure TiO ₂	180
Figure E.2 ln (C/C ₀) versus reaction time data of thin film 49 wt% SiO ₂	180
Figure E.3 ln (C/C ₀) versus reaction time data of thin film 60 wt% SiO ₂	181
Figure E.4 ln (C/C ₀) versus reaction time data of thin film containing 74 wt% SiO ₂	181
Figure E.5 ln (C/C ₀) versus reaction time data of thin film containing 85 wt% SiO ₂	182

Figure E.6 $\ln(C/C_0)$ versus reaction time data of thin film containing 92
wt% SiO_2 182

NOMENCLATURE

Symbols

- C/C_0 : The reduction in the number of viable cells
- N : Number of attached bacteria at time t
- N_{eq} : Number of attached bacteria at equilibrium state
- $H_{o/w}$: Relative hydrophobicity between microorganism and support
- C_e : The equilibrium concentration of remaining MB in the solution after adsorption (ppm)
- x/m : The quantity of MB adsorbed per unit glass substrate area (mg/cm^2)
- x_m : The amount of MB adsorbed at monolayer per unit area of thin film (mg)
- A_m : The cross-sectional area occupied by the adsorbed MB on the surface (m^2)
- MW_{MB} : The molecular weight of methylene blue
- N : The coverage factor
- A_0 : The initial absorbance value of feed stock solution
- A : The final absorbance value of MB solution after adsorption
- C_{int} : Initial concentration of MB solution (ppm)
- θ : Contact angle
- γ_{sl} : The solid/liquid interfacial free energy
- γ_{sv} : The solid/vapor interfacial free energy
- γ_{lv} : The liquid/vapor interfacial free energy
- π : Spreading pressure term
- $\gamma_{\text{surface}}^{\text{tot}}$: Surface free energy of solid
- γ^{LW} : Lifshitz-van der Waals force
- γ^- : Basic (electron-donor) component
- γ^+ : Acidic (electron acceptor) component
- $\gamma_{\text{surface}}^{\text{AB}}$: Acid-base component

- ΔG_{sl} : Free energy of cohesion
- ΔG^{LW} : Van der Waals interactions
- ΔG^{DL} : Electrostatic double layer interactions
- d : Separation distance between cell and substratum
- Ψ : Surface potential
- κ : Debye length
- ΔF_{Adh} : Work of adhesion (mN/m)
- ΔG_{adh} : Gibbs energy owing to bacterial adhesion (interfacial energy) (mN/m)
- γ_{sb} : The solid-bacterium interfacial free energy (mN/m)
- γ_{sl} : The solid-liquid interfacial free energy (mN/m)
- γ_{bl} : The bacterium-liquid interfacial free energy (mN/m)
- ΔG^{AB} : Acid-base interactions (mN/m)
- ψ : Surface potential
- ε : Relative dielectric permittivity of medium
- ε_0 : Permittivity in vacuum
- ΔG_{bb} : Free energy of aggregation

Abbreviations

AFM: Atomic Force Microscop

CAH: Contact angle hysteresis

D: Di-iodamethane

DLVO: Deryagin, Landau, Verwey and Overbeek

G: Glycerol

Gr (-): Gram negative bacterium

Gr (+): Gram positive bacterium

LPS: Lipopolysaccharide

LW-AB: Lifshitz-van der Walls acid-base approach

MB: Methylene blue

Min: Minute

NHE: Normal hydrogen electrode

Ox-Red: Oxidation and reduction reactions

PBS: Phosphate buffer solution

PEG: Polyethylene glycol

RMS: Root-Mean Square surface roughness

ROS: Reactive oxygen species

RSA: Relative surface area

SEM: Scanning electron Microscop

SFE: Surface free energy

TTIP: Titanium tetra-isopropoxide

UV: Ultraviolet

W: Water

XDLVO: Extended DLVO Theory

XRD: X-Ray diffraction

CHAPTER 1

INTRODUCTION

TiO₂ is the most widely studied metal oxide semiconductor due to its stability, biocompatibility, nontoxicity, physical, optical and electrical properties. Since, TiO₂ is stable, water insoluble and has suitable band gap energy to ensure reductive and oxidative processes; it is used as a photocatalyst for a wide range of applications. The most common applications are, purification of polluted water (Hoffman *et al.*, 1995), reduction of CO₂ (Fox and Dulay, 1993; Hoffmann *et al.*, 1995; Mills and Hunte, 1997; Kaneco *et al.*, 1998) and decomposition of NO_x (Anpo, 2000; Zhang *et al.*, 2001; Nonami *et al.*, 2004) in the atmosphere. Furthermore, due to its non-toxic quality and unique white color it is also used in food, cosmetics, biomaterial industry (Meacock *et al.*, 1997; Hewitt, 1999) and paints.

Surface disinfection is performed to control infections and reduce the contamination risks. Manual disinfection of surfaces is mostly achieved by the use of chemical agents or UV-C irradiation (200-280 nm). However these methods are impractical and ineffective in long term. The disinfection chemicals are generally toxic, corrosive, and have polluting properties and UV-C irradiation is hazardous and is difficult to control. The more complex but effective alternative of manual disinfection is the use of antimicrobial materials or surface coatings. Antimicrobial surfaces can be developed by using different strategies such as; contact killing, biocide leaching and adhesion resistance (Jenny *et al.*, 2009). TiO₂ can also be used as coating to get surfaces with self-cleaning and/or antimicrobial properties. Photocatalytic antimicrobial surface coatings are successful, environmentally friendly and economic alternatives for continuous surface

disinfection (Matsunaga *et al.*, 1988; Saito *et al.*, 1992; Maness *et al.*, 1999; Erkan *et al.*, 2006).

In all strategies that are used for getting antimicrobial surfaces, microbial adhesion plays an important role. Considering the photocatalytic antimicrobial surface coatings as an example of contact killing and/or biocide leaching strategies, microbial adhesion may also become an important parameter for photocatalytic activity of TiO₂ coatings.

Microbial adhesion is affected by surface hydrophobicity, surface free energies of the material, microorganism and suspending medium. These physicochemical properties can be explained by the chemical structure, surface charge, roughness, surface area, and pore structure of the material surfaces (Satou *et al.*, 1988; van der Mei *et al.*, 1998; Ong *et al.*, 1999; Liu *et al.*, 2004; Li and Logan, 2004; Ahn *et al.*, 2009).

Different types of bacteria such as *Escherichia coli* (*E. coli*), *Staphylococcus aureus*, *Lactobacillus acidophilus*, *Streptococcus sobrinus*, and *Salmonella choleraesuis* have been employed as model microorganisms to clarify the mechanism for the photocatalytic inactivation of TiO₂ (Matsunaga *et al.*, 1985; Saito *et al.*, 1992; Erkan *et al.*, 2006;). *E. coli* has been widely used as a model microorganism for the photocatalytic antibacterial activity of TiO₂ because of its rapid growth, short life cycle and the amount of huge information present in the literature.

Photocatalytic disinfection of *E. coli* over TiO₂ has been widely examined to explain the inactivation mechanism of TiO₂. Proposed mechanisms are inhibition of cell respiration (Matsunaga *et al.*, 1985; Matsunaga *et al.*, 1988), the decomposition of the lipopolysaccharide layer of the cell by reactive oxygen species (ROS), such as hydroxy ($\bullet\text{OH}$), super oxygen radicals ($\bullet\text{O}_2^-$) and hydrogen

peroxide (H_2O_2) (Lan *et al.*, 2007), decomposition of outer membrane of the cell (Sunada *et al.*, 1998) and structural disarrangement of the cytoplasmic membrane because of lipid peroxidation (Maness *et al.*, 1999; Huang *et al.*, 2000). Although the mechanism of photocatalytic disinfection is not clear yet, there is a consent in the literature on the inactivation of bacteria that is initiated with the attack of generated reactive oxygen species (ROS), which are produced as a result photocatalytic processes of TiO_2 on the cell surface (the outer membrane and peptidoglycon layer) (Saito *et al.*, 1992; Sunada *et al.*, 2003).

The photocatalytic processes of TiO_2 is initiated by activation of TiO_2 by UV-A irradiation (320-400 nm), which can be provided from natural sun light or artificial illumination. The photocatalytic processes depend on the generation of electron-hole (e^-/h^+) pairs as a result of absorption of photons having energy exceeding the band gap of TiO_2 (Mills and Hunte, 1997; Diebold, 2003; Lasa *et al.*, 2005). The electrons (e^-) and holes (h^+) diffuse to the crystal surface and react with adsorbed oxygen and water species over the surface to generate free radicals such as, hydroxy ($\bullet\text{OH}$) and super oxide ions ($\bullet\text{O}_2^-$) having very high oxidation potential (Anpo *et al.*, 1986; Fox and Dulay, 1993; Mills and Hunte, 1997; Fujishima *et al.*, 2000). The photocatalytic efficiency can be defined as the effectiveness of the photons on the free radical generation and generally less than 10 % (Serpone *et al.*, 1993). Many factors affect the photocatalytic efficiency such as defects in the crystal structure, impurities, particle size (Zhang *et al.*, 1998; Yu and Zhao, 2002), specific surface area (Ding *et al.*, 2005; Erdural *et al.*, 2008), porosity (Ding *et al.*, 2005; Novotná *et al.*, 2007), surface acidity (Zhao *et al.*, 2001; Guan *et al.*, 2003; Guan, 2005; Zhou *et al.*, 2006), electron-hole recombination, hydrophobicity (Fu *et al.*, 1996; Hattori *et al.*, 2000; Zhao *et al.*, 2001; Guan and Yin, 2005; Guan 2005; Novotná *et al.*, 2007) and crystal phases (Kato *et al.*, 1994; Negishi and Takeuchi, 1999; Jung and Park, 1999). To enhance the photocatalytic efficiency of TiO_2 , many attempts have been reported in the literature by modifying its electronic band structure and surface structure. Doping of semiconductor with

various transition metal ions, surface sensitization, coupling of two semiconductor and the use of support such as Al_2O_3 , SiO_2 , activated carbon are studied and reported techniques in literature (Wu *et al.*, 2004; Ou and Lo, 2007; Marciono *et al.*, 2009 Ma *et al.*, 2011). SiO_2 is one of the most commonly used oxide support because it has large surface area, high adsorption capacity (Anderson and Bard, 1997), high thermal stability (Viswananth and Ramasamy, 1998; Periyat *et al.*, 2008) good mechanical strength (Guan *et al.*, 2003) and optical transparency. It has been shown that, the addition of SiO_2 to TiO_2 enhances photocatalytic activity of TiO_2 (Anderson&Bard, 1995; Quan *et al.*, 2004; Su *et al.*, 2010; Suzuki *et al.*, 2011; Bui *et al.*, 2011). The increase of photocatalytic efficiency of TiO_2 with SiO_2 addition can be explained by the following mechanisms;

- The dispersion of TiO_2 in SiO_2 phase results with the decrease of TiO_2 grain size due to the limitation of growth of TiO_2 crystallites. High dispersion of titania in silica matrix and the formation of Si -O -Ti bonding limit crystallite size (Sankur and Gunning, 1985; Zhai *et al.*, 1999; Lin *et al.*, 1999; Yu *et al.*, 2002). As a result of a smaller grain or crystallite size, larger surface area can be obtained which has higher adsorption capacity for reactants (Zhang *et al.*, 1998; Yu and Zhao, 2002; Corp *et al.*, 2004). In addition, the mobility of electrons and holes in crystallite are enhanced significantly by crystallite size and the accessibility of photons to the lattice increases drastically (Zhang *et al.*, 1998; Gao and Wachs, 1999; Kamat 2002; Zhang *et al.*, 2009). However when the amount of SiO_2 exceeds a certain extent the distance between neighboring titania nanoparticles tends to increase. In this case, accessibility of ROS on the active sites of TiO_2 to adsorbed molecules decreases and photocatalytic activity reduces because of unstable ROS and the formation of recombination of the photogenerated radicals. As a result the radicals cannot reach adsorbed molecules (Suzuki *et al.*, 2011) .
- Heat treatment is a critical step for crystallinity. The transport properties of electrons and holes can be improved by removing internal stresses and

lattice defects by calcination process. Anatase phase is considered as more active than other crystal forms of TiO₂ (rutile, brookite). However the anatase phase is transformed into rutile phase as a result of heat treatment above 500 °C. Rutile formation takes place by crystal growth as a result of sintering and the use of oxide support inhibits rutile formation to certain a extent (Anderson and Bard, 1997; Gao *et al.*, 1998; Kumar *et al.*, 1999; Ding *et al.*, 2000; Zhao *et al.*, 2001; Yu *et al.*, 2008).

- The surface acidity can be increased by dispersion which increases the amount of available hydroxyl groups over the surface which are hole acceptors. Surface acidity has a vital role on the production of [•]OH radicals (Fu *et al.*, 1996; Guan and Yin, 2005; Zhou *et al.*, 2006).

TiO₂-SiO₂ binary mixtures have been utilized especially for environmental purification. The effect of SiO₂ addition on the photocatalytic degradation efficiency of TiO₂ against different type of organic compounds (Fu *et al.*, 1996; Anderson and Bard 1997; Jung and Park, 1999; Yu and Zhao, 2002) was reported extensively. Moreover in the relevant literature antifogging and self cleaning properties of TiO₂-SiO₂ coated thin film surface have been investigated (Anderson and Bard, 1997; Machida *et al.*, 1999; Hattori *et al.*, 2000; Zhao *et al.*, 2001; Guan 2005; Guan and Yin, 2005; Permpoon *et al.*, 2008; Chien *et al.*, 2009). However there are few reports on the antibacterial properties of TiO₂-SiO₂ coated thin films for continuous surface disinfection (Xu *et al.*, 2004; Sun *et al.*, 2007; Garther *et al.*, 2008).

In this study, the effects of SiO₂ on the photocatalytic antibacterial and self-cleaning activities of TiO₂ thin films were investigated. The thin films having various SiO₂/TiO₂ ratios were synthesized by sol-gel method and crystallinity, surface area, surface free energy and band gap of the samples were characterized. Photocatalytic self-cleaning and antibacterial activities of the thin films were investigated through the degradation of methylene blue (MB) and inactivation of *E. coli*, respectively.

According to the experimental results, photocatalytic self-cleaning and antibacterial activities were observed on all the samples containing TiO₂. The addition of silica enhanced the photocatalytic activity to a certain extent. However, the antibacterial and self-cleaning activities reached their maximum values on thin films having different SiO₂ contents. In this study, some arguments were presented for reasoning out why the antibacterial and self-cleaning activities reached their maximum values at different SiO₂ ratios. For this purpose, the surface structure and physicochemical properties of thin film surfaces were attempted to relate with the bacterial adhesion and antibacterial activity.

CHAPTER 2

LITERATURE SURVEY

A photocatalyst can be defined as a substance that is activated by the absorption of photons and accelerates reaction without being consumed (Mills and Hunte, 1997; Lasa *et al.*, 2005).

Metal oxide semiconductors have been found to be the most suitable photocatalysts (Fox and Dulay, 1993). In literature, various n-type semiconductor metal oxides, such as TiO₂, ZrO₂, SnO₂, WO₂, MoO₃ are successfully applied as photocatalysts for many liquid and gas phase oxidation-reduction reactions (Hoffman *et al.*, 1995; Kaneco *et al.*, 1998; Anpo, 2000) . In the presence of irradiated semiconductors, environment remediation (Anpo, 2000), the purification of polluted water (Hoffman *et al.*, 1995), the decomposition of NO_x (Zhang *et al.*, 2001), the reduction of CO₂ (Kaneco *et al.*, 1998) in the atmosphere can be achieved. When compared with the chemical methods, in the presence of semiconductor photocatalysts, it is possible to obtain a complete mineralization of toxic substrate even in the absence of toxic, corrosive, and polluting reagents.

2.1. General remarks about semiconductors

Filled and unfilled bands exist in the lattice of any material. Gap between filled and unfilled bands is called band gap. The lower energy valance band is completely filled and the upper energy conduction band is completely empty at the temperature of absolute zero. The energy gap between filled valance band and empty conduction band is defined as band gap energy. Up to Fermi level, all energy levels completely filled with electrons. The size and the gap between

bands define the electrical conductivity nature of material. Semiconductors are group of materials having electrical conductivity between that of metals and insulators. In insulators the chance of motion of electrons between the valance band and the conduction band is very little due to large band gap. In metals, electrons are free to move because of the overlap between the valance band and conduction band (Figure 2.1) and there is at least one valance electron per atom in these bands. In semiconductors, this situation is similar to that in insulators, but semiconductors have narrower band gap than insulators and there are excess electrons, and/or holes (Hannay, 1959; Mills and Hunte, 1997).

Due to their electronic configuration, semiconductors have been widely applied on the production of anti-static coatings, gas sensors, production of touch screen LCD monitors, optical filters and photocatalysts.

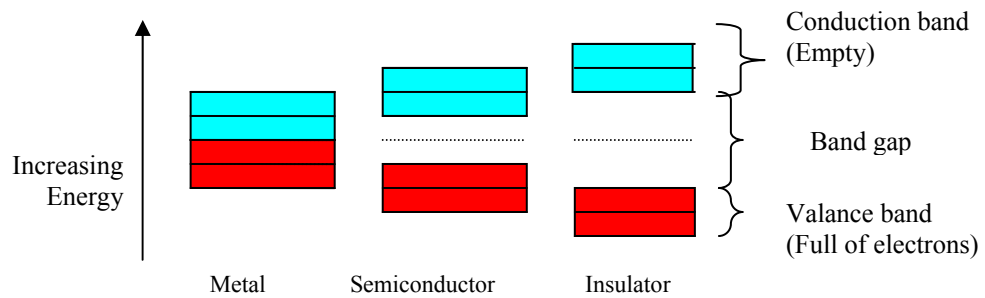


Figure 2.1 Comparison of the band gaps for a metal, a semiconductor and insulator

The excitation of valence band electrons requires the existence of photons having proper energy which is greater than the band gap energy of semiconductor. Ultraviolet (UV) or visible light radiations are frequently used to provide photons with sufficient energy. The wavelength range of visible light is between 400 to 720 nm and UV radiation is divided into three categories according to wavelength range as; UVA: 315 -400 nm, UVB: 280- 315 nm, and UVC: 200 - 280 nm. The band gap energy and corresponding wavelength of common semiconductor metal oxides are listed in Table 2.1.

The photocatalytic processes depend on the generation of electron-hole (e^-/h^+) pairs which is a result of absorption of photons having energy exceeding the band gap of semiconductor material. The electrons (e^-) and holes (h^+) diffuse to the surface and react with adsorbed oxygen and water species over the surface generating hydroxy ($\bullet\text{OH}$) and super oxide ions ($\bullet\text{O}_2^-$) having very high oxidation potential.

Table 2.1 Band gap energies and corresponding radiation wavelengths of various semiconductors (Lasa *et al.*, 2005)

Semiconductor	Band gap energy (eV)	Wavelength (nm)
TiO ₂ (rutile)	3.0	413
TiO ₂ (anatase)	3.2	388
ZnO	3.2	388
ZnS	3.6	335
CdS	2.4	516
Fe ₂ O ₃	2.3	539
WO ₃	2.8	443

Photocatalytic activity of semiconductors is a function of catalyst properties, the organic species to be degraded and the experimental conditions. Catalyst having the highest activity with one compound might not necessarily be the best catalyst for the destruction of other species (Lasa *et al.*, 2005). In Figure 2.2 valence and conduction band positions of various semiconductors at a pH of 7 (versus normal hydrogen electrode (NHE)) and redox potentials of adsorbates can be seen. The possibility of photocatalytic process occurrence depends on the position of conduction band and valence band of semiconductor and level of redox potential of adsorbates. Adsorbates can be electron donor or electron acceptor. The conduction band of semiconductor must be more negative than the redox potential level of the adsorbate (donor) and the valence band of the semiconductor must be more positive than the redox potential level of the adsorbate (acceptor). Oxidation and reduction mechanisms can be defined as the process of electron transfer from the adsorbate to the semiconductor and transfer of electron from the semiconductor to the adsorbate, respectively. At the surface of the semiconductor particle photogenerated electrons can reduce an electron acceptor and photogenerated holes can oxidize an electron donor.

Although, semiconductors such as CdS and Fe₂O₃ have low band-gap energies which need irradiation with low energy light, they cannot be used as photocatalyst because of their photocorrosive effect under irradiation during the reaction and positions of their conduction bands, respectively (Schiavello, 1997; Mills and Hunte, 1997). On the other hand metal oxide semiconductors have been found to be the most suitable photocatalysts due to their photocorrosion resistance, their wide band gap energies and having suitable band energy positions to ensure reductive and oxidative processes (Fox and Dulay, 1993).

A semiconductor photocatalyst must be photoactive, photo-stable, inexpensive and inert (Mills and Hunte, 1997). TiO_2 and ZnO are the most widely studied semiconductor metal oxides. (Hoffmann *et al.*, 1995).

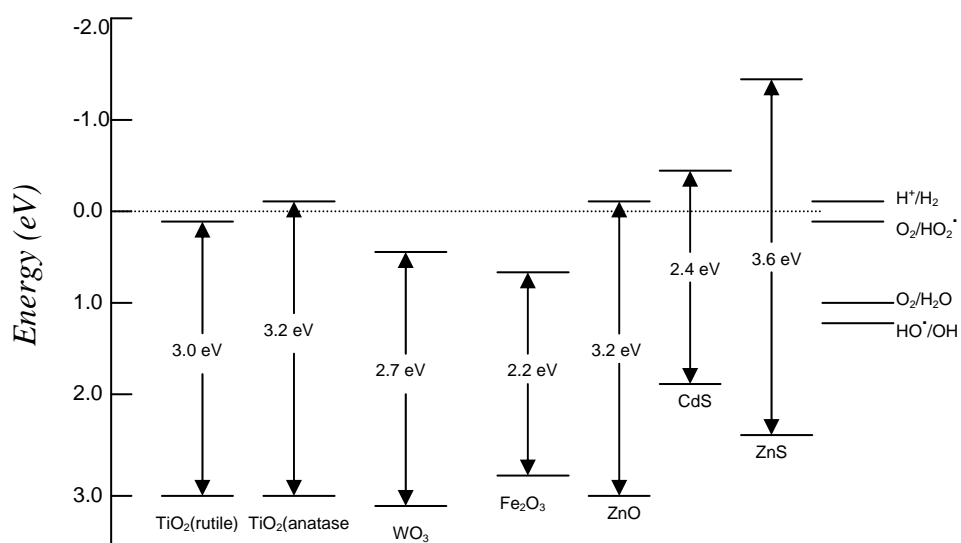


Figure 2.2 Valence and conduction band positions for various semiconductors (Adapted from Mills A., Hunte Le S., “An overview of semiconductor photocatalysis” *Journal of Photochemistry and Photobiology A* 108 (1997) 1

2.2 TiO_2

TiO_2 , titania, is an inert, nontoxic, biocompatible and abundant transition metal oxide. Rather than other semi-conductor metal oxides, TiO_2 plays an important role in permanent disinfection and photo-degradation of unwanted and toxic organic substances from contaminated air and water due to its inert structure, photo-stability, high efficiency, water insolubility and low cost.

Rutile, anatase and brookite are the different mineral forms of TiO_2 (Diebold, 2003). As seen from Figure 2.3, although both anatase and rutile possess chains of octahedral groups of oxygen atoms around titanium (TiO_6 octahedron) in their crystal structures, the distortion of each octahedron and assembly form of octahedron chains are different. Each octahedron in rutile and anatase is in contact with ten and eight neighbor octahedrons, respectively. In rutile structure, two of the neighbor octahedrons share edge oxygen pairs and the remaining eight share corner oxygen atoms. In anatase structure, four of the neighbor octahedrons share edge oxygen pairs and the other four share corner oxygen atoms. As a result of these differences in lattice structures, different mass densities and electronic band structures are seen between the two forms. Brookite form of TiO_2 has an orthorhombic crystalline structure (Macwan and Dave, 2011).

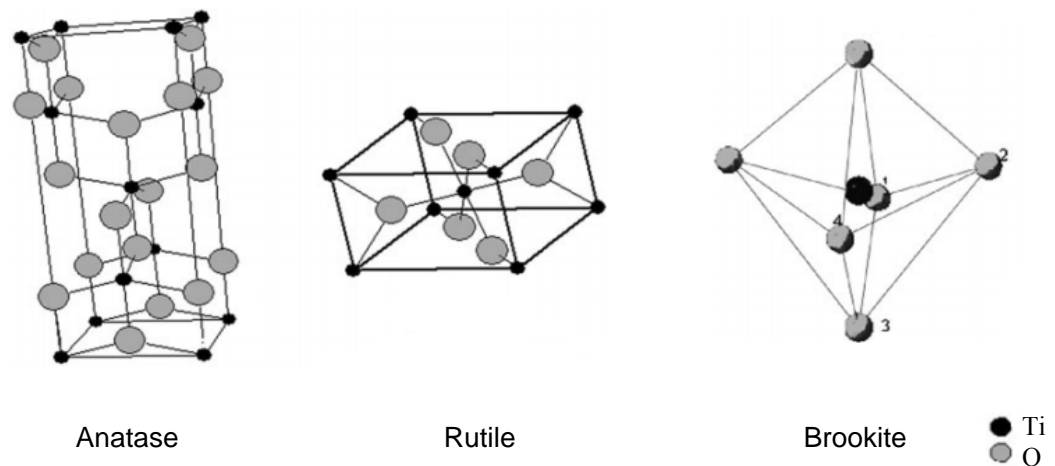


Figure 2.3 Forms of TiO_2 (Macwan and Dave, 2011)

Brookite is not suitable for photocatalytic reactions because of thermal instability. Rutile is the most stable phase thermodynamically (Reddy *et al.*, 2002; Diebold, 2003;). Anatase is the most popular crystalline phase used in photocatalytic processes due to having a more negative conduction band edge potential (higher potential energy of photo-generated electrons) rather than rutile (Yu *et al.*, 2008). Yet there are studies in literature that show that rutile phase or mixture of rutile and anatase phases has higher photocatalytic activity than a pure anatase phase (Mahanty *et al.*, 2004; Lasa *et al.*, 2005).

TiO₂ has a wide application area. It can be used as white pigment in paint (especially rutile type), paper (Macwan and Dave, 2011), rubber, plastics and cosmetics industry (Meacock *et al.*, 1997; Hewitt, 1999) and optical coatings (Yoldas and Partlow 1985), dye-sensitized photoelectrochemical cells and gas sensors are the examples of applications of TiO₂. Furthermore, TiO₂ thin film photocatalysts prepared on glass, tile, various architectural materials and cotton fabrics have been described as promising antibacterial, self-cleaning and deodorization systems (Kikuchi *et al.*, 1997; Erkan *et al.*, 2006; Vliet *et al.*, 2009; Hadnadjev *et al.*, 2010; Wu and Long, 2011)

2.3 Photocatalytic reactions of TiO₂

When TiO₂ absorbs photons having sufficient energy which is larger than the band gap energy, electrons in the valance band, excite to the energy level of conduction band generating holes in the valance band. Therefore photo-excited TiO₂ generates energetic electron-hole (e⁻-h⁺) pairs. The e⁻-h⁺ pair formation is the first step of heterogeneous photocatalytic reactions (Turchi and Ollis, 1990; Hoffman *et al.*, 1995; Fujishima *et al.*, 2000; Abdullah and Gaya, 2008; Chong *et al.*, 2010).

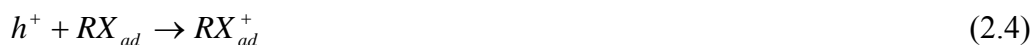


The electrons (e-) and holes (h+) over the catalyst surface have great potential for many oxidation and reduction reactions (Ox-Red). The resulting electron-hole pairs in the bulk of TiO₂ particle are transferred to the outer surface by lattice transport properties and interact with the molecules that exist in the environment (e.g. water (H₂O), and oxygen (O₂)). The steps of charge-carrier trapping of valance band hole and conduction band electron are given in Equation 2.2 and 2.3, respectively.



Where $Ti(IV)OH$ represents the primary hydrated surface functionality of TiO₂ (Hoffman *et al.*, 1995).

The holes react with adsorbed substrate (Eq. 2.4)



In most of the applications, the photocatalytic reactions are performed in air or in aqueous phase (Hoffman *et al.*, 1995; Chong *et al.*, 2010). In this case ionization of water is the reduction step which yields OH^- species (2.5).



In addition, the holes also react with surface adsorbed H₂O (2.6) or OH⁻ with the following reactions; (Eq. 2.7)



Hydroxyl groups on the surface are very important for photocatalytic reactions because holes and hydroxyl groups work together to produce reactive OH^\bullet radicals which then decompose organic pollutant.

Similarly, electrons reach to the particle surface via diffusion and react with the molecular oxygen yielding superoxygen that has unique oxidation potential.



The super-oxide anions (O_2^-) (Equation 2.6) might be involved in the following reactions (Equation 2.9 and 2.10) if water species exists in the environment.



The hydrogen peroxide is a very active oxidant and is mostly used as oxidant in waste water treatment and manual sterilization (Kikuchi *et al.*, 1997). Photoconversion of hydrogen peroxide also yields OH^\bullet free radicals.



The hydroxyl radicals (OH^\bullet) and super oxide ions (O_2^-) are very active species for the oxidation of organic adsorbed pollutants and inactivation of microorganisms (Cho *et al.*, 2003; Cho *et al.*, 2004).

The chain reaction initiated by the photon absorption ends up with the Ox-Red reactions which occur over the particle surface. The effectiveness of the photons on the free radical generation defines the photocatalytic efficiency. The transport properties of the lattice do not allow the successful diffusion of

electrons and holes to the surface most of the time. The charge recombination centers such as imperfections, impurities, lattice defects trap the charges and the energy dissipated as heat.



The charge recombination is the major limitation for many photocatalysts which yield low photon efficiency. In the absence of electron scavengers (O_2 and H_2O), an electron recombines with the hole in the valance band as given in Equation 2.12 (Chong *et al.*, 2010). During electron-hole recombination reaction, heat energy comes out (Eq. 2.12). If there is adsorbed $(O_2)_{ads}$ and (OH_{ads}^{-}) on the surface of TiO_2 , a photoexcited electron reacts with $(O_2)_{ads}$ (Eq. 2.8) and the hole reacts with (OH_{ads}^{-}) (Eq. 2.7) to produce $O_2^{\cdot -}$ and OH^{\cdot} , respectively.

Besides electron-hole recombination, descent of absorbed photon energy by light reflection and transmission can decrease photocatalytic activity. Hence, the ratio of the number of free radicals produced to the number of photons absorbed is defined as photocatalytic efficiency (Equation 2.13) (Grela *et al.*, 1996).

$$\text{Photocatalytic efficiency} = \frac{\text{Number of free radicals produced}}{\text{Number of photons absorbed}} \quad (2.13)$$

The photocatalytic efficiency of TiO_2 is mostly less than 10% (Serpone *et al.*, 1993) due to its large band gap and considerable recombination of charge carriers.

2.4 Improving the photocatalytic activity of TiO_2

The photocatalytic activity of TiO_2 can be influenced by its specific surface area, particle size, crystal structure, porosity, band-gap and surface hydroxyl

group density (Zhang *et al.*, 1998; Guan and Yin, 2005 Černigoj *et al.*, 2006; Zhou *et al.*, 2006; Erdural *et al.*, 2008).

Many attempts have been reported in literature regarding the improvement of photocatalytic efficiency of TiO₂ by modifying its electronic band structure and surface structure. There are several methods to make this modification; doping the TiO₂ surface with transition metal ions such as, Pd²⁺, Pt⁴⁺, Au³⁺, Ag⁺, Fe³⁺, oxides (ZnO, WO₃, SiO₂, CrO₃) or non-metals (C, N, S, P, F), sensitization by dyes and metal complexes, coupling of semiconductors with suitable energy levels, and use of binary metal oxides can be accounted as promising approaches (Wu *et al.*, 2004; Ou and Lo, 2007; Marciono *et al.*, 2009; Ma *et al.*, 2011).

Doping with transition metal ions increases the light absorption capacity by decreasing the band gap of TiO₂. Alkaline earth ions such as; Ca²⁺, Sr²⁺ (Al-Salim *et al.*, 2000), Fe³⁺ (Kim *et al.*, 2004; Naeem and Ouyang, 2010; Zhao *et al.*, 2010), rare earth ions such as; La³⁺, Er³⁺, Pr³⁺ (Xu *et al.*, 2002) and noble metals and its ions (Pd²⁺, Pt⁴⁺, Au³⁺, Ag⁺) can be used for doping process. Fe³⁺ is frequently used as metal ion since it enhances the absorption of light in the visible region of TiO₂ (Trapalis *et al.*, 2003).

The reason for the enhancement of photocatalytic activity of TiO₂ with deposition of transition metal ions such as Au³⁺ (Chandrasekharan and Kamat, 2000), Ag⁺ (Dobosz and Sobczykński, 2003) Pt⁴⁺ (Teoh *et al.*, 2007) and Pd²⁺ (Wang *et al.*, 1992) is ascribed to;

- reduction of recombination probability of electron-hole pairs due to Schottky effect at the interface of metals and TiO₂, which act as a trap for photogenerated electrons (Li *et al.*, 2002; Sakthivel *et al.*, 2004; Ou and Lo, 2007, Teoh *et al.*, 2007)

- enhancement of the formation of Ti^{3+} ions which are necessary for adsorption of oxygen on the titania surface (Li and Li, 2002; Sakthivel *et al.*, 2004; Ou and Lo, 2007).

However, doped metals can be detrimental to the photo-oxidation activity when they cover Ti^{3+} (Sakthivel *et al.*, 2004) and when metal ion centers disperse the lattice. With the dispersment of the lattice, recombination centers are formed. (Sakthivel *et al.*, 2004; Ou and Lo, 2007).

Number of organic dyes such as, erythrosin B, thionine, and phthalocyanine (Moser and Gratzel, 1984; Carp *et al.*, 2004) are used for surface sensitization of TiO_2 which also increases its sensitivity in the visible region (Moser and Gratzel, 1984). This can be achieved by injection of electrons from an excited level of the dye into the semiconductor conduction band.

Furthermore, to obtain better charge separation, bicrystals or tricrystals of heterogeneous titania nanostructure have also been used. Indeed, according to many reports, the photocatalytic activity of anatase structure is usually higher than that of rutile (Kato *et al.*, 1994; Hoffman *et al.*, 1995; Jung and Park, 1999; Yin *et al.*, 2001; Hidalgo *et al.*, 2002; Deng *et al.*, 2002; Mills *et al.*, 2003; Sakatani *et al.*, 2006) due to the decrease in the probability of electron-hole recombination in wide band gap lattice structure of anatase (Linsebigler *et al.*, 1995; Sumita *et al.*, 1999), lower oxygen adsorption capacity and higher hydroxylation performance of anatase (Tanaka *et al.*, 1991; Bickley *et al.*, 1991). However, there are few cases in which higher photocatalytic activity for rutile than anatase is reported (Testino *et al.*, 2007; Nag *et al.*, 2008). Enhancement of photocatalytic activity was also observed for bicrystalline TiO_2 containing anatase-rutile (Bickley *et al.*, 1991), anatase-brookite (Kang and Chen, 2010) and rutile-brookite (Xu and Zhang, 2009).

2.4.1. Improving photocatalytic activity of TiO₂ by addition of SiO₂

SiO₂ is one of the most commonly used support materials because it has larger surface area and adsorptive property (Anderson and Bard, 1997), high thermal stability (Viswananth and Ramasamy, 1998; Periyat *et al.*, 2008) and good mechanical strength (Guan *et al.*, 2003). The use of TiO₂/SiO₂ binary mixtures on the photocatalytic degradation of organics with higher efficiency has been widely studied in the last two decade (Anpo *et al.*, 1986; Anderson and Bard, 1997; Gao *et al.*, 1998; Jung and Park, 1999; Yu and Zhao, 2002; Kwon *et al.*, 2003; Novotna *et al.*, 2007). The addition of SiO₂ enhances the photocatalytic activity of TiO₂ which might be explained by the following effects;

- reduction of grain size of TiO₂ and increase of specific surface area of TiO₂ particles
- elimination of bulk defects, enhancing the thermal stability of TiO₂, stabilizing the anatase crystalline form of TiO₂ even at high calcination temperatures
- formation of new active sites on the SiO₂ -TiO₂ grain boundaries by Si-O-Ti bond formation
- increase in the band-gap energy of TiO₂

Particle size is an effective parameter on the photocatalytic efficiency of semiconductor metal oxides. With smaller particle size, electron-hole recombination probability and diffusion path-way decreases whereas accessibility of photons to the lattice increases drastically (Zhang *et al.*, 1998; Kamat, 2002). According to the literature, a larger surface area can be obtained by a smaller particle size which also enhances the adsorption of reactants over the TiO₂ surface (Zhang *et al.*, 1998; Yu and Zhao, 2002; Corp *et al.*, 2004).

SiO₂ addition causes the reduction of grain size of TiO₂ due to the limitation of grain boundary growth of TiO₂ nanoparticles in SiO₂ phase due to the high dispersion of titania in the silica matrix and formation of Si-O-Ti bonding which could inhibit grain growth of TiO₂ and decrease crystallite size (Sankur and Gunning, 1985; Zhai *et al.*, 1999; Lin *et al.*, 1999; Yu *et al.*, 2002).

The structural defects can be observed both on the surface and on the bulk of TiO₂ particles. Mostly, the surface defects act as active sites for adsorption and reactions by enhancing the photocatalytic activity while the bulk defects promote the charge recombination reaction (Jung and Park, 1999). Calcination at high temperature is a useful technique to remove internal stresses and lattice defects. However, heat treatments at high temperatures may cause phase transformation. Over 500 °C, anatase phase can transform to rutile since anatase is a metastable phase. This is an undesirable process for the photo-degradation of organic dye molecules because anatase phase has higher adsorption capacity against organic dye molecule than rutile phase (Jung and Park, 1999; Negishi and Takeuchi, 1999; Daoud and Xin, 2004; Qi *et al.*, 2006). Usage of SiO₂ as a dopant has been reported to be an effective solution to increase the thermal stability of the anatase phase and blocks the transformation of anatase phase to rutile phase even at high temperature calcinations. Prevention of phase transformation with SiO₂ addition has been explained by high dispersion capacity of the TiO₂ clusters in the SiO₂ surface and possible bonding of Si-O-Ti in SiO₂/TiO₂ interface which stabilize the crystallite transformation (Anderson and Bard, 1997; Gao *et al.*, 1998; Ding *et al.*, 2000; Zhao *et al.*, 2001).

Surface acidity which is the result of charge imbalance is an important parameter for photocatalytic activity. It increases the amount of hydroxyl groups on the surface which are the acceptors of holes and these groups have a vital role in production of [•]OH radicals (Itoh *et al.*, 1974; Fu *et al.*, 1996; Guan and Yin, 2005; Zhou *et al.*, 2006). The higher surface concentration of OH_{ad}⁻ species yields higher photocatalytic efficiency (Ding *et al.*, 2000; Liu *et al.*,

2008). For TiO₂-SiO₂ binary mixtures, as a result of migration of SiO₂ atoms into lattice of TiO₂ and migration of TiO₂ atoms into lattice of SiO₂, positive and negative charge imbalances can be formed, respectively (Fu *et al.*, 1996; Zhang *et al.*, 2009). Migrating atoms and lattice of oxide, which is migrated, are called as dopant oxide cation and host oxide, respectively. As a result of migration, charge imbalance occurs because dopant cation which is already bonded to the same number of oxygens migrate to host oxide even though oxygen atoms are now of a new coordination. Brønsted sites and Lewis sites are expected to form when the charge imbalance is negative and positive, respectively. According to many reports, SiO₂ atoms are more likely to migrate into the lattice of TiO₂ since Si⁴⁺ (0.041 nm) has smaller radius than that of Ti⁴⁺ (0.064 nm). If a silicon atom enters a titania lattice, Lewis acid sites are formed and more hydroxyl groups would be absorbed on the colloid core of TiO₂-SiO₂. However, migration of titanium into silicon sites was also investigated by only a few researchers. In this case, acidic sites are created by Brønsted acid character instead of Lewis acid character (Liu and Davis, 1994).

It was reported that the band gap energy of TiO₂ increases with SiO₂ addition. The reasons of increase in the band-gap energy (Dagan *et al.*, 1995) of TiO₂ were attributed to quantum size effect (Anpo and Takeuchi, 2003) and occurrence of interface interaction between SiO₂ and TiO₂ atoms. The band gap of TiO₂ (anatase) and SiO₂ is 3.3 eV and 11.7 eV, respectively. It was reported in the literature that, when TiO₂-SiO₂ binary mixture was used, the band gap of TiO₂ increased up to 4.1 eV (Gao and Wachs, 1999; Jafry *et al.*, 2011). According to band theory in quantum mechanics, as the particle size of TiO₂ decreases, the band gap between valance band and conduction band increases (Anderson and Bard, 1997) due to rising of conduction band and lowering of the valance band (Gao and Wachs, 1999; Zhang *et al.*, 2009). As a result, the oxidizing potential of the photon generated holes (h⁺) and the reducing potential of the photon generated electrons (e⁻) increases.

2.4.2 Interactions of TiO₂ with SiO₂

Interaction between TiO₂ and SiO₂ can be divided into two categories: physically mixed (weak interaction forces occur such as Van der Waals forces) and chemically bonded (i.e., the formation of Ti-O-Si bonds). When chemical bonding is formed, the textural and surface properties of TiO₂ particles change extremely. As a result, photocatalytic reactivity of TiO₂-SiO₂ binary mixture enhances when compared to pure TiO₂.

The degree of interaction between TiO₂ and SiO₂ is directly affected from the content of TiO₂ and SiO₂ in the mixed oxide (Stakheev *et al.*, 1993; Anderson and Bard, 1997; Kwon *et al.*, 2003; Guan, 2005; Zhou *et al.*, 2006), preparation methods, and synthesis conditions (Gao and Wachs, 1999).

According to Stakheev *et al.*, (1993) the atomically mixed TiO₂-SiO₂ oxides can only be obtained when TiO₂ content is lower than 15 wt%. However, when TiO₂ content is above 50 wt%, TiO₂ crystallites tend to form aggregated nanoparticles as a separate phase (Gao and Wachs, 1999; Anpo and Takeuchi, 2003). TiO₂-SiO₂ binary oxides have been extensively used in the form of thin film or powder for a variety of reactions. In Table 2.2, examples of photocatalytic reactions of TiO₂-SiO₂ binary mixtures, the effect of surface composition on photocatalytic activity and the proposed reasons why the photocatalytic activity of these binary mixtures reach their maximum values at different SiO₂ ratios are given. As seen from Table 2.2, the maximum photocatalytic activity was reported for different catalyst compositions varied between 4-80 wt% SiO₂ in TiO₂-SiO₂ binary mixture.

Table 2.2 Various reactions for TiO₂-SiO₂ in powder or thin film form

SiO ₂ (wt%)	Form	Reactions	Proposed reason for increasing activity with SiO ₂ addition	Proposed reason for decreasing activity with further addition of SiO ₂	References
50	Thin film	Photocatalytic decomposition of rhodamine B	Having higher surface adsorption capacity and higher surface hydroxyl group in the composite thin film	Deducing amount of the surface acidity sites and photocatalytic center	Zhou et al., (2006)
80	Powder	<ul style="list-style-type: none"> • Photocatalytic decomposition of rhodamine-R-6G • Photocatalytic decomposition of phenol/ 	SiO ₂ was considered as an adsorbent which increases the concentration of phenol and rhodamine-R-6G near the TiO ₂ sites, and, by this way, diffusion of reactive oxygen species from TiO ₂ surface to phenol and R-6G molecules become easier.		Anderson and Bard, (1995)/ Anderson and Bard, (1997)
4	Thin film	Photocatalytic degradation of methyl orange	Decrease in the grain size of TiO ₂ , higher adsorptivity toward organic contaminants, increase in hydroxyl content	Decrease in the quantum yield, increase in the amount of amorphous TiO ₂	Yu and Zhao (2002)

Table 2.2 (cont'd)

SiO ₂ (wt%)	Form	Reactions	Proposed reason for increasing activity with SiO ₂ addition	Proposed reason for decreasing activity with further addition of SiO ₂	References
60	Powder	Photocatalytic degradation of methylene blue	Increase in surface area and adsorption capacity due to formation of mesoporous silica/titania composites.	Recombination of the photogenerated radicals due to increase in the distance between neighboring titania nanoparticles	Suzuki et al., 2011
5	Hydrosol	Photocatalytic degradation of methylene blue	Decrease in particle size, increase of Lewis sites on the surface of TiO ₂ due to formation of Ti-O-Si bonds, generation of more adsorption sites and hence, adsorption of more hydroxide ion		Zhang et al., 2009
20	Powder	Inactivation of bacteriophage MS2	Enhancement of adsorptive capacity of MS2 to the catalyst and/or increase in band gap energy with SiO ₂ addition		Jafry et al., (2011)

2.5 Application of TiO₂ for hydrophilicity and self cleaning effect

Self cleaning activity of TiO₂ can be used in ceramic tiles, kitchen and bathroom components, interior furnishing, plastic surfaces, curtains, fabrics, materials for roads and tunnel walls (Ramamurthy and Schanze, 2003).

In nature, the lotus leaf can be given as an example of a self-cleaning surface. Lotus leaf has a super-hydrophobic surface, and when water drops contact with the lotus leaf surface, they are repelled from the surface collecting hydrophilic contaminants over the surface. In the literature, much effort has been performed to imitate the self-cleaning property of lotus leaf (Feng *et al.*, 2002). However, little success has been attained. On the other hand, production of self-cleaning surfaces by using super-hydrophilic and photocatalytic properties of TiO₂ is a promising method (Yu and Zhao, 2001; Doshi *et al.*, 2003; Lee and Choi, 2004; Zhang *et al.*, 2005; Guan, 2005; Hadnadjev *et al.* 2010). Both self cleaning and hydrophilic properties of TiO₂ can be applied on the same surface though their mechanisms are totally different (Fujishima *et al.*, 2000; Guan, 2005).

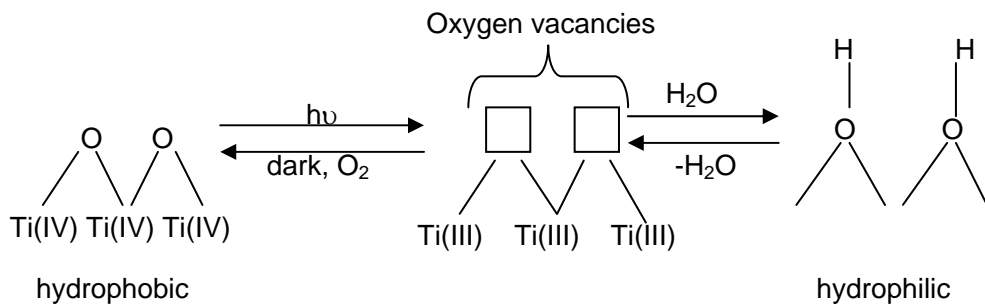


Figure 2.4 Mechanism of photo-induced hydrophilicity

Super-hydrophilicity effect of TiO_2 has been recently searched. This effect was first investigated, accidentally, in a study that was being carried out at the laboratories of TOTO Inc., in 1995. TiO_2 films became superhydrophilic surfaces by exposing UV irradiation. In literature, this method is called as photo-induced superhydrophilicity. In this process, photo-generated electrons reduce Ti^{4+} cations to Ti^{3+} and holes oxidize $\text{O}_2^{\cdot-}$ radical to O_2 (Watanabea *et al.*, 1999; Fujishima *et al.*, 2000; Carp *et al.*, 2004; Ren *et al.*, 2004; Thompson and Yates, 2006; Thompson and Yates, 2006). During reduction and oxidation reactions, the bond between titanium and lattice oxygen become weaker which forms free oxygen atoms over the surface and oxygen vacancies. Oxygen vacancies can be filled by OH^- species which can be produced by the ionization of water. The increase of chemisorbed OH^- causes increasing of van der Waals forces and hydrogen bonding interactions between H_2O and OH^- (Carp *et al.*, 2004). Figure 2.4 is summarizes the mechanism for photo-induced hydrophilicity (Fujishima *et al.*, 2000).

If TiO_2 is coated on glass, because of hydrophilic nature of the irradiated semiconductor, water has tended to spread perfectly across the surface. Provided the glass is illuminated, it can undergo self-cleaning by rainfall. Other applications for the hydrophilic glass include antifogging windows and mirrors, where instead of forming individual water droplets, the surface of the glass is covered by a uniform thin layer of water (Wardle, 2009).

However, hydrophilic nature of TiO_2 is slowly reversed in the dark as the Ti^{3+} sites are oxidized by atmospheric oxygen and the vacancies are filled by the O^{2-} ions produced by the oxidation reaction (Wardle, 2009). On the other hand, SiO_2 addition improves the hydrophilic property of TiO_2 (Zhao *et al.*, 2001; Yu and Zhao, 2001; Guan *et al.*, 2003; Ren *et al.*, 2004; Novotá *et al.*, 2007). Fu *et al.* (1996) and Guan *et al.* (2003) and reported that, with addition of SiO_2 to TiO_2 thin films hydrophilicity of surface could preserve for a long time because of enhancement of surface acidity.

2.6 TiO₂ photocatalysis for disinfection

Destruction of different types of bacterial species (Matsugana *et al.*, 1985; Saito *et al.*, 1992; Kühn *et al.*, 2003) viruses (Watts *et al.*, 1995; Cho *et al.* 2005; Jafry *et al.*, 2011) and fungi (Seven *et al.*, 2004; Lonnen *et al.*, 2005; Erkan *et al.*, 2006; Maneerat and Hayata, 2006; Chen *et al.*, 2009) from contaminated water, air and surfaces by using TiO₂ has been reported more than two decades.

To achieve photocatalytic disinfection of waste water, air and surfaces, TiO₂ has been utilized in two forms; a powder and immobilized form. In the powder form, TiO₂ particles are suspended in the reaction solution. In the immobilized form, TiO₂ thin films are prepared on suitable supports. When TiO₂ is utilized in the powder form, mass transfer limitations can be eliminated during the photocatalytic process. However, at the end of the photocatalytic reaction TiO₂ particles must be removed from the solution and the separation process of TiO₂ particles is a slow and expensive process. Moreover in the powder form, the penetration depth of UV light can be limited due to strong absorption of dissolved organic species and the suspension (Chen *et al.*, 2001; Chen *et al.*, 2005; Camera-Roda and Santarelli 2007). On the other hand, utilization of thin films overcomes these disadvantages. Firstly, separation step can be eliminated and continuous treatment of contaminated water and air can be achieved (Grieken *et al.*, 2009), secondly, by using porous thin films, specific surface area can be increased, thirdly electron-hole recombination can be reduced and photocatalytic efficiency can be enlarged (Chen *et al.*, 2001). However, utilization of TiO₂ thin films generates also problems such as; external mass transfer resistance during the diffusion of the pollutant from bulk solution to the catalyst surface and prevention of accessibility of photons and reactants to active catalyst surface (Periyathamby and Ray, 1999).

Different types of microorganisms such as, *Escherichia coli*, *Lactobacillus acidophilus* (Matsugana *et al.*, 1985), *Saccharomyces cerevisia* (Matsugana *et al.*, 1985; Seven *et al.*, 2004; Erkan *et al.*, 2006), *Streptococcus sobrinus* (Saito *et al.*, 1992), *Pseudomonas aeruginosa* (Kühn *et al.*, 2003), *Salmonella choleraesuis* and *Aspergillus niger* (Erkan *et al.*, 2006) have been used as model microorganisms to clarify the mechanism for the photocatalytic inactivation of TiO₂. *E. coli* which is a typical G (-) bacterium has been widely used as model microorganism to study photocatalytic antibacterial activity of TiO₂ because of its rapid growth, short life cycle and being an indicator bacterium of contaminated environments.

It has been reported that the complexity and density of the cell walls affect the photocatalytic inactivation efficiency of TiO₂ significantly. Therefore, before discussing the photocatalytic effects of TiO₂ for disinfection, brief information is given about composition of cell walls of gram positive (G(+)) bacteria, gram negative (G(-)) bacteria and fungi.

Most bacteria have envelope layers over the cell membranes that provide structural support and protection from host defense. Gram stain method is used to categorize bacteria depending on envelope composition. As seen from Figure 2.5 there are significant differences between cell envelope structures of G(+) and G(-) bacteria.

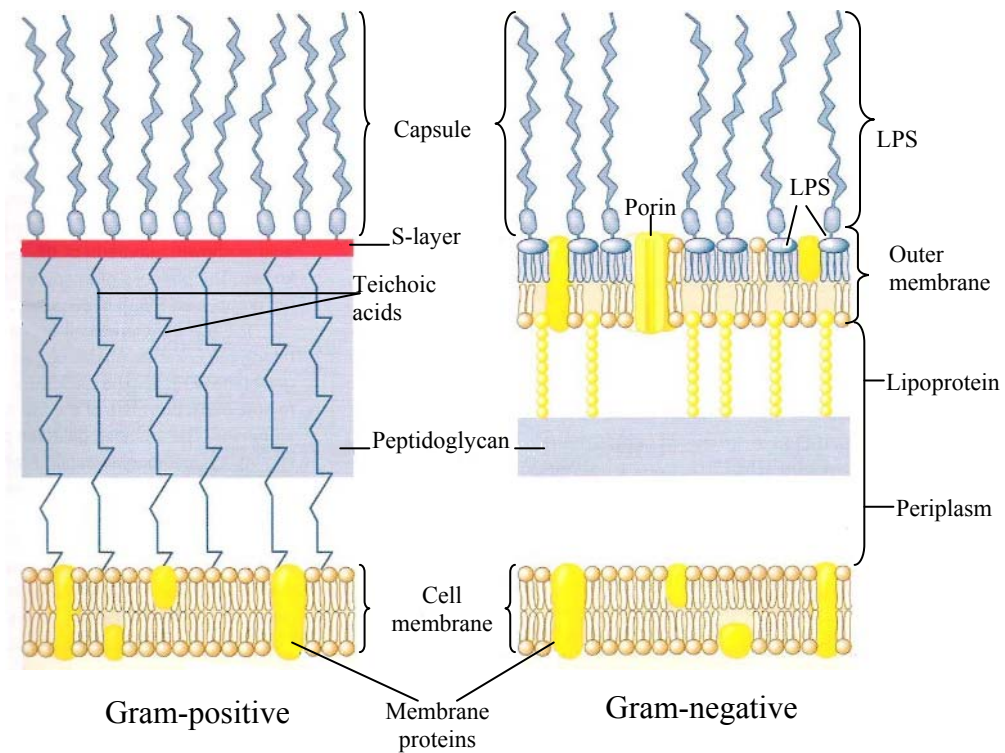


Figure 2.5 Schematic patterns of cell envelope of Gram-positive and Gram-negative bacteria (Slonczewski *et al.*, 2009)

G(+) bacteria have thick cell wall containing multiple layers of 15-80 nm thick peptidoglycan, and teichoic acid. The cell wall may be covered by an S-layer. Surface-layer which is an additional protective layer of G(+) bacteria consisting of protein or glycoprotein (protein with attached sugars). S-layer can be also found in G(-) bacteria. In some G(+) species, carbohydrate filaments form a capsule. The capsule polysaccharides form a slippery mucous layer that inhibits phagocytosis by macrophages.

As observed from Figure 2.5, there is no space between peptidoglycan layers in G(+) bacteria. The peptidoglycan is reinforced by teichoic acids threaded through its multiple layers. Outside the cell wall, G(+) cells are often encased in capsule consisting of weakly bound polysaccharides. On the other hand, G(-) bacteria possess a thin cell wall (single layer peptidoglycan (1-2 nm)) which is sandwiched between the outer membrane containing lipopolysaccharides and lipoproteins and the inner membrane. The outer membrane is responsible of transportation of molecules such as, charged species.

For G(-) cell envelope, the peptidoglycan is covered by an outer membrane. The G(-) outer membrane possesses defensive abilities and toxigenic properties to many pathogens. As seen from Figure 2.5, the inward-facing and outward-facing of the outer membrane have different kind of phospholipids. The inward-facing side of outer membrane consist of phospholipid composition which is similar to that of cell membrane (in G(-) species, it is called the inner membrane or inner cell membrane). The outward-facing side consists of special kind of phospholipid called lipopolysaccharide (LPS). LPSs are a class of lipids, attached to long polysaccharides (sugar chains). G(+) bacteria do not contain LPS. The LPS has crucial medical importance because it acts as endotoxin. LPS molecules consist of lipid A, core polysaccharide, and O antigen. Degradation of LPS layer by reactive oxygen species (ROS) such as; $\cdot\text{OH}$, $\text{O}_2^{\cdot-}$, H_2O_2 was attributed to reason of photocatalytic inactivation performance of TiO_2 by several reports (Sökmen *et al.*, 2001; Sunuda *et al.*, 2003).

There is a separate membrane-bounded compartment of the G(-) bacteria cell which is known as the periplasm. The periplasm is an aqueous layer containing specific enzymes and nutrient transporters that not found within the cytoplasm, such as periplasmic binding protein for sugars, amino acids or other nutrients.

As outer membrane is porous to most ions and organic molecules, periplasmic proteins are usually subjected to fluctuations in pH and salt concentration.

The peptidoglycan layer of G(+) bacteria and the outer membrane of G(-) bacteria contain different chemicals and molecular surface structures such as, fimbriae, fibrils and flagellae. Electron microscopy can be used to scan these surface appendages (Poortinga *et al.*, 2002). Dimensions of fimbriae are 0.2-2.0 μm in length and 2-10 nm in diameter. Fimbriae can be rigid or flexible. Fibrils are shorter than fimbriae, their length is less than 0.2 μm . Flagellae, the biggest structure among these three structures, has a length of 10-20 μm , a diameter of about 20 nm and is responsible for the cell mobility.

In the literature, nearly 200,000 fungal species has been described. Although, fungi provide essential support for all communities of multicellular organisms, approximately 500 species have been reported as pathogenic or potentially pathogenic to animals, including humans, and plants. Usually fungi are considered as a primary contributor to the problem of indoor air and outdoor environment quality. The inactivation of fungi by using TiO_2 is difficult when compared to bacteria due to sporulation and having cell walls with different composition, structure and thickness (Chen *et al.*, 2009). The major difference between fungal and bacteria cell wall is that fungal cell walls contain chitin and bacteria cell walls contain peptidoglycan. Chitin is an acetylated amino-polysaccharide. The tensile strength of chitin is stronger than steel (Slonczewski *et al.*, 2009).

2.6.1 Photocatalytic effects of TiO_2 suspension for disinfection

Studies on the photocatalytic inactivation of microorganisms were started in 1985 by Matsugana *et al.* According to their results, after 120 min., the complete deactivation of *L. acidophilus*, *S. cerevisia* and *E. coli* was achieved

by platinum-loaded TiO₂ under irradiation. Reason of cell death was attributed to oxidation of coenzyme A and the inhibition of cell respiration.

The effects of TiO₂ concentration on inactivation performance of TiO₂ powders was firstly investigated by Saito *et al.* (1992). *Streptococcus sobrinus* AHT was used as model microorganism. The complete inactivation was achieved when TiO₂ concentration was 1 g/ml in the reaction mixture within 1 min under irradiation. However further addition of TiO₂ reduced the inactivation performance. Decline in inactivation performance was attributed to limited light penetration (Saito *et al.*, 1992).

The effects of TiO₂ concentration, light intensity and irradiation time on the photocatalytic inactivation of *E. coli* by Degussa P25 TiO₂ suspension were studied by Wei *et al.* (1994). First order kinetic model was applied to calculate inactivation performance of suspension TiO₂. It was emphasized that existence of oxygen in the reaction medium is important to obtain higher photocatalytic activity. Bacterial inactivation rate constant was reported as proportional to the square root of the concentration of TiO₂ and to the light intensity in the range of 180 to 1660 $\mu\text{E/s m}^2$ (Wei *et al.*, 1994). In addition similar relationships between TiO₂ concentration and light intensity for photocatalytic inactivation of *E. coli* cells were also reported by Huang *et al.* (1998).

Watts *et al.*, (1995) achieved the inactivation of coliform bacteria and the polio virus in wastewater under F40BL fluorescent lights irradiation. The time needed for complete inactivation by using the photocatalyst was compared to time needed for complete inactivation by chlorination. Complete inactivation by using TiO₂ and chlorination took longer than 150 min and less than 60 min, respectively. Considering better performance of chlorination, it was proposed as more feasible method than usage of TiO₂ for inactivation of bacteria and viruses (Watts *et al.*, 1995). However, in the relevant literature, considering

long term antibacterial effect without creating secondary pollution and stability of TiO₂, disinfection with TiO₂ has been mostly proposed as being more effective method than the disinfection with chlorine or ozone (Carp *et al.*, 2004; Chong *et al.*, 2010; Markowska-Szczupak *et al.*, 2011).

To investigate the effects of external conditions such as pH, additives, etc. on photocatalytic inactivation performance of TiO₂, photocatalytic antibacterial test was performed against *E. coli* in distilled water and river water, respectively. When irradiation was stopped, although no bacterial re-growth was observed in distilled water with TiO₂, in river water with TiO₂, bacteria recovered after 24 h. Occurrence of bacterial re-growth in river water showed that, under favorable conditions, bacteria can repair itself when “bacteria entered a viable but non-culturable stage” because of self defense mechanism (Wist *et al.*, 2002). Existence of self defense mechanism was also observed by Rincón and Pulagarin (2003). It was reported that, when irradiation was interrupted at different time periods bacteria could repair itself against superoxide anions O₂^{•-} (precursors •OH) due to having superoxide dismutase (SOD) enzymes.

The effect of light intensity, concentration of TiO₂, continuous irradiation time and temperature on the inactivation performance of TiO₂ powders were also studied by Rincón and Pulagarin (2003). According to their results, the effect of temperature was different on the inactivation of G(+) bacteria such as *enterococci*, and G(-) bacteria such as *E. coli*. Although the photocatalytic inactivation reaction rate of TiO₂ against G(+) bacteria increased with increasing temperature, the photocatalytic inactivation reaction rate of TiO₂ against gram-negative bacteria decreased (Rincón and Pulagarin, 2003). Moreover, the existence of self defense mechanism of *E. coli* against reactive oxygen species (ROS) was reported for the first time in this study.

In 2004 again Rincón and Pulagarin found the effect of additives on the inactivation rate of Degussa P25 TiO₂ under solar illumination against *E. coli*

and observed that inactivation rate improved with addition of H_2O_2 . Furthermore, the effects of addition of inorganic ions such as HCO_3^- , HPO_4^{2-} , Cl^- , NO_3^- and SO_4^{2-} on the sensitivity of bacteria under sunlight with and without TiO_2 were investigated. Although, addition of HCO_3^- , HPO_4^{2-} reduced photocatalytic antibacterial activity significantly, there was little influence of Cl^- , NO_3^- and SO_4^{2-} . The positive and negative effects of inorganic compounds were explained with the enhancement of ROS production and competing with bacteria for the photo generated oxidative species, respectively.

Desai and Kowshik revealed that uniform stirring of reaction mixture containing TiO_2 particles and microorganism enhanced the photocatalytic performance of TiO_2 considerably due to increase in amount of dissolved oxygen and contact between TiO_2 particle and the cells (Desai and Kowshik, 2009).

2.6.2 Photocatalytic effects of TiO_2 thin films for disinfection

In the relevant literature, several authors reported that, the utilization of TiO_2 films could be effective as suspended form (Matsugana *et al.*, 1988; Huang *et al.*, 1998; Sunada *et al.*, 2003; Grieken *et al.*, 2009)

To eliminate separation step during the treatment of contaminated water by powder TiO_2 , immobilization of TiO_2 on acetyl cellulose membranes was firstly achieved by Matsunaga *et al.* (1988). Continuous sterilization system was constructed with TiO_2 -immobilized acetylcellulose membrane reactor, a mercury lamp, and a masterflex pump. After 16 mins under irradiation, which had light intensity of 1100 microeinsteins/ $\text{m}^2\cdot\text{s}$, 99% of *E. coli* cells were inactivated in the contaminated water.

In 1993, to reveal the effect of $\bullet\text{OH}_{\text{ads}}$ on the cell death of *E. coli*, anatase TiO_2 was utilized in the flow through water reactor because of high oxidation potential and non selectivity properties of $\bullet\text{OH}_{\text{ads}}$ (Ireland *et al.*, 1993).

In 1997, to investigate the role of ROS in photocatalytic inactivation reaction, TiO_2 thin films was used against *E. coli* as model microorganism (Kikuchi *et al.*, 1997). H_2O_2 is proposed as the main source of inactivation process. According to Kikuchi *et al.* results, after diffusion of H_2O_2 and $\bullet\text{O}_2^-$ into the cell, $\bullet\text{OH}$ radical was generated by Haber-Weiss reaction



The mechanism for inactivation of *E. coli* cells on TiO_2 thin films was disclosed by Sunada *et al.* (2003), as well. Compare to the spheroplasts, lower photocatalytic reaction rate constant was achieved during inactivation of *E. coli* cells. This was attributed to existence of the cell wall of *E. coli* which was suggested as a barrier for photocatalytic inactivation.

The effect of complexity of cell walls on the antibacterial activity of coated plexiglass with Degussa P25 TiO_2 was determined by Kühn *et al.* (2003). Photocatalytic inactivation tests were performed against *E. coli*, *P. aeruginosa*, *S. aureus*, *E. faecium*, and *C. albicans*. It was reported that, improvement of complexity and density of cell wall decreased the photocatalytic efficiency. A similar study was also performed by Erkan *et al.* (2003) over the Pd doped SnO_2 and TiO_2 thin films. It was reported that the antibacterial efficiencies of the TiO_2 , SnO_2 and their Pd doped thin film samples against different microorganisms and fungal spores were found to decrease in following order *E. coli* > *S. aereus* > *S. cerevisiae* > *A. niger* spores with increase in complexity and strength of the cell walls.

The effect of nitrogen doping on photocatalytic antibacterial activity of TiO₂ thin films was investigated by Văcăroiu *et al.* (2009). Enhancement of photocatalytic antibacterial activity of thin films with nitrogen doping, which was enhanced by thermal treatment at high temperature, was attributed to having more free $\cdot\text{OH}$ surface radicals (Văcăroiu *et al.*, 2009).

2.6.3 Mechanism of cell death

A variety of explanations have been used to clarify the mechanisms of cell death by photocatalytic reactions in the literature. There is consensus on the fact that cell membrane damage starts the inactivation of microorganisms which leads to the destruction of intracellular components, and causes the death of the cell. Therefore, as mentioned above, the efficiency of photocatalytic activity of TiO₂ can be changed according to cell envelope thickness and complexity. Photocatalytic inactivation studies have revealed that the sensitivity of bioparticulates to TiO₂ photocatalysis is likely in the following order:

Virus > G(-) bacteria > G(+) bacteria > endospores > yeast > filamentous fungi (Markowska-Szczupaka *et al.*, 2011). On the other hand, Wolfrum *et al.* (2002) reported that there were no significant differences between the performance of TiO₂ against G(+) and G(-) bacteria.

The first mechanism for inactivation by TiO₂ was proposed by Matsugana *et al.* (1985). The oxidation of the intracellular coenzyme A (CoA), which takes place in a variety of biochemical reactions, was reported as being responsible for the inhibition of cell respiration and death of the cell (Matsugana *et al.*, 1985; Matsunaga *et al.*, 1988).

Cell permeability and cell wall decay were proposed as the reasons of bacterial inactivation by Saito *et al.* (1992). In that study, *Streptococcus sobrinus* AHT was used as model microorganism. Decomposition of cell was observed after 60 min irradiation with TiO₂. Saito *et al.* (1992) demonstrated that, cell viability

decreased as a result of rapid outflow of potassium ions and slow leakage of RNA and proteins from bacteria.

Ireland *et al.* (1993) reported that in the presence of inorganic thiosulfate which was a scavenger of $\bullet\text{OH}$, no antibacterial activity was detected. Consequently, $\bullet\text{OH}$ radical was proposed as the main source of formation of antibacterial activity (Ireland *et al.*, 1993).

Sjogren and Sierka (1994) reported that, the inactivation performance of TiO_2 suspensions against MS-2 phage enhanced 200% under irradiation in the presence of 2 μM ferrous sulfate. The enhancement of inactivation performance was attributed to increase in $\bullet\text{OH}$ radical concentration resulting from Fenton reaction ($\text{Fe}^{2+} + \text{H}_2\text{O}_2 \rightarrow \text{Fe}^{3+} + \text{OH}^- + \bullet\text{OH}$) (Sjogren and Sierka; 1994).

Cho *et al.* (2004) obtained a linear correlation between $\bullet\text{OH}$ radical concentration and *E. coli* inactivation rate of TiO_2 powders. According to their results, in the presence of methanol which acts as scavenger of hole and $\bullet\text{OH}$ radical, the inactivation performance of TiO_2 declined by 85%. As a result, $\bullet\text{OH}$ radical and other ROS such as $\bullet\text{O}_2^-$ and H_2O_2 were defined as the main and minor photo oxidants, respectively.

Photocatalytic disinfection performance of TiO_2 in the powder form was investigated against MS-2 phage and *E. coli* to clarify role of ROS during the photocatalytic reaction. As a result, Cho *et al.* (2005) hypothesized that during the inactivation MS-2 phage only hydroxyl radical in the solution bulk play a major role and other ROS such as; $\text{O}_2^{\bullet-}$, H_2O_2 has negligible effects. But during the inactivation of *E. coli* both free hydroxyl radicals in the bulk solution and surface-bound hydroxyl radicals on the surface of TiO_2 play major role and other ROS have minor role (Cho *et al.*, 2005).

On the other hand, $\cdot O_2^-$ and H_2O_2 was also proposed as a major source of photocatalytic inactivation process (Kikuchi *et al.*, 1997; Maness *et al.*, 1999).

To clarify the effect of hydroxyl radicals ($\cdot OH$) and H_2O_2 on the inactivation mechanism of TiO_2 , photocatalytic reaction of TiO_2 thin films was performed against *E. coli* in the presence of mannitol which is the scavenger of $\cdot OH$ and catalase which decompose H_2O_2 to H_2O and O_2 . In the presence of catalase the photocatalytic reaction was much more limited than in the presence of mannitol. As a result, H_2O_2 was proposed as the main source for photocatalytic inactivation (Kikuchi *et al.*, 1997).

Photokilling mechanism of TiO_2 against *E. coli* was attributed to ROS attack to the cell wall of *E. coli*. The lipid peroxidation reaction of polyunsaturated phospholipids was suggested as the reason for the death of *E. coli* cells. To estimate membrane damage of *E. coli* cells, production of malondialdehyde (MDA), a product of lipid peroxidation, was examined (Maness *et al.*, 1999).

It was demonstrated that formation of peroxidation products such as carboxylic acids is parallel to destruction of cell wall membrane by ROS (Kiwi and Nadtochenko 2004). Similar results were also reported by Sunada *et al.* (1998). They investigated that, TiO_2 thin films not only inactivate the bacteria but also degrade toxic compounds which are synthesized by bacteria.

To clarify the change of cell permeability during the photocatalytic reaction of TiO_2 suspension against *E. coli*, leakage of intracellular β -D--galactosidase enzyme was detected by hydrolysis of o-nitrophenol β -D--galactopyranosideside (ONPG) which is a substrate of the enzyme. For sonicated- TiO_2 slurry the hydrolysis of ONPG was faster than unsonicated TiO_2 slurry. This was attributed to increasing of the surface area and decreasing the size of TiO_2

particles which eliminate mass transfer resistance and make easier to entry of TiO₂ particles in to the cell (Huang *et al.* 2000).

Sunada *et al.* (2003) compared the inactivation performance of TiO₂ thin films against intact *E. coli* cells and the spheroplasts. Two different regions were observed during the inactivation kinetics of intact *E. coli* cells. Initially a lag time period and then a higher inactivation rate were obtained. On the contrary, the inactivation reaction against spheroplasts without cell wall, illustrated only a single-step kinetics with a higher reaction rate, which showed that the cell wall of *E. coli* cell behaves as a barrier to the inactivation process.

The decay of the cell wall and cell membrane of *E. coli* and *Staphylococcus aureus* was detected by TEM in AgBr/TiO₂ suspension by Lan *et al.* (2007). TEM investigation indicated that lipopolysaccharide layer and peptidoglycan layer was decomposed by active species ([•]OH, O₂^{•-}, H₂O₂) generated by AgBr/TiO₂ particles under irradiation. It was reported that, damaging of the cell wall and the membrane caused the intracellular substances of the cell to leak. The permeability of the cell membrane was determined by the measured amount of K⁺ leakage. Because K⁺ involving in bacteria and acting in the regulation of polysome content and protein synthesis. After irradiation, the leakage of K⁺ was observed from *E. coli* and *S. aureus* cells, and its concentration increased with irradiation time. These results implied that photocatalytic reaction caused a change in the cell membrane permeability and the resultant leakage of intracellular substances Lan *et al.* (2007).

Pigeot-Rémy *et al.* (2011) reported that, the RNA of *E. coli* was more sensitive to destructive action of reactive oxygen species than DNA. According to their results contact of TiO₂ with *E. coli* in the dark increased the cell wall sensitivity of *E. coli* to ROS because TiO₂ with particles could penetrate into the cell wall and achieved photocatalytic process inside the cell.

The initial inactivation seems to be a partial disintegration of the outer membrane by the active species which are produced by TiO₂ photocatalysis. This process does not cause completely decomposition of the cell membrane. However, the partial decomposition of the membrane changes the permeability to reactive species (Saito *et al.*, 1992; Sunada *et al.*, 1998; Maness *et al.*, 1999). In this way, reactive species can easily reach to the cytoplasmic membrane causing them attack to the cytoplasmic membrane that leads to the peroxidation of membrane lipid. The change of permeability and decomposition of the cytoplasmic membrane by lipid peroxidation cause cell death. Supported by many reports, a disorder of the cytoplasmic membrane is the main reason of photocatalytic inactivation by TiO₂ photocatalysis (Sunada *et al.*, 1998; Maness *et al.*, 1999; Huang *et al.*, 2000).

2.6.4 Kinetic models of photocatalytic inactivation of microorganisms

Due to complex mechanism of the photocatalytic inactivation process, different kinetic profiles have been reported for the photocatalytic inactivation of *E. coli* in aqueous suspensions by using TiO₂ (Cho *et al.*, 2004; Benabbou *et al.*, 2007; Marugán *et al.*, 2008; Erdural *et al.*, 2008). Graphic display of proposed kinetic models for photocatalytic inactivation reaction of *E. coli* can be seen in Figure 2.6. Kinetic profiles change due to initial bacterial concentration, type of model microorganism, light intensity, temperature, total reaction time and amount of catalyst. Time lag periods and log-linear inactivation region can be observed in these kinetic profiles. Time lag periods at the beginning and at the end of bacterial inactivation performance are usually called as “shoulder” and “tail”, respectively (Benabbou *et al.*, 2007; Marugán *et al.*, 2008).

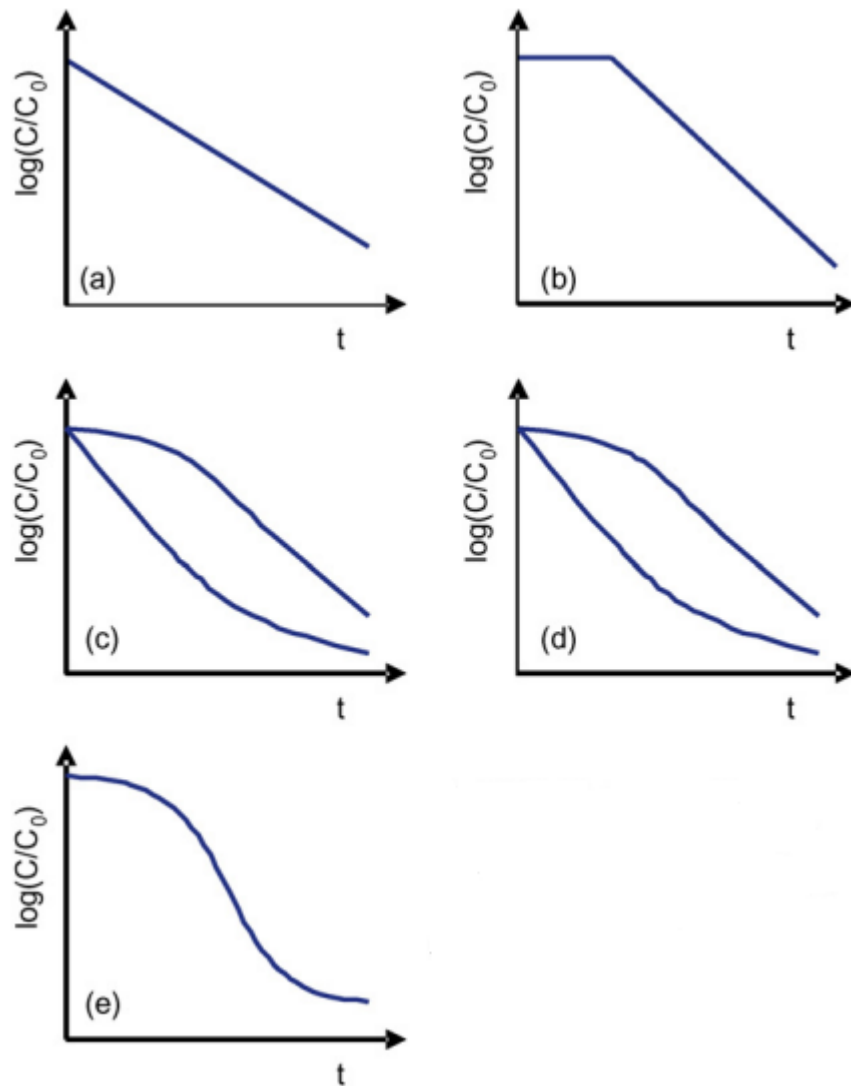


Figure 2.6 Graphical display of proposed kinetic models for photocatalytic inactivation reaction of *E. coli* (a) Chick-Watson equation (b) Delayed Chick-Watson equation (c) Modified Chick-Watson equation (d) Hom equation (e) Modified Hom equation.

Five different empirical equations have been proposed in the literature for bacterial inactivation process;

- Chick-Watson equation
- Delayed Chick-Watson equation
- Modified Chick-Watson equation
- Hom equation
- Modified Hom equation.

The first inactivation model was proposed in 1908; Chick-Watson equation is given by ;

$$\log\left(\frac{C}{C_0}\right) = -kt [c]^n \quad (2.14)$$

Where; C/C_0 is the reduction in the number of viable cells, k is disinfection kinetic constant, t is time, n is reaction order, c is the concentration of disinfection agent. For photocatalytic reactions the concentration of disinfection agent can be assumed constant, then the equation becomes,

$$\log\left(\frac{C}{C_0}\right) = -kt \quad (2.15)$$

This pseudo-first order kinetic model has been widely used to evaluate inactivation rate constants for comparing inactivation performances (Figure 2.6.a). However, this kinetic model can be only applied in the log-linear period. In this case, if there is time lag period at the beginning of the reaction (Figure 2.6.b) (Cho *et al.*, 2004) following equation can be used which is called as Delayed Chick-Watson equation; where t_0 is the time of delay and k' is disinfection kinetic constant.

$$\log\left(\frac{C}{C_0}\right) = \begin{cases} 0 & t \leq t_0 \\ -k'(t-t_0) & t > t_0 \end{cases} \quad (2.16)$$

When time lag period occur after long time treatment (Figure 2.6.c) because of low concentration of remained bacteria than modified Chick–Watson model can be used.

$$\log \frac{C}{C_0} = k_1 [1 - \exp(-k_2 t)] \quad (2.17)$$

Where k_1 and k_2 disinfection kinetic constants of shoulder and log-linear period of inactivation reaction, respectively. When there is a shoulder and tail in addition to log-linear period during the inactivation reaction (Figure 2.6.d), Hom equation can be also applied.

$$\log \frac{C}{C_0} = -k' t^h \quad (2.18)$$

Where h is the degree of deviating from the classical log-linear behaviour. When $h = 1$, this equation turn to the Chick–Watson linear equation; for $h > 1$ and $h < 1$ the equation can be used to evaluate rate constants in existence of a shoulder and a tail, respectively.

However Equation 2.17 and 2.18 can not be used in the existence of shoulder and tail region at the same time (Figure 2.6.e), then modified Hom equation has been proposed (Cho *et al.*, 2003)

$$\log \frac{C}{C_0} = -k_1 [1 - \exp(-k_2 t)]^{k_3} \quad (2.19)$$

Where k_1 k_2 and k_3 is the kinetic constants of shoulder, log-linear and tail periods of inactivation reaction, respectively

The formation of shoulder is attributed to the self-defense mechanism of bacteria in response to oxidative stress, volumetric rate of reactive oxygen species generation and volumetric rate of photon absorption. On the other hand, the formation of tail is attributed to competition for $\cdot\text{OH}$ usage which occurs between remaining alive bacteria and organic species released during the photo-process (Rincon and Pulgarin, 2004; Benabbou *et al.*, 2007; Marugán *et al.*, 2008).

2.7 Relationship Between Bacterial Adhesion and Antibacterial Activity

According to the strategy used for the design of antibacterial surfaces, bacterial adhesion can be desirable or undesirable.

Antibacterial activity has been described as anti-adhesion in different reports related with different areas such as; bio-fouling (Zhao *et al.*, 2005; Bayoudh *et al.*, 2006; Lin *et al.*, 2008), oral microbiology (Ahn *et al.*, 2009; Bendavid *et al.*, 2009; Kinnari *et al.*, 2010), biomaterial infection (Asadinezhad *et al.*, 2010) and food processing equipment (Shi and Zhu, 2009).

Antibacterial activity is also defined as the result of bacteria's inactivation by getting expose to an irreversible damage produced by ROS on semiconductor surface under irradiation. During this process, biocide species are produced and they diffuse over time from a semiconductor surface to bacteria surface to inactivate either non-adhered bacteria or adhered bacteria (Kikuchi *et al.*, 1997; Erkan *et al.*, 2006; Jenny *et al.*, 2009; Hadnadjev *et al.*, 2010; Wu and Long, 2011).

2.7.1 Bacterial Adhesion

Bacterial adhesion to the surface normally occurs because bacteria prefer to grow on the suitable surfaces rather than in a surrounding aqueous phase (An and Friedman, 1997; Katsikogianni; and Missirlis, 2004).

The bacterial adhesion process is comprised of two phases. The first one is initial, non-specific, reversible, physical phase and the second one is slower, time dependent, irreversible, molecular or cellular phase (An and Friedman, 1997; Hermansson, 1999; Pereni *et al.*, 2006).

2.7.1.1 Interactions between bacteria and material surface during the first phase:

The initial phase of adhesion is called as attachment which refers formation of physical contact between bacteria and material surface rather than chemical and cellular interactions (Hermansson, 1999). Thus, the first phase of bacterial adhesion is reversible.

During the movement of planktonic bacteria to a material surface, physical forces such as; Brownian motion, van der Waals forces, gravitational forces and hydrophobic interactions play a major role (An and Friedman, 1998; Katsikogianni and Missirlis, 2004). Physical interaction between the bacteria and material surface can be classified as long-range interactions and short-range interactions (An and Friedman, 1998; Gottenbos *et al.*, 2002).

Long range interactions are responsible for transportation of bacteria to the surface from solution and occur when distances between cells and material surfaces bigger than 150 nm. Electrostatic and attractive Lifshitz- van der Waals (LW) interactions are considered as long-range interactions. (An and Friedman, 1997; Poortinga *et al.*, 2002).

Short range interactions occur 3 nm distances between the surface and the cells. It is responsible for closer contact of bacteria and the surface. Ionic and dipole interactions, hydrogen bonding, Lewis acid-base interactions are accounted as short-range interactions (Busscher *et al.*, 1984; Bos&Busscher, 1999; Wang *et al.*, 2004; Bayouhd *et al.*, 2006).

2.7.1.2 Interactions between bacteria and material surface during the second phase:

The second phase is irreversible phase. At this stage, the bacterial adhesion becomes more stable as a result of reactions between the bacterial and material surfaces. Bacterial surface structures include surface polymeric structures such as; capsules, fimbriae, pili or slime (An and Friedman, 1998; Gottenbos *et al.*, 2002). Once bacteria attach to the surface, the formation of extra cellular polymers occurs. When compared to the formation period of the first phase of bacterial adhesion, second phase takes much longer time. According to relevant literature second phase of bacterial adhesion takes several hours (Hermansson, 1999)

2.8 Factors affecting the bacterial adhesion

Bacterial adhesion is controlled by different factors including, surface charge, hydrophobicity (Gallardo-Moreno *et al.*, 2004; Lin *et al.*, 2004; Li and Logan 2004; Teixeira *et al.*, 2006) and the surface free energy (SFE) (Liu *et al.*, 2004; Zhao *et al.*, 2007; Hamadi *et al.*, 2009) of bacteria, material surface and suspending medium. In addition to these, chemical compositions of material and surface roughness also control the bacteria adhesion (An and Friedman, 1998; Harnett *et al.*, 2007; Ahn *et al.*, 2009; Kinnari *et al.*, 2010).

2.8.1 Surface free energy

The atoms, which are at the external surface, are different compared with those in the bulk material in terms of coordination and energy. This difference arises due to the asymmetrical environment. The asymmetrical environment occurs due to the exposure of a atom in the bulk to cohesive forces with other atoms in all directions, while those at the surface subject to this remain only on one side of the interface. Therefore, different distribution of atoms at the surface forms different surface energy which is to be measured. Surface energy or surface free energy (SFE) or surface tension of solids comes from the force acting on the molecules at the surface or it can be explained as the excess energy at the surface of material compared to the bulk. This energy is a function of surface tension. Contact angle analysis is a method widely used in order to measure the surface properties of solid materials (Giese and van Oss, 2002).

Contact angle is defined as the mechanical equilibrium of liquid droplet at equilibrium with the solid surface and vapor at “three phase boundary”. This definition was firstly proposed by Thomas Young in 1805 (Sharma and Rao, 2002). Young’s equation gives the correlation between liquid-vapor interfacial free energy, liquid-solid interfacial free energy and solid-vapor interfacial free energy with contact angle (Equation 2.20)

$$\gamma_{lv} \cos \theta = \gamma_{sv} - \gamma_{sl} \quad (2.20)$$

Where θ is the contact angle,

γ_{sl} is the solid/liquid interfacial free energy,

γ_{sv} is the solid/vapor interfacial free energy,

γ_{lv} is the liquid/vapor interfacial free energy.

In 1937, the Young's equation was developed including spreading pressure term (π) by Bangham and Razouk as given in Equation 2.21. According to Bangham and Razouk adsorption of vapor to surfaces can not be neglected. This term is the difference between surface free energy of solid ($\gamma^{tot}_{surface}$) and solid/vapor interfacial energy (γ_{sv})

$$\pi = \gamma^{tot}_{surface} - \gamma_{sv} \quad (2.21)$$

Then Equation 2.20 becomes

$$\gamma_{lv} \cos \theta = \gamma^{tot}_{surface} - \gamma_{sl} - \pi \quad (2.22)$$

However, according to relevant literature, when contact angles are bigger than 10° , spreading pressure term can be neglected and Young's equation becomes (Schneider, 1996);

$$\gamma_{lv} \cos \theta = \gamma^{tot}_{surface} - \gamma_{sl} \quad (2.23)$$

Different methods such as; Zisman, Saito, Fowkes, Berthelot, Geometric and Harmonic mean, and Lifshitz-van der Waals-acid/base (LW-AB) approach can be used to calculate surface free energy of the solid surface. In this study Lifshitz-van der Waals-acid/base approach was used to calculate surface free energy of thin films.

2.8.1.1 Lifshitz-van der Waals-acid/base approach

Lifshitz-van der Waals acid-base (LW-AB) approach was expanded by van Oss (Van Oss *et al.*, 1986; Van Oss *et al.*, 1988) to explain interaction between biopolymers (human serum albumin, human immunoglobulin) and low energy solids (polytetrafluoroethylene, polystyrene). Until 1986, the attachment of

biopolymers to low energy solids was attributed only to the existence of apolar interactions. However a new term “Lewis acid-base interaction” was introduced to literature by Lifshitz-van der Waals acid-base (LW-AB) approach (Van Oss *et al.*, 1986). According to LW-AB approach, SFE is divided into two main components; Lewis acid-base (polar) and dispersive (apolar) components.

Lifshitz-van der Waals (γ^{LW}) force is the dispersive or apolar component. Lifshitz-van der Waals component contains London, Keesom and Debye forces (Van Oss *et al.*, 1986). London, Keesom and Debye forces are electrodynamic interactions present at the interface. As a result of randomly oriented dipole-dipole, dipole-induced dipole and fluctuating dipole-induced dipole interactions, Keesom (“orientation”), Debye (“induction”) and London (“dispersion”) forces occurs, respectively.

Hydrogen bonding compounds (Brønsted acids (proton donor) - Brønsted bases (proton acceptor)) and compounds that interact as Lewis acids (electron acceptors) and Lewis bases (electron donors) on the surface of any material are sources of polar component of surface energy (Sharma and Rao, 2002). Surface tension, which occurs due to proton acceptor and electron donor functionality is symbolized as “ γ^- ” and is called as basic (electron-donor) component. Surface tension, which occurs due to proton donor and electron acceptor functionality is symbolized as “ γ^+ ” and is called as acidic (electron acceptor) component.

The polar component includes short-range interactions which come especially from hydrogen bonding. The electron donor (γ^-) component, which is a part of polar component, influences bacterial adhesion significantly (Zhao *et al.*, 2007).

The geometric mean of acidic and basic components gives the acid-base component ($\gamma_{surface}^{AB}$) (Volpe and Siboni, 2000; Giese and Van Oss, 2002; Li and Logan 2004):

$$\gamma_{surface}^{AB} = 2\sqrt{\gamma_s^- \gamma_s^+} \quad (2.24)$$

The number of oxygen-based functional groups such as; carboxyl group (-COOH), hydroxyl anion (OH⁻) and hydroperoxyl radical (HO₂•) over the surface causes increase in polar component (γ^{AB}) (Van Oss *et al.*, 1988; Marciano *et al.*, 2009; Kinnari *et al.*, 2010) on the surface. These groups are important for the formation of chemical bonds between bacteria and surface (Boland *et al.*, 2000; Asadinezhad *et al.*, 2010).

In the van Oss approach, the sum of LW and acid-base components is defined as the total surface energy of pure substance.

$$\gamma_{surface}^{tot} = \gamma_{surface}^{LW} + \gamma_{surface}^{AB} \quad (2.25)$$

The total surface energy ($\gamma_{surface}^{tot}$) can be calculated by using Young's equation. In Young's equation (Equation 2.23) γ_l and $\cos\theta$ are knowns and $\gamma_{surface}^{tot}$ and γ_{sl} are the unknowns. However with one equation two unknowns can not be calculated. For this reason when Equation 2.23 is combined with Duprè equation (given in Equation 2.26) (Busscher, 1984; Van Oss *et al.*, 1988; Giese and Van Oss, 2002).

$$\Delta G_{sl} = \gamma_{sl} - \gamma_s - \gamma_l \quad (2.26)$$

Equation 2.23 becomes

$$(1 + \cos \theta) \gamma_l = -\Delta G_{sl} \quad (2.27)$$

where ΔG_{sl} is free energy of cohesion. This equation is known as Young-Durpé equation. The components of ΔG_{sl} can be defined as following equations;

$$\Delta G_{sl}^{LW} = -2\sqrt{\gamma_s^{LW} \gamma_l^{LW}} \quad (2.28)$$

$$\Delta G_{sl}^{AB} = -2(\sqrt{\gamma_s^+ \gamma_l^-} + \sqrt{\gamma_s^- \gamma_l^+}) \quad (2.29)$$

Considering definition of ΔG_{sl} which is given in Equations 2.28 and 2.29 and combining Equations 2.28 and 2.29 in Equation 2.27, one can obtain complete Young-Durpé equation

$$(1 + \cos \theta) \gamma_l^{tot} = 2\left(\sqrt{\gamma_s^{LW} \gamma_l^{LW}} + \sqrt{\gamma_s^+ \gamma_l^-} + \sqrt{\gamma_s^- \gamma_l^+}\right) \quad (2.30)$$

The subscripts (s) and (l) indicate solid surface and liquid phases, respectively. Therefore, the acid/base and Lifshitz-van der Waals components of the solid surface ($\gamma_s^+, \gamma_s^-, \gamma_s^{LW}$) can be calculated by Young-Durpé Equation by the experimental measurement of the contact angles of three probe liquids with known surface tension parameters ($\gamma_l^+, \gamma_l^-, \gamma_l^{LW}$) of the surface. van-Oss method requires contact angle measurements with at least three probe liquids. Two of them must be polar and one liquid must be non-polar (Schneider, 1996; Marciano *et al.*, 2009) with the known values of $\gamma_l^{LW}, \gamma_l^+, \gamma_l^-$. Hence, considering Equation 2.30 there will be three unknowns (i.e. $\gamma_s^{LW}, \gamma_s^+$ and γ_s^-) with three equations which suitable for calculation of components of SFE.

2.8.1.2 Explanation of bacterial adhesion by theoretical models

In the relevant literature, bacterial adhesion mechanism has been explained by three theoretical approaches. DLVO (Deryagin, Landau, Verwey and Overbeek)

theory (Marshall *et al.*, 1971), thermodynamic approach (Absolom *et al.*, 1983; Fletcher, 1983), extended DLVO theory (van Oss *et al.*, 1986). All these theories based on the adhesion/deposition of colloidal particles.

DLVO theory

DLVO theory was initially developed to describe interactions between non-biological colloids, but Marshall *et al.*, (1971) used this theory, for the first time, to explain bacterial adhesion mechanism. According to DLVO theory, as given in Equation 2.31, interaction between a cell and a surface (ΔG_{tot}) can be described as balance between attractive (ΔG^{LW}) (van der Waals interactions, (LW)) and the repulsive interactions (electrostatic double layer interactions) (ΔG^{DL}). Repulsive interactions occur as a result of Coulomb interactions between charged molecules. Strength and range of repulsive interactions are under the influence of surrounding ions. Although DLVO theory accounts electrostatic interactions, it can not describe short-range Lewis acid-base interactions. According to DLVO theory, first physical phase of bacterial adhesion process consists of only long-range interactions. Interaction energy in DLVO theory is distance dependent (Hermansson, 1999; Katsikogianni and Missirlis, 2004)

$$\Delta G_{tot} = \Delta G^{LW} + \Delta G^{DL} \quad (2.31)$$

where $\Delta G^{LW} = -\frac{Ar}{6d}$ and $\Delta G^{DL} \propto \Psi^2 e^{-\kappa d}$

where A is the Hamaker constant, d is the separation distance between cell and substratum, r is the radius of the cell and Ψ is the surface potential, κ is the Debye length.

Although DLVO theory gives an opinion about whether an organism can overcome electrostatic barrier or not during the adhesion process, it does not reveal predictions on molecular interactions which occur as a result of interaction between polymers at the bacterial surface and molecular groups on the substratum.

Thermodynamic Theory

The thermodynamic theory is the second approach that is used to describe bacterial adhesion to surfaces (Absolom *et al.*, 1983). The thermodynamic theory, describes bacterial adhesion considering attractive and repulsive interactions such as van der Waals, electrostatic or dipole and expresses them in terms of surface free energy (SFE). Contact angle measurements are used to calculate surface free energy terms. In addition to van der Waals forces, acid/base interactions which include hydrophobic/hydrophilic interactions are also expressed in thermodynamic approach. Adhesion process is assumed to be reversible in this approach. In other words, by this approach the first phase of adhesion can be explained. Thermodynamic approach is an equilibrium model and it ignores distance dependence. Owing to thermodynamic approach being an equilibrium model, kinetic interpretation about bacterial adhesion process can not be achieved.

Thermodynamically, mechanism of bacterial adhesion can be explained by work of adhesion (ΔF_{Adh}) or Gibbs energy owing to bacterial adhesion (interfacial energy) (ΔG_{adh}). For this purpose, numerical values of surface free energy of the bacteria and substratum surfaces and surface free energy (or surface tension) of the suspending solution must be calculated (Busscher *et al.*, 1984; Wang *et al.*, 2004; Harnett *et al.*, 2007; Liu *et al.*, 2008; Marciano *et al.*, 2010). For this purpose Dupré equation can be used (Absolom *et al.*, 1983).

$$\Delta F_{Adh} = \gamma_{sb} - \gamma_{sl} - \gamma_{bl} \quad (2.32)$$

where γ_{sb} the solid-bacterium, γ_{sl} the solid-liquid and γ_{bl} is the bacterium-liquid interfacial free energy. The interfacial free energy between substance i and j can be defined as (Van Oss *et al.*, 1986):

$$\gamma_{ij} = \gamma_i + \gamma_j - 2\left(\sqrt{\gamma_i^{LW}\gamma_j^{LW}} + \sqrt{\gamma_i^+\gamma_j^-} + \sqrt{\gamma_i^-\gamma_j^+}\right) \quad (2.33)$$

or

$$\gamma_{ij} = \left(\sqrt{\gamma_i^{LW}} - \sqrt{\gamma_j^{LW}}\right)^2 + 2\left(\sqrt{\gamma_i^+} - \sqrt{\gamma_j^+}\right)\left(\sqrt{\gamma_i^-} - \sqrt{\gamma_j^-}\right) \quad (2.34)$$

Surface free energy of a substance (γ_s and γ_p) must be known to calculate the interfacial free energy between two substances. However, surface free energy of a substance can not be measured directly. As mentioned previously, they can be estimated indirectly from the contact angle data of probe liquids by LW-AB approach (Van Oss *et al.*, 1986; Van Oss *et al.*, 1988).

Finally, combining Equation 2.33 or 2.34 in 2.32, the work of bacterial adhesion can be determined by using the following equation (Busscher *et al.*, 1984; Wang *et al.*, 2004; Chen and Zhu, 2005; Harnett *et al.*, 2007; Liu *et al.*, 2008; Marciano *et al.*, 2010).

$$\Delta F_{Adh} = 2 \left(\begin{array}{l} \sqrt{\gamma_s^{LW}\gamma_l^{LW}} + \sqrt{\gamma_s^+\gamma_l^-} + \sqrt{\gamma_s^-\gamma_l^+} \\ + \sqrt{\gamma_b^{LW}\gamma_l^{LW}} + \sqrt{\gamma_b^+\gamma_l^-} + \sqrt{\gamma_b^-\gamma_l^+} \\ - \sqrt{\gamma_s^{LW}\gamma_b^{LW}} - \sqrt{\gamma_s^+\gamma_b^-} - \sqrt{\gamma_s^-\gamma_b^+} - \gamma_l \end{array} \right) \quad (2.35)$$

If thermodynamic function ΔF_{Adh} decreases or is negative, the bacterial adhesion process will be favored. On the contrary, if ΔF_{Adh} increases or is

positive, the process will not be favored (Chen and Zhu, 2005; Harnett *et al.*, 2007; Liu *et al.*, 2008; Marciano *et al.*, 2010).

Although thermodynamic approach has been criticized due to assuming that the adhesion process is reversible, being an equilibrium model and ignoring the distance dependence (Hermansson, 1999; Katsikogianni and Missirlis, 2004), it has been widely used in literature. In such studies adopting the thermodynamic approach, the effects of various environmental factors such as; cell and substratum surfaces, hydrophobicity (Busscher *et al.*, 1984; Schneider, 1996; Marciano *et al.*, 2009; Soumya *et al.*, 2011), DMSO concentration in suspending medium (Absolom *et al.*, 1983) and pH of suspending medium (Hamadi *et al.*, 2009) on bacterial adhesion process are examined.

Extended DLVO Thoery

Bacterial adhesion can be also explained by extended DLVO theory (XDLVO). Short-range interaction is firstly denoted by Van Oss *et al.* in XDLVO theory (Van Oss *et al.*, 1986). Gibbs energy owing to bacterial adhesion (interfacial energy) (ΔG_{adh}) is explained by the following equation:

$$\Delta G_{adh} = \Delta G^{LW} + \Delta G^{DL} + \Delta G^{AB} \quad (2.36)$$

where ΔG^{LW} , ΔG^{DL} and ΔG^{AB} are Lifshitz-van der Walls, double layer and acid-base interactions respectively.

$$\Delta G^{LW} = -\frac{Ar}{6d} \quad (2.37)$$

$$\Delta G^{AB} = 2\pi r \lambda \Delta G_{d_0}^{AB} \exp\left(\frac{d_0 - d}{\lambda}\right) \quad (2.38)$$

$$\Delta G^{DL} = \pi r \epsilon \epsilon_0 (2\psi_{01}\psi_{02} \ln\left(\frac{1 + e^{-\kappa d}}{1 - e^{-\kappa d}}\right) + (\psi_{01}^2 + \psi_{02}^2) \ln(1 - e^{-2\kappa d})) \quad (2.39)$$

where A is the Hamaker constant, d is the separation distance between cell and substratum, r is the radius of the cell and ψ_{01} and ψ_{02} are the surface potentials of bacteria and substratum surfaces, ε and ε_0 are the relative dielectric permittivity of medium and the permittivity in vacuum, respectively and κ is the Debye length.

Different from DLVO theory, the effect of ionic and dipole interactions, hydrogen bonding, Lewis acid-base interactions on bacterial adhesion can be predicted by using XDLVO theory. XDLVO theory is distance dependent. By XDLVO theory, interaction energies between bacteria and substrates at different distances can be calculated using Equation 2.37-2.39.

In general, the interaction energy calculated by the DLVO or XDLVO theory shows two energy minima, a primary minimum and secondary minimum. When the interaction energy between bacteria and substrate is at its primary minimum, the irreversible/second phase of bacterial adhesion forms. This means that there is very small distance ($d = 0$ nm) between cell and substrate, and direct contact can be achieved. When interaction energy between bacterium and substrate is at its secondary minimum, the reversible/first phase of bacterial adhesion forms where the distance between bacterium and substrate is larger than 5–100 nm (Hermansson, 1999; Wang *et al.*, 2011). In most cases, an energy barrier exists which goes from the secondary minimum to the primary minimum.

Compared with DLVO theory, XDLVO theory could provide better qualitative prediction for bacterial adhesion. For example, although adhesion of positively charged *Stenotrophomonas (Xanthomonas) maltophila* was expected to have attached to glass in high numbers by using the classical DLVO theory, it showed a low adhesion degree (Jucker *et al.*, 1996). The reason of this lower adhesion degree than expected was explained later by Jucker *et al.*, (1997). According to Jucker *et al.* (1997), adhesion became low as a result of having

low affinity of LPS for SiO₂, which was isolated from *S. maltophila*. “The extended DLVO theory also predicted that the LPS–SiO₂ interaction would be repulsive” (Hermansson, 1999).

Degree of bacterial adhesion of *Pseudomonas aeruginosa*, *Escherichia coli* and *Pseudomonas putida*, on glass and modified glass was correlated with the interaction energies by using XDLVO theory (Wang *et al.*, 2011). It was reported that adhesion increased with the reduction in radius of bacteria which contacted with the surface. This was attributed to formation of less repulsion due to surface structures/polymers of bacteria at the secondary minima.

There have also been experimental studies which could not be explained by XDLVO theory. For example, Bayouhd *et al.* (2006) revealed that, XDLVO theory was acceptable only for the first phase of bacterial adhesion. Because, during the adhesion of *Staphylococcus epidermisstrain* strain to ITO-coated glass an inconsistency was observed between theoretical approach and adhesion tests after 2 h of adhesion. Since they proposed that a specific biological approach affected the adhesion in the second phase (Bayouhd *et al.*, 2006). However, XDLVO theory is claimed to explain both irreversible and reversible phases of bacterial adhesion. Deviation of experimental results from XDLVO theory are explained by the existence of specific properties of bacteria cell such as formation of polymeric bridges between cell and substratum surface, significant deviation of the bacterial cells from a round shape to an elongated shape (Wang *et al.*, 2011).

2.8.2 Influence of Surface Hydrophobicity and SFE on Bacterial Adhesion

Surface free energy and hydrophobicity (water contact angle value) of the surface are the most important characteristics that influence bacterial adhesion (Liu *et al.*, 2004; Zhao *et al.*, 2007; Hamadi *et al.*, 2009).

Relationship between SFE and bacterial adhesion is controversial issue. According to thermodynamic rules, more bacteria can hold on to the material with low SFE than the material with high SFE (Busscher *et al.*, 1984; Schneider, 1996; Ahn *et al.*, 2009;; Marciano *et al.*, 2009; Hamadi *et al.*, 2009; Kinnari *et al.*, 2010). However, according to some studies, the bacterial adhesion does not correlate well with the surface energy of the substratum. When the surface free energy of substratum was about 20-30 mJ/m², adhesion of microorganism was minimal. Substrata having surface energies below 20 and above 30 mJ/m² exhibited appreciable amounts of adsorbed biomass. This called as “Barrier’s law“ in the literature (Zhao *et al.*, 2004; Pereni *et al.*, 2006; Zhao *et al.*, 2007).

Faille *et al.*, investigated that although the apolar component of different kinds of substratum surface free energy, γ^{LW} , did not effect the bacterial adhesion of *B. cereus* spores, the polar components (γ^+ and γ^-) of substratum surface free energies affected the bacterial adhesion directly (Faille *et al.*, 2002).

Besides, hydrophobicity (water contact angle value) of both surface and bacterium are significant parameters for the formation of first phase of adhesion (Mafu *et al.*, 1991; van der Mei and Busscher, 1998; Faille *et al.*, 2002; Li and Logan, 2004; Liu *et al.*, 2008; Mafu *et al.*, 2011). In other words, bacterial adhesion can be controlled by changing wettability of surfaces.

Adhesion to either hydrophilic or hydrophobic surfaces can be affected by hydrophobicity of bacteria. Hydrophobicity of bacteria can be obtained by

different methods such as; contact angle measurements (Li and Logan, 2004; Mafu *et al.*, 2011), salt aggregation test (Mafu *et al.*, 1991), hydrophobic interaction chromatography (Mozes *et al.*, 1987). Contact angle measurement method is incomparably more precise than the other methods. Growth medium, strain type and age of bacteria influence the hydrophobicity of bacterial species. For example, the length of lipopolysaccharide (LPS) molecule was found to affect the bacterial adhesion significantly (Ong *et al.*, 1999; Li and Logan, 2004). Strong correlation was reported between the chain length of LPS of different *E. coli* strains and contact angle value of cell surfaces. The strains having shorter LPS chain length have more hydrophobic surfaces (Ong *et al.*, 1999; Burks *et al.*, 2003).

Cell surface hydrophobicity has been also evaluated in terms of free energy of aggregation (ΔG_{bb}) as given in the following equation (Mei *et al.*, 1998; Mafu *et al.*, 2011).

$$\Delta G_{bb} = -4(\sqrt{\gamma_b^{LW}} - \sqrt{\gamma_l^{LW}})^2 - 4(\sqrt{\gamma_b^+ \gamma_b^-} + \sqrt{\gamma_l^+ \gamma_l^-} - \sqrt{\gamma_b^+ \gamma_l^-} - \sqrt{\gamma_b^- \gamma_l^+}) \quad (2.40)$$

If the value of ΔG_{bb} is positive than cell surface is hydrophilic, on the other hand if the value of ΔG_{bb} is negative than bacterial surface is hydrophobic and bacteria tend to aggregate in aqueous suspension (Mei *et al.*, 1998).

Several mathematical models have been proposed in the relevant literature to explain effect of cell surface hydrophobicity and/or substratum surfaces on bacterial adhesion mechanism.

Liu *et al.*, (2004) proposed a mathematical model to explain correlation between bacterial adhesion and surface hydrophobicity of bacteria and /or substratum as given in Equation 2.41.

$$N = N_{eq} \frac{(H_{o/w})^{a/b}}{\left[\exp((\Delta G_{adh}^0 - \Delta G_{adh})/RT) \right]^{1/b} + (H_{o/w})^{a/b}} \quad (2.41)$$

where N ; number of attached bacteria at time t

N_{eq} ; number of attached bacteria at equilibrium state

$H_{o/w}$; relative hydrophobicity between microorganism and support

surface and was defined as; $H_{o/w} = \frac{H_m + H_s}{(1 - H_m) + (1 - H_s)}$

where H_m and H_s are the relative hydrophobicity of microbial cell (%) and substratum surface (%), respectively.

According to Liu *et al.* (2004), hydrophobicity of bacterial surface is the significant parameter for bacterial adhesion degree. Bacteria with hydrophobic surface are much more willing to adhere on both hydrophilic and hydrophobic material surface than hydrophilic bacteria (Satou *et al.*, 1988; Mei *et al.*, 1998; Liu *et al.*, 2004).

On the other hand, Li and Logan also conducted series of experiments in order to understand the effect of surface hydrophobicity of metal-oxide surface on bacterial adhesion, for this purpose they measured the adhesion of 8 strains of bacteria, to 11 different metal-oxide surfaces. Based on their results, rather than hydrophobicity of bacteria surface, substratum hydrophobicity played an important role in determining bacterial adhesion (Li and Logan, 2004).

Wiencek and Fletcher (1995) reported that hydrophilic surfaces do not favor bacterial adhesion by preferential bonding with water molecules to the surface which acts as a barrier for irreversible adhesion of cells. In addition, Teixeira *et al.*, (2006) indicated the higher adhesion of *Staphylococcus epidermidis* to hydrophobic polymers rather than the hydrophilic elastomer materials. On the

other hand, some of studies reported the preferential adhesion of hydrophobic bacteria to hydrophobic substratum while the affinity of hydrophilic bacteria to hydrophilic surfaces (Hogt et al., 1983; Satou et al., 1988; Vacheethasanee *et al.*, 1998).

Absolom *et al.*, (1983) reported the importance of surface tension of suspending medium for bacterial adhesion. According to their results, different kinds of bacteria *Staphylococcus aureus* (strain 049), *Staphylococcus epidermidis* (strain 047), *E. coli* (strains 055 and 2627), and *Listeria monocytogenes*, showed higher adhesion to hydrophilic substrata when the bacterial surface energy was greater than that of the suspending liquid. However, when the bacterial surface energy was smaller than that of the suspending medium, bacteria preferred to adhere onto hydrophobic surfaces.

2.8.3 Influence of Surface Roughness on Bacterial Adhesion

The effect of surface roughness on the bacterial adhesion can not be clarified alone. In many cases, the change in surface roughness causes a change in contact angle and SFE of substratum (Gallardo-Moreno *et al.*, 2004; Ahn *et al.*, 2009). In some studies, increasing bacterial adhesion with increasing surface roughness was attributed to the increase in surface area (Shellenberger and Logan, 2002). However, in some reports no significant correlation was obtained between bacterial adhesion and surface roughness (Li and Logan, 2004; Teixeira *et al.*, 2006).

Genzer and Efimenk (2006) reported that, the roughness of surfaces can cause contact angle hysteresis. The contact angle hysteresis is the measure of surface non-ideality (Gao *et al.*, 2006). It can be defined as the difference between the advancing and receding of contact angles. Depending on the surface roughness, measured contact angle can be different than the true contact angle. On the other hand, when roughness value of surface is smaller than 0.1 μm , contact

angle measurement can be performed accurately (Busscher *et al.*, 1984; Kinnari *et al.*, 2009).

The variation between the measured contact angle and true contact angle can be classified as Wenzel and Cassie-Baxter regimes according to the degree of roughness (Figure 2.7). In Wenzel regimes, “roughness promotes either wettability or non-wettability, depending on the chemical nature of the substratum” (Genzer&Efimenk 2006). When the surface possesses small protrusions, Cassie-Baxter regime forms because when protrusions are very small, they can be filled with air instead of liquid as shown in Figure 2.7.c.

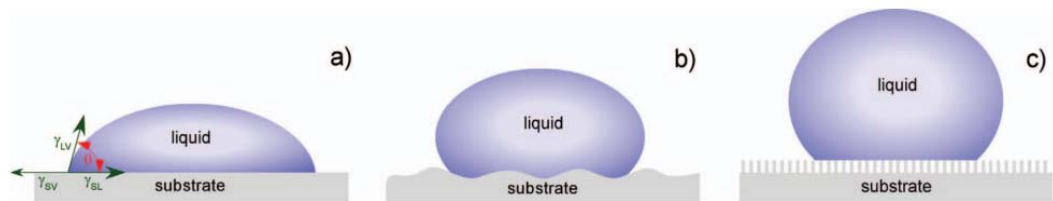


Figure 2.7. The spread of the liquid droplet on the surface according to roughness degree (a) on a flat substratum, (b) rough substrata Wenzel regime, (c) rough substrata Cassie-Baxter regime (Genzer and Efimenko, 2006)

Wettability of a substratum is relevance with adhesion between the liquid and the substratum. In cassie regime adhesion is small and the drop can easily be separated from the substratum. Yet in Wenzel regime droplets adhere to the substratum more strongly. Contact angle hysteresis is high for the Wenzel regime and low for the Cassie regime (Genzer and Efimenk, 2006).

The effect of contact angle hysteresis (CAH) on biofouling was reported by Schmidt *et al.* (2004). According to their results, biofouling released from the perfluoroalkyl and acrylate coatings easily when the contact angle hysteresis of coating surfaces was lower (Schmidt *et al.*, 2004).

Effect of surface roughness and surface free energy characteristics of the orthodontic materials and bacterial adhesion were analyzed by Ahn *et al.* (2009). According to their results, when surface roughness is less than 0.2 μm , surface roughness has no significant effect on the bacterial adhesion. In this case, bacterial adhesion is rather affected by surface free energy.

Asadinezhad *et al.* (2010) reported that the adhesion of *E. coli* and *S. aureus* were favored by both hydrophilicity and roughness of polyvinyl chloride (PVC) samples (Asadinezhad *et al.*, 2010). But they could not explain the effect of roughness alone.

The separation of adhered *Candida parapsilosis* from hydrophilic glass and hydrophobic silicone rubber were tested by Gallardo-Moreno *et al.* (2004) to explain the relationships between the adhesion mechanism, hydrophobicity and morphology of cells and roughness. It was reported that, adhesion of microorganisms was stronger over the hydrophobic rough silicone surface than the hydrophilic and smooth glass surfaces. Similarly, Kinnari *et al.* (2009), reported the favored adhesion of *Staphylococcus aureus* and *Staphylococcus epidermidis* on the ultra-high molecular weight polyethylene surfaces by the increase of roughness and polar component of surface free energy.

2.9 Synthesis of TiO₂ Thin Films

TiO₂ can be synthesized by using various techniques by both vacuum deposition (such as; chemical vapor deposition (CVD), plasma assisted chemical vapor deposition (PECVD) and wet methods (such as; sol-gel

process). However, vacuum deposition techniques are not feasible to provide thin films on large surfaces due to requiring expensive equipments and conditions such as high vacuum, high deposition temperature and magnetic waves (Ding *et al.*, 2001).

Sol-gel method is one of the wet techniques that can be used to synthesize both powder and thin films TiO₂. Sol-gel film formation requires less equipment without vacuum and high temperature environment. It is cheaper than other processes. In sol-gel process, new crystalline phase can be obtained from noncrystalline solids and final film is obtained with high homogeneity. Furthermore, microstructure of coated film (i.e, pore volume, pore size and surface area) can be controlled during this process (Brinker and Scherer, 1990). On the other hand, there are some limitations for sol-gel process. In this process, the precursors are expensive and sensitive to moisture. Moreover, long processing time can be required. There is large shrinkage during the processing. Heat treatments at high temperatures (≥ 400 °C) are required for removal of organic parts of precursors and crystallization (Kwon *et al.*, 2003; Carp *et al.*, 2004).

2.9.1 Sol-gel Process

Sol-gel method has been used for the preparation of thin film coatings on glass (Sato *et al.*, 2002; Rizzo *et al.*, 2003; Kwon *et al.*, 2003), ceramics (Djambazov *et al.*, 1998), membrane (Carp *et al.*, 2004) and fabrics (Xu *et al.*, 2006).

Sol-gel procedure can be defined as the formation of a metal oxo polymer network from molecular precursors such as metal alkoxides or metal salts (Wang and Ying, 1999).

Hydrolysis, alcohol condensation and water condensation are three reactions that generally used to describe the sol-gel process at the functional group level.

pH, nature, concentration and nature of catalyst, water:alkoxide ratio and temperature are factors that affect the rate of hydrolysis and condensation reactions. By controlling precursor chemistry and processing conditions, products can be obtained with excellent chemical homogeneity and metastable structures at low reaction temperatures (Livage *et al.*, 1988; Brinker and Scherer, 1990)

For sol-gel synthesis of metal alkoxides, both hydrolysis and condensation reactions occur rapidly. To control the size of the products and to form small colloidal clusters with more uniform particles size, separation and reduction of rates of hydrolysis and condensation step are vital. For this purpose, bulky, branched alkoxy groups (i.e., isopropoxides) or acid catalysed are utilized (Brinker and Scherer, 1990; Yin *et al.*, 2001; Wright and Sommerdijk, 2003).

Sol-gel route starts with hydrolysis of precursor. Alkoxides of transition metals such as ethyl, propyl and butyl are utilized in the sol-gel process because they react easily with water (Brinker and Scherer, 1990) at room temperature. In this step, according to rate of reaction, alkoxide groups (OR) of precursor partially or exactly replaced with hydroxyl groups as given in Equation 2.42. The hydrolysis step is catalyzed by both acids and bases. The control of hydrolysis reaction rate is vital to obtain homogeneous titanium oxide networks (Wright and Sommerdijk, 2003; Su *et al.*, 2004).

Hydrolysis



Where M is a metal species (Ti, Si, Al, Zr, etc) and R is an alkyl group (methyl, butyl, ethyl, etc) (Su *et al.*, 2004; Xu *et al.*, 2006).

Hydrolysis reaction occurs with condensation reaction (Equation 2.43-2.44) in the same media and at the same time and partially hydrolyzed molecules may

combine in condensation reaction, as well. However, in this case reaction rate gradually slows down because hydrolysis of polymeric alkoxy groups formed by condensation reactions is limited by mass transfer.

Alcohol elimination (Equation 2.43) or water elimination (oxolation) (Equation 2.44) may take place during the condensation step. As a result of combination of the constitute particles of the gel into a compact mass, condensation reactions build up the metal oxide crystals (Su *et al.*, 2004).

Condensation (alcohol elimination)



Condensation (water elimination)



Addition to hydrolysis and condensation reactions, side reactions are also take place during sol-gel processing. The most important kind of side reactions is olation reactions (Equation 2.45-2.46). As a result of reaction between two hydroxyl-metal groups olation reactions occur.



The overall reaction can be given as Equation 2.47 for sol-gel synthesis



During the sol-gel synthesis, well polymerization can be provided when hydrolysis reaction, which is limited by mass transfer, is accelerated by using catalysts. Catalyst nature affects hydrolysis rate. When acid catalyst (HCl, H₂SO₄, etc) is utilized instead of basic catalyst (NH₄, etc.) the hydrolysis rate increases. In addition, concentration of acid catalyst used in sol-gel synthesis also affects the rates of condensation, olation and oxolation reactions. The rates of these reactions directly affect crystal structure and photocatalytic activity of sol-gel product. On the contrary, based catalyst induces the condensation reactions and amorphous powders can be synthesized with unhydrolyzed alkoxide ligands (Wright and Sommerdijk, 2003; Carp *et al.*, 2004).

The rates of reactions are also affected by amount of water in the reaction mixture (Wang and Ying, 1999). If there is low amount of water at the beginning, reaction system will be controlled by alkoxides and condensation and oxolation reactions will firstly occur. As a result, closely packed three dimensional crystallite structures of Ti-O-Ti derivatives will be formed. If there is stoichiometric amount of water, while rate of oxolation reactions will be very small, the reaction system will be governed by hydrolysis reaction and derivatives of Ti(OH)₄ will be formed (Brinker and Scherer, 1990; Brinker *et al.*, 1992; Hague and Mayo; 1994; Wang and Ying, 1999; Kwon *et al.*, 2003). However, by adding more water, the formation of Ti-O-Ti derivatives, which are the desired product, can be obstructed due to increase in rate of oxolation reaction. As a result, in stead of Ti-O-Ti derivatives, Ti-OH derivatives form. In this case, gel phase is obtained with low density without three dimensional and closely packed (Su *et al.*, 2004). In addition when there is too much water, formation of Ti(OH)₄O⁺H₂ derivatives and Ti-O-Ti chains with high density is also achieved through solvation and olation reactions, respectively. Consequently, the structure and photocatalytic activity of TiO₂ are directly affected by water amount.

After hydrolysis and condensation of titanium alkoxide, amorphous titanium dioxide is obtained. Therefore to convert amorphous titanium dioxide to crystallize either anatase or rutile TiO₂ and to remove the organic part from the final molecule, calcination process is applied at high temperatures (450–600 °C) (Wang and Ying, 1999). During the calcination, air pump should be used to oxidize the material.

As a result of the calcination at high temperatures, particle agglomeration and grain growth form, surface area can decrease and glassy surfaces without porosity can be form. To provide micro- and mesoporosity to thin films is very important for photocatalytic activity of thin films which produced by sol-gel process. For this purpose, water-soluble polymeric materials such as polyethylene glycol (PEG) and carboxymethyl cellulose (CMC), which are burned and vanished during the calcination step, have been used in the relevant literature (Kajihara *et al.*, 1998, Černigoj *et al.*, 2006; Ubonchonlakate *et al.*, 2012).

2.9.2 Dip-Coating

In sol-gel process before the gelation, the fluid sol or solution can be used for preparation of thin films by dipping, spinning or spraying processes. In this study dip coating method was used to obtain TiO₂-SiO₂ thin films. There are some advantages of preparation of TiO₂ thin films by dip coating method such as; transfer efficiency is very high, all contact areas are coated, multi-layer coating can be obtained on the substrate and equipment requirements are simple.

Immersion, start up, deposition, drainage and evaporation are the stages of dip-coating process (Brinker and Scherer, 1990).

- Immersion: The moving substrate is dipped into the coating solution at constant speed.

- Start-up: The substrate is remained in the solution motionless for a while according to type of substrate.
- Deposition: Thin layer deposits on the substrate while it is pulled up. This process must be at constant speed and without any judders.
- Drainage: Excess liquid will drain from the surface.
- Evaporation: The solvent evaporates from the liquid, forming the thin layer (Rahaman, 2007).

In this process moving substrate is dipped into and withdrawn from coating liquid at the constant velocity to obtain uniform coating. In addition to velocity of dipping and withdrawal step, viscosity, surface tension of coating solution and evaporation rate is also affected the film formation.

CHAPTER 3

MATERIALS AND METHODS

3.1 Materials

Deionized water was used in all experiments. Titanium tetra-isopropoxide (TTIP, extra pure grade, Sigma-Aldrich CAS No: 546-68-9) and colloidal silica solution Ludox SM-30 (30 wt% suspension in water, Sigma-Aldrich CAS No: 7631-86-9) were used as titania and silica precursors, respectively. 65 % HNO₃ (CAS No: 7697-37-2), polyethylene glycol (PEG-4000, CAS No: 25322-68-3), methylene blue (MB, 82%, CAS No: 61-73-4) and KOH (CAS No: 71769-53-4) were purchased from Merck. Acetic acid (CH₃COOH, 99-100%, CAS No: 9522-05) was purchased from JT Baker. Na₂HPO₄ (Merck, CAS No: 7632-05-5) and NaH₂PO₄ (Merck, CAS No: 89140-32-9) were used to prepare buffer solution. Luria Bertanmi (LB) agar and LB broth (CAS No: 9002-18-0) were purchased from Merck.

3.2 Synthesis of TiO₂, and SiO₂-TiO₂ colloidal mixture

Titanium tetra-isopropoxide hydrolysis was performed by adding 5 ml of TTIP and 1 ml of acetic acid (CH₃COOH) to 200 ml of deionized water which is catalyzed by 700 µl of nitric acid (HNO₃). The mixture stirred and heated to 80 °C for 30 min. The resulting TiO₂ colloidal solution was kept under stirring for 2 h before adding Ludox SM-30. The samples having different SiO₂/TiO₂ ratios (0, 50, 40, 26, 15, 8, 5 and 100 wt % TiO₂) were obtained by mixing proper amount of Ludox SM-30 solution with TiO₂ colloidal solution for 24h at room temperature (20°C). Finally, 21.3 ml of PEG-4000 solution (50g PEG 4000/ 100 ml distilled water) was added to the TiO₂-SiO₂ mixture to improve the consistency of solution.

Thin films of SiO₂-TiO₂ samples were obtained by coating the glass substrates with TiO₂-SiO₂ colloidal solution by using dip coating method. Pyrex glass plates were pretreated and cleaned before coating. In the pretreatment step, the glass plates was treated with 1 M KOH solution for 24 h and rinsed with water followed by ultrasonication in distilled water for 10 min and drying at 120 °C for 2 h. The plates were coated by colloidal solution by dipping and withdrawing at a constant speed of 0.75 mm/s from the solution and dried at 120°C for 20 min. In order to achieve desired film thickness, the coating-drying steps were repeated five times for each sample. Finally, the samples were calcined at 500°C in air flow (Protherm 1000W, PTF 12/50/250). The experimental procedure is also depicted in Figure 3.1.

3.3 Characterization of thin films

The prepared thin film samples were characterized by XRD, SEM and AFM. The relative surface areas and the surface free energies of the samples were measured by methylene blue adsorption technique and contact angle measurements, respectively.

3.3.1 X-Ray Diffraction (XRD)

The crystal structure of the thin films was characterized by the grazing incidence XRD technique by using X-ray diffractometer (Rigaku Ultima-IV) with Cu target and Ni filter ($\lambda_{\text{Cu}} K_{\alpha} = 1.54 \text{ \AA}$) between 20 and 60 Bragg angles at the scan rate of 1.000 deg/min.

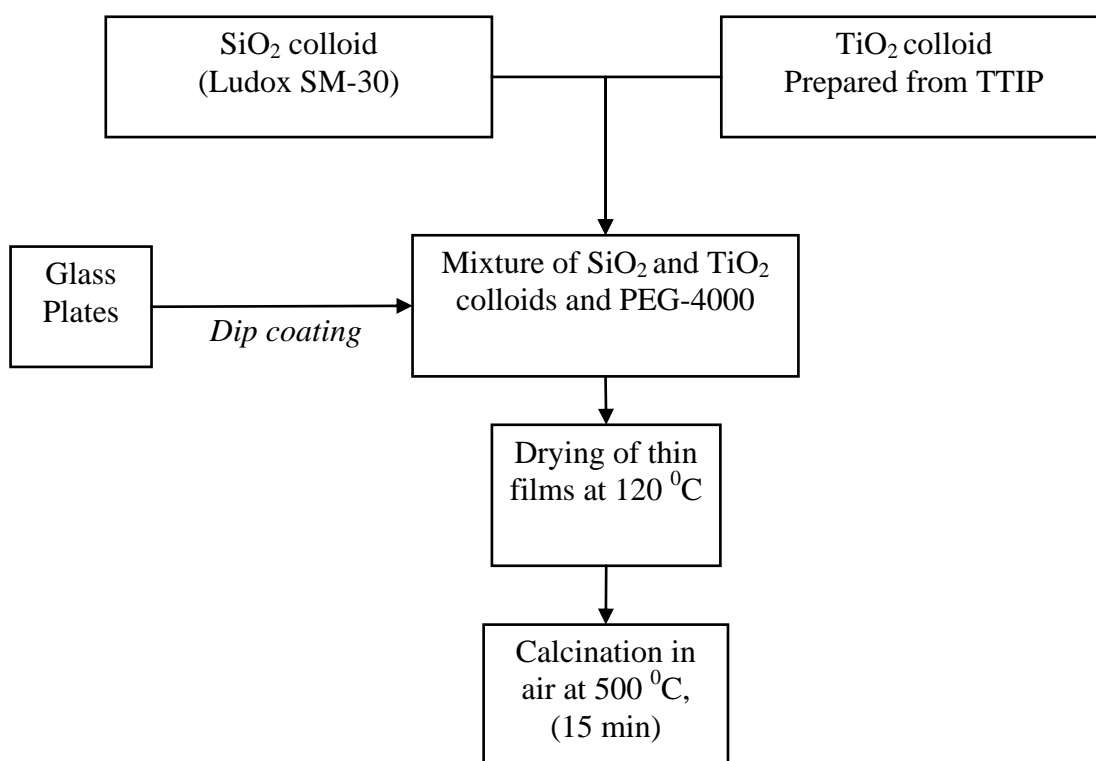


Figure 3.1 TiO₂- SiO₂ colloid and thin film preparations

3.3.2 SEM Imaging

The morphology and thickness of thin films were analyzed by using Scanning Electron Microscope (Quanta 400F Field Emission) imaging. The accelerating voltage was 30 kV. Before SEM examination the thin films were coated with Au-Pd to obtain conductivity. The thickness of the TiO₂-SiO₂ thin films was measured by the SEM analysis of cross-sections of the samples.

3.3.3 Imaging with Atomic Force Microscopy (AFM)

The surface imaging was performed by using AFM (Nanosurf easyScan 2). The images obtained by non-contact dynamic force mode (190 Hz) by using silicon

SPM tips and the data were analyzed to obtain surface roughness of the thin films. Data taken from 3-D images were analyzed to calculate the surface roughness based on RMS.

Root-Mean-Square (RMS) surface roughness, (S_q)

$$S_q = \sqrt{\frac{1}{MN} \sum_{k=0}^{M-1} \sum_{l=0}^{N-1} (z(x_k, y_l))^2} \quad (3.1)$$

M : is a number of points of per profile (scan line)

N : is the number of profiles

z : amplitude at (x,y) point

3.3.4 Surface area measurement of thin films

Brunauer-Emmett-Teller (BET) method is based on the volumetric or gravimetric analysis of the adsorbed amount of N_2 over the surface and it has been extensively used to determine the surface area of powder samples. However, this technique is not suitable for thin films having very small mass (several micrograms per sample) of semiconductor. In this study, the methylene blue (MB) adsorption technique (Adamson, 1997) was adopted to determine the relative surface area of the samples by applying Langmuir isotherm. The adsorption tests were performed by saturation of thin films by MB in solution. The experiments were performed by immersing the thin film coated samples in 25 ml of 2 ppm MB solution for 72 h at room temperature. In order to prevent MB photo-degradation, the adsorption experiments were performed in dark. To determine the amount of MB adsorbed over the metal oxide surfaces, the MB concentration in solution was performed by UV-Visible (Nicolet Evolution 100) spectrophotometer at 663 nm with respect to time. The adsorption equilibrium was usually achieved within 12 h. Adsorbed

amount of MB over the surface was determined from the difference between initial and final (equilibrium) concentrations of MB in solution.

3.3.5 Contact angle measurements

Contact angle measurements of thin film surfaces were performed by sessile drop technique at room temperature using contact angle analyzer (KSV-CAM 100). Contact angle data was collected for di-iodomethane (apolar), glycerol (polar) and water (polar) by applying 5 µl droplets. The measurements were repeated at least at ten different positions over the same sample surface and the average values were obtained. One particular contact angle image is shown in Figure 3.2.

3.4 Microorganism and Growth Conditions

In this study, *Escherichia coli* XL1-blue (Invitrogen Life Technologies, USA) was used as a probe microorganism and the main culture was stored at -80 °C in a freezer. To prepare a working culture, *E. coli* was grown on Luria Bertani (LB) agar in petri dishes at 35 °C overnight then stored at 4 °C until use. A liquid *E. coli* suspension was prepared by transferring a single colony from the LB agar plate to sterile LB broth containing 1% Bacto tryptone, 0.5% Bacto yeast extract, and 1% NaCl in distilled water and incubating on a rotary shaker at 35 °C.

3.5 Preparations of *E. coli* cells

A single colony of *E. coli* from LB agar slants was taken and inoculated into 25 ml LB broth medium in 100 ml Erlenmeyer flasks containing 25 ml of medium and cultivated at 35 °C on rotary shaker (170 rpm) overnight. After cultivation, 1.5 ml of culture sample containing *E. coli* cells were centrifuged at 5000xg for 10 min and harvested cells were washed with sterilized 0.2 M phosphate buffer solution at pH 7.2 (PBS) for 2 times. The cells were then re-suspended in PBS to adjust the number of cells suitable (in a range of 10⁶-10⁸ cells/ml) for the purpose. The

number of cells in *E. coli* suspensions was determined using viable cell count method in which 100 μl serially diluted *E. coli* suspensions in PBS were pipetted onto LB agar plates and the number of colonies were counted after overnight incubation at 35 °C.

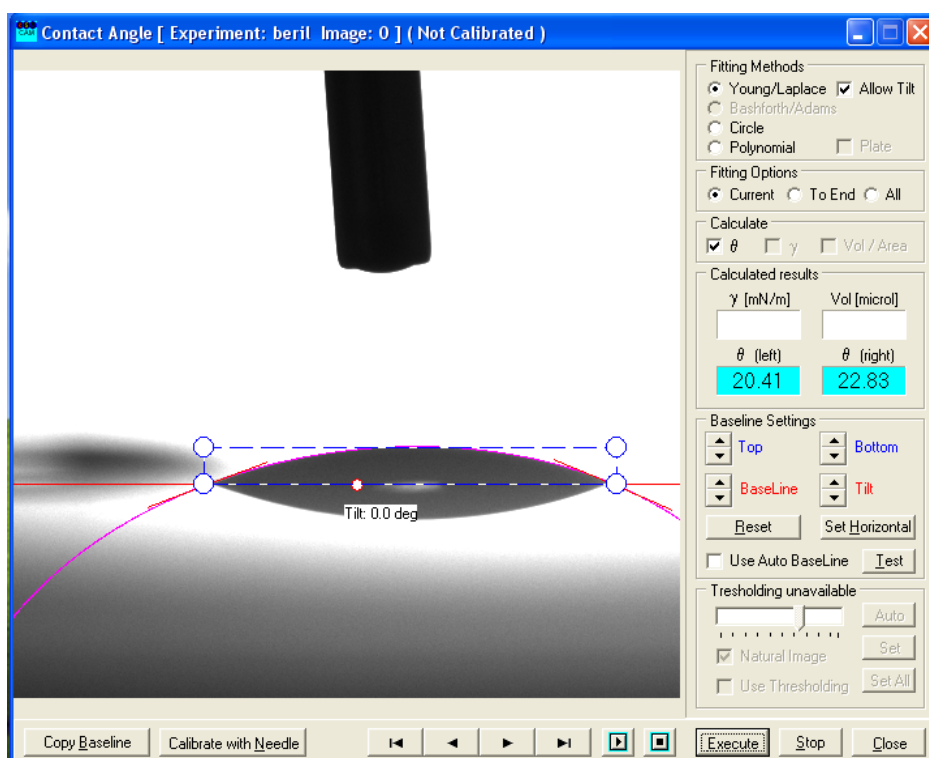


Figure 3.2 Example image of contact angle measurement performed by contact angle analyzer.

3.5.1 Surface-adhered *E. coli* cell preparation

The cell count of the *E. coli* cell suspension (section 3.5) was adjusted to 10^6 - 10^7 cells/ml in PBS. Coated and uncoated glass plates with equal substrate area (7.5

cm²) were immersed in 20 ml of *E. coli* cell suspension and incubated at 37 °C on rotary shaker (170 rpm) for 24 h in the dark. After that, plates were removed and washed with PBS to remove non-adherent bacteria. To determine the number of adhered bacteria, samples were immersed in 50 ml glass beakers, containing 10 ml of sterile PBS and the adhered *E. coli* cells were removed from the surface in an ultrasonic bath applied for 25 min. There was no effect of ultrasonic bath on the bacteria death. The number of cells were determined as explained in section 3.5.

3.5.2 Preparation of *E. coli* cells for contact angle measurements

The bacterial count of the cells (section 3.5) was adjusted to 10⁶-10⁷ cells/ml in sterilized de-ionized pure water. Bacterial lawns were obtained by filtering of 20 ml bacterial suspension under vacuum on cellulose membrane filters (0.45 µm, Millipore) and dried for 1 h at room temperature. Contact angle measurements were performed within 30 min as given in section 3.3.5.

3.5.3 Preparation of *E. coli* cells for Scanning Electron Microscopy

SEM analysis was performed to observe the effect of irradiation on *E. coli* cells in the presence and absence of the photocatalyst in Prof. Dr. Zekiye Suludere's laboratory at Biology Department of Gazi University.. For this purpose, after irradiation for 1 h, 0.2 M sterilized PBS was added to 100 µl of *E. coli* suspension over the thin film surfaces (13 mm*13 mm) and kept at 4 °C overnight. After 24 h, 4% glutaraldehyde solution was used for fixation. Dehydration was performed with the use of a graded series of ethanol and the sample was subjected to critical point drying with CO₂ (Polaron, CPD 7501). Gold coating was performed by Polaron SC502 sputter coater for the SEM examination. The scanning electron microscope micrographs were taken at 10-15 kV with the Jeol JSM 6060.

3.6 Determination of photocatalytic antibacterial activity of TiO₂-SiO₂ thin films

Photocatalytic bacterial inactivation experiments were carried out using *E. coli* cells which are either surface-adhered or in cell suspensions contacting with surfaces. *E. coli* cells were counted before and after irradiation and antibacterial activity was calculated using the following equation:

$$\% \text{ Antibacterial Activity} = \frac{\text{Initial Number of Microorganisms} - \text{Number of Microorganisms}}{\text{Initial Number of Microorganisms}} \times 100 \quad (3.2)$$

The photocatalytic antibacterial activity test experiments were also performed on the coated samples in the dark and on the bare glass substrates under irradiation in order to validate the photocatalytic effect.

3.6.1 Photocatalytic inactivation of *E. coli* cells in suspensions

The bacterial count of the prepared *E. coli* cell suspension (section 3.5) was adjusted to 10⁷-10⁸ cells/ml in PBS. Then, 200 µl suspension was pipetted onto TiO₂-SiO₂ thin films containing different amounts of SiO₂ and placed in a Suntest solar simulator (Atlas CPS+) at 35 °C for 1 h equipped with Xenon lamp. The spectral distribution was controlled by soda lime filter which simulates indoor daylight conditions ($\lambda = 310\text{-}800 \text{ nm}$ at 300 W/m²). The spectral distribution of the filter is given in Appendix A. The schematic notation of antibacterial activity test is given in Figure 3.3. Cell suspensions were removed from the surfaces at different time intervals and the number of remaining viable cells was determined.

In addition, photocatalytic antibacterial activity of the thin film surface containing 92 % SiO₂ was measured five times after cleaning with deionized water and incubation at 45⁰C in the dark for one night to determine the surface reusability.

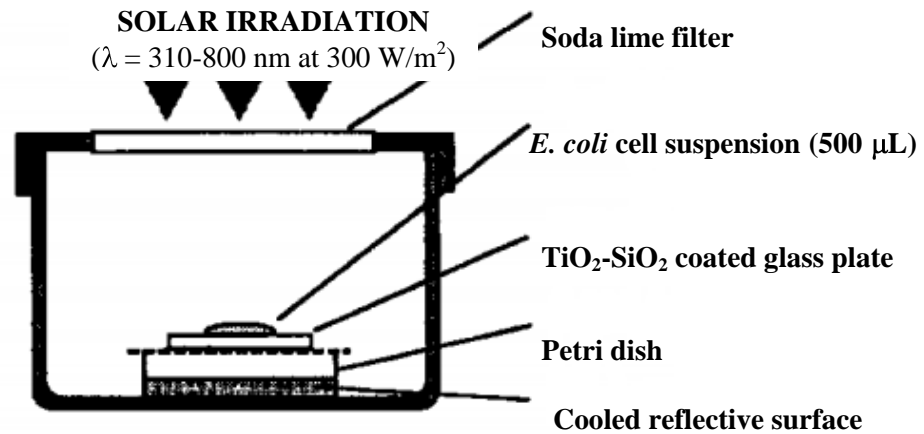


Figure 3.3 Antibacterial activity test

3.6.2 Photocatalytic inactivation of surface-adhered *E. coli* cells

Before the photocatalytic activity test, the adhered cells from one side of the glass plates (section 3.5.1) were removed by rubbing with 70% ethanol. Then, the glass plates containing adhered bacteria on the top surface were irradiated in Suntest solar simulator (Atlas CPS+) under the same conditions given in section 3.6.1 at 35 °C for 1 h. To determine the effect of irradiation time on photocatalytic inactivation of adhered cells, samples were removed from the simulator cabin at different time intervals, the adhered *E. coli* cells were removed from the surface and the number of viable cells on the thin films was determined as explained in section 3.5.1.

3.7 Photocatalytic self-cleaning activity of thin films

The photocatalytic self cleaning activity of the samples was measured by analysis of the degradation rate of surface-adsorbed methylene blue (MB) under irradiation. For this purpose, coated and uncoated glass plates having 10 cm² plate areas were immersed in 20 ml of 100 ppm MB solution for 24 h in the dark at room temperature. To determine the initial MB concentration on the sample surfaces, MB in solution was analyzed by UV-Vis spectrometer as mentioned in part 3.3.4. MB adsorbed on the opposite side of the coated surface was wiped off by using 70% ethanol. The samples were dried for 2 h in the dark at room temperature and the photocatalytic self cleaning activity test was performed under simulated sun light (Atlas CPS, Xe 1000W (Atlas Suntest CPS) with 300W/m² irradiation power for 4 h. To determine the MB degradation rate, samples were removed at different time intervals and the absorbance at 663 nm were measured using UV-Vis spectrometer (Nicolet Evolution 100). Absorbance values were converted to surface MB concentration using calibration curves. The calibration data for MB absorbance versus concentration was obtained by using stains of 20 ml of MB solutions having various concentrations in a range of 2-100 ppm over 10 cm² thin film samples. The details can be found in Appendix D.

3.8 Characterization of photo-induced hydrophilicity of thin films

The photo-induced hydrophilicity of the thin films was determined by contact angle measurements against ultra pure distilled water. The change in contact angle of water before and after irradiation was used to determine the photo-induced hydrophilicity of the thin films. For this purpose water contact angle measurements were performed on the thin films as mentioned in part 3.3.5 after treatment under an UV source (AAT UV Sterilizer cabin with a 15 W- 254 nm UV lamp) for 4 h and incubated in the dark for 24 h at room temperature.

CHAPTER 4

RESULTS AND DISCUSSION

In this study, binary mixtures of $\text{TiO}_2\text{-SiO}_2$ were synthesized by sol-gel technique and coated over soda-lime glass plates as thin films by using dip-coating method. The samples were synthesized to obtain various $\text{SiO}_2/\text{TiO}_2$ ratios which corresponds to 0, 49, 60, 74, 85, 92, 95, and 100 wt% SiO_2 in TiO_2 respectively. The samples were characterized by using different techniques including X-ray diffraction (XRD), scanning electron microscope (SEM), atomic force microscope (AFM) and contact angle measurement. Afterwards, the effect of SiO_2 on the photocatalytic self-cleaning and antibacterial activity over the thin film samples were studied.

4.1 Structure of $\text{TiO}_2\text{-SiO}_2$ thin films

4.1.1 SEM results

SEM images of samples coated with pure TiO_2 and $\text{TiO}_2\text{-SiO}_2$ composite films were obtained. The images of samples containing pure TiO_2 and $\text{TiO}_2\text{-SiO}_2$ mixtures in the range of 60 wt% to 95 wt% SiO_2 are given in Figures 4.1 to 4.5, respectively. Thin film surfaces containing pure TiO_2 are glassy, smooth with no roughness and grains. The addition of SiO_2 enhances the grain structure, surface roughness and porosity to a great extent as shown in Figures 4.2, 4.3, and 4.4. The SiO_2 containing TiO_2 thin films are comprised of spherical particles with approximately 10 nm diameter.

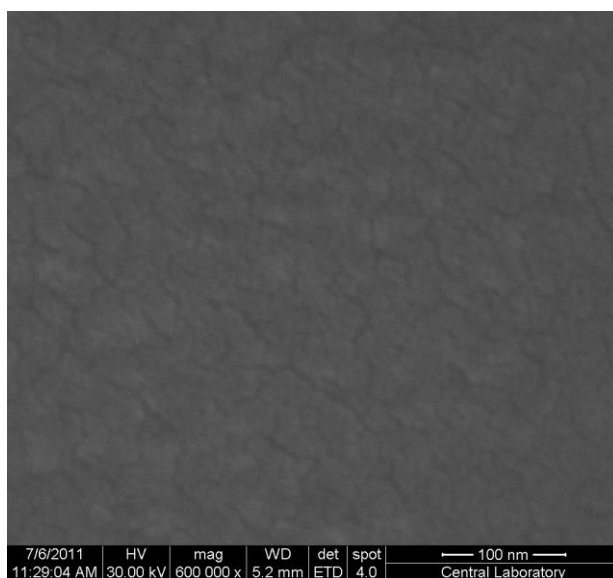


Figure 4.1 SEM image of a thin film surface containing pure TiO_2 .
Image at the 600 000 x magnification

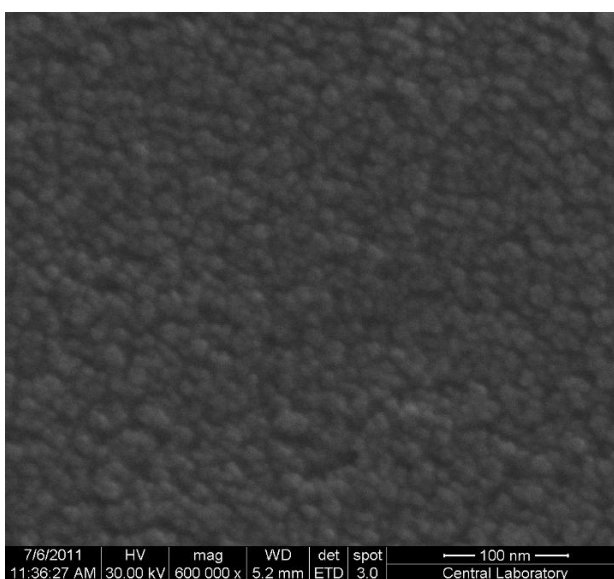


Figure 4.2 SEM image of a TiO_2 - SiO_2 thin film surface containing 60 wt% SiO_2 .
Image at the 600 000 x magnification

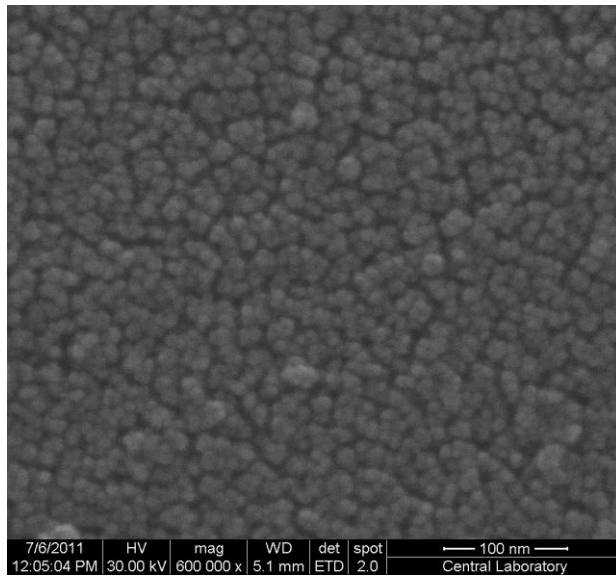


Figure 4.3 SEM image of a $\text{TiO}_2\text{-SiO}_2$ thin film surface containing 74 wt% SiO_2 . Image at the 600 000 x magnification

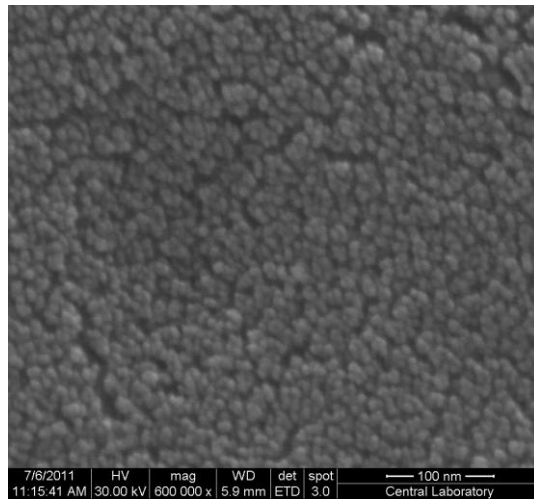


Figure 4.4 SEM image of a $\text{TiO}_2\text{-SiO}_2$ thin film surface containing 92 wt% SiO_2 . Image at the 600 000 x magnification

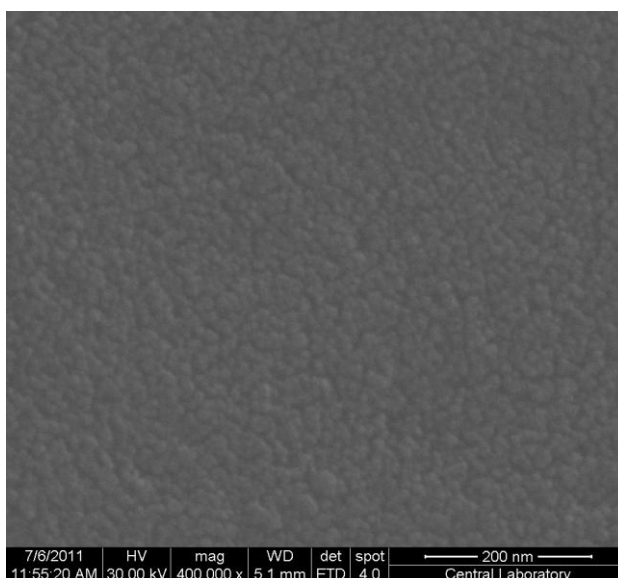


Figure 4.5 SEM image of a $\text{TiO}_2\text{-SiO}_2$ thin film surface containing 95 wt% SiO_2 . Image at the 400 000 x magnification

The cross section of the samples were also analyzed by SEM. The samples were cut to 10 mm*10 mm squares and mounted vertically on the sample holder. The sample images of the thin film crosssections are presented in Figure 4.6. As observed, continuous, homogenous and uniform $\text{TiO}_2\text{-SiO}_2$ thin film layers were obtained. The film thickness increases consistently with the SiO_2 loading which can be explained by the consistency of ludox 30 solution. Film thickness in dip coating method is strongly affected by the viscosity and consistency of the solution as well as withdrawn speed. The thickness of thin films varied between 30 nm to 1 μm within the range of 0- 92wt% SiO_2 which were coated by five consecutive dip coating-drying steps before calcination.

4.1.2 AFM results

The surface morphology of TiO₂-SiO₂ thin films having different SiO₂ contents was also studied by AFM. Surface topography was measured approximately on a 3 x 3 μm² area. In Figures 4.7 and 4.8, the top view of the AFM height-mode image and three-dimensional AFM images of TiO₂-SiO₂ films are shown, respectively. The top view of the AFM height-mode image of pure TiO₂ and 50 wt%, to 95 wt% SiO₂ containing TiO₂-SiO₂ samples are given in Figure 4.7. Pure TiO₂ film surface consists of smaller particles (Figure 4.7(A)) than the SiO₂ containing samples. The addition of SiO₂ enhances the surface roughness and porosity as seen from Figure 4.7(B), (C) and (D). When three-dimensional AFM images of thin film surfaces are examined, as seen from Figure 4.8, the undulation scales and spaces of thin films change drastically. As seen from Figure 4.8(A) thin film surface with pure TiO₂ possesses relatively uniform undulations with smaller amplitudes. With addition of SiO₂ undulation becomes non-uniform with higher amplitudes which causes the increase in surface roughness. Table 4.1 shows the average surface roughness of thin film surfaces which were measured by analysis of AFM images based on RMS values. The surface roughness enhanced by the addition of SiO₂ to great extents which is in good agreement with SEM images.

Table 4.1 Surface roughness values of thin films

SiO ₂ content (wt %)	0	49	60	74	85	92	95
Roughness (RMS, nm)	2.0±1.0	3.6±0.2	4.1±0.7	5.4±1.0	6.6±1.0	7.0±1.0	9.4±2.0

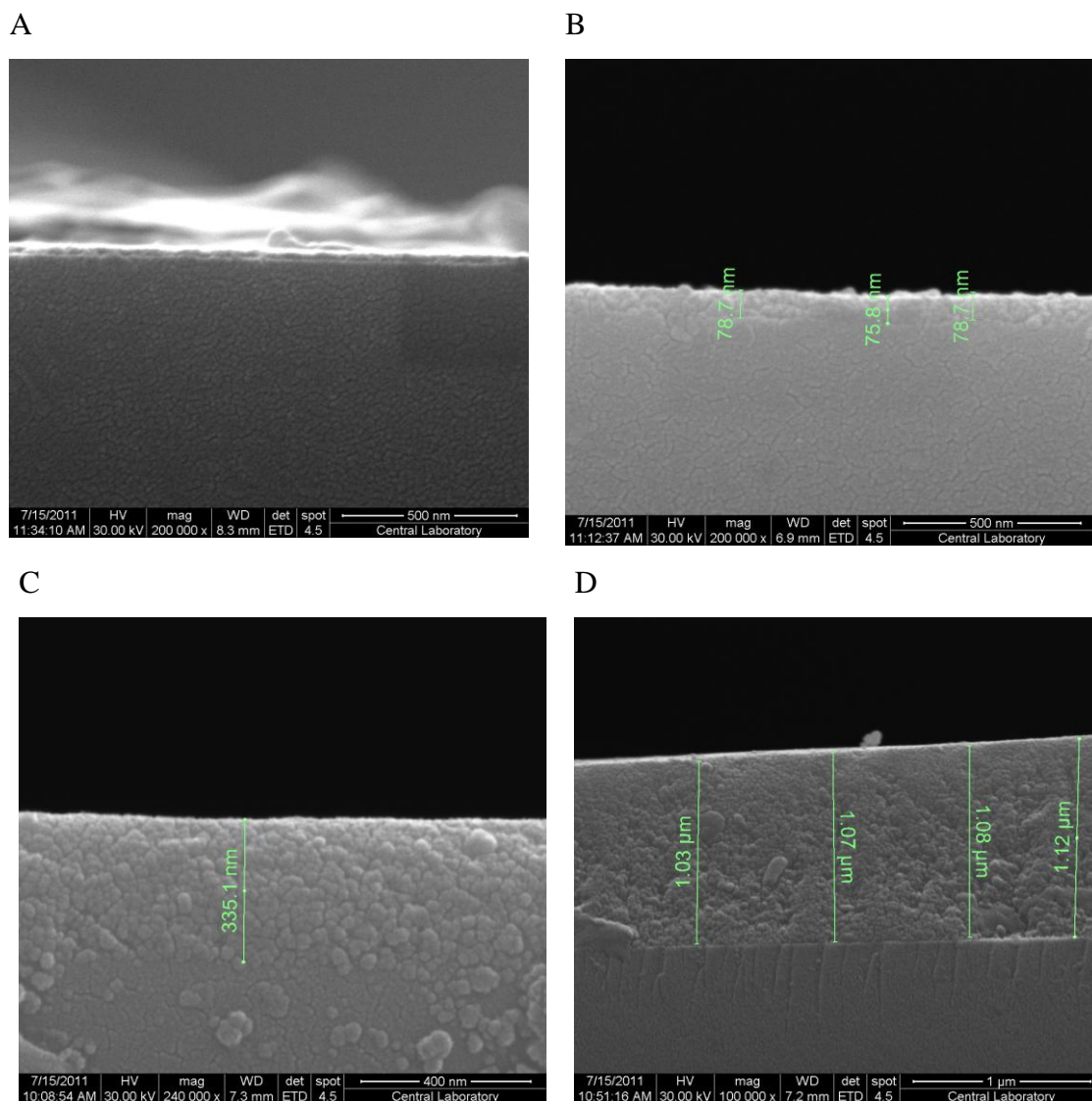


Figure 4.6 Cross sectional view of $\text{TiO}_2\text{-SiO}_2$ thin films. (A) Pure TiO_2 (B) 60 wt% SiO_2 (C) 74 wt% SiO_2 (D) 92 wt% SiO_2

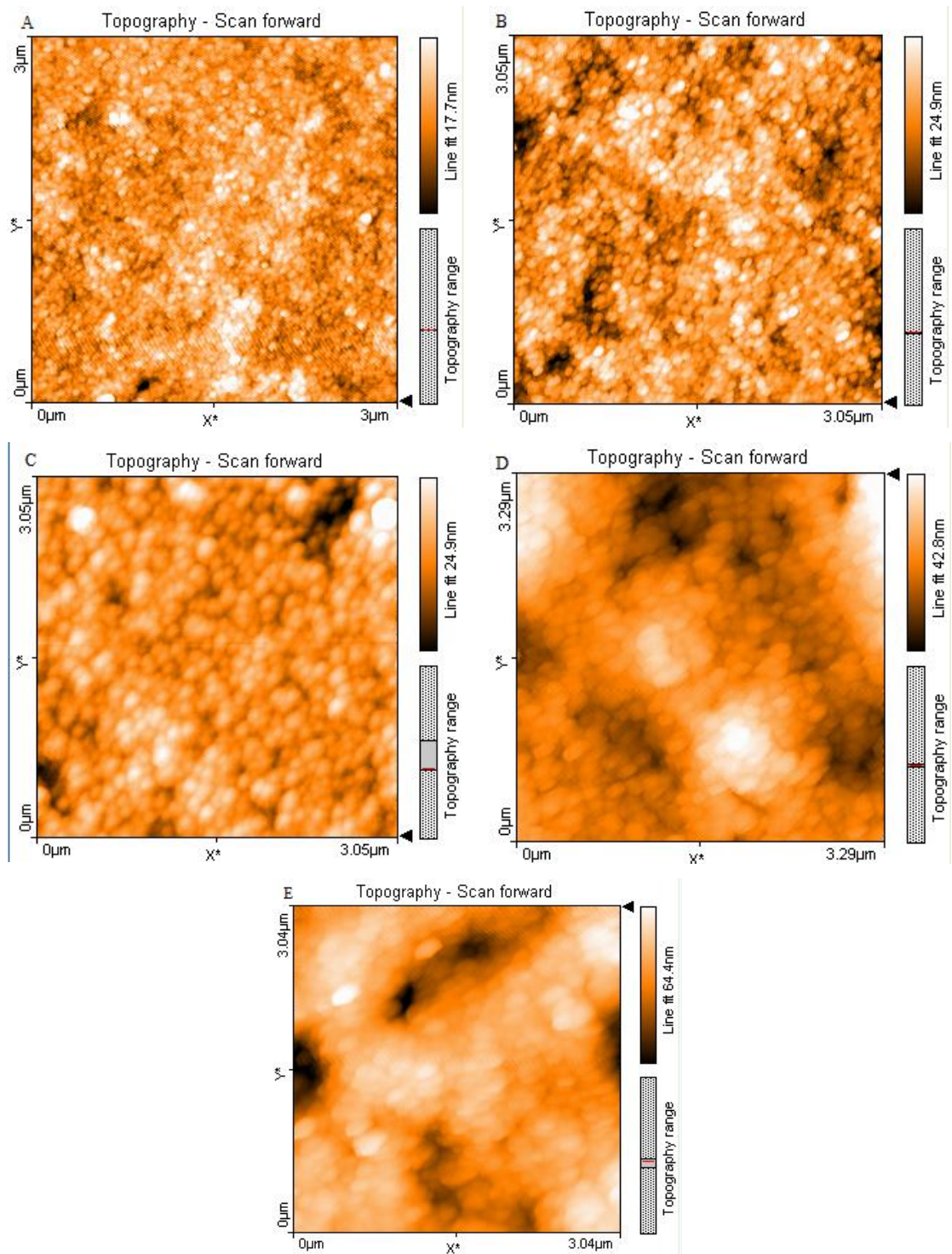


Figure 4.7 Top view of the AFM height mode images of the $\text{TiO}_2\text{-SiO}_2$ thin films. (A) Pure TiO_2 (B) 49wt% SiO_2 (C) 60wt% SiO_2 (D) 92wt% SiO_2 (E) 95wt% SiO_2

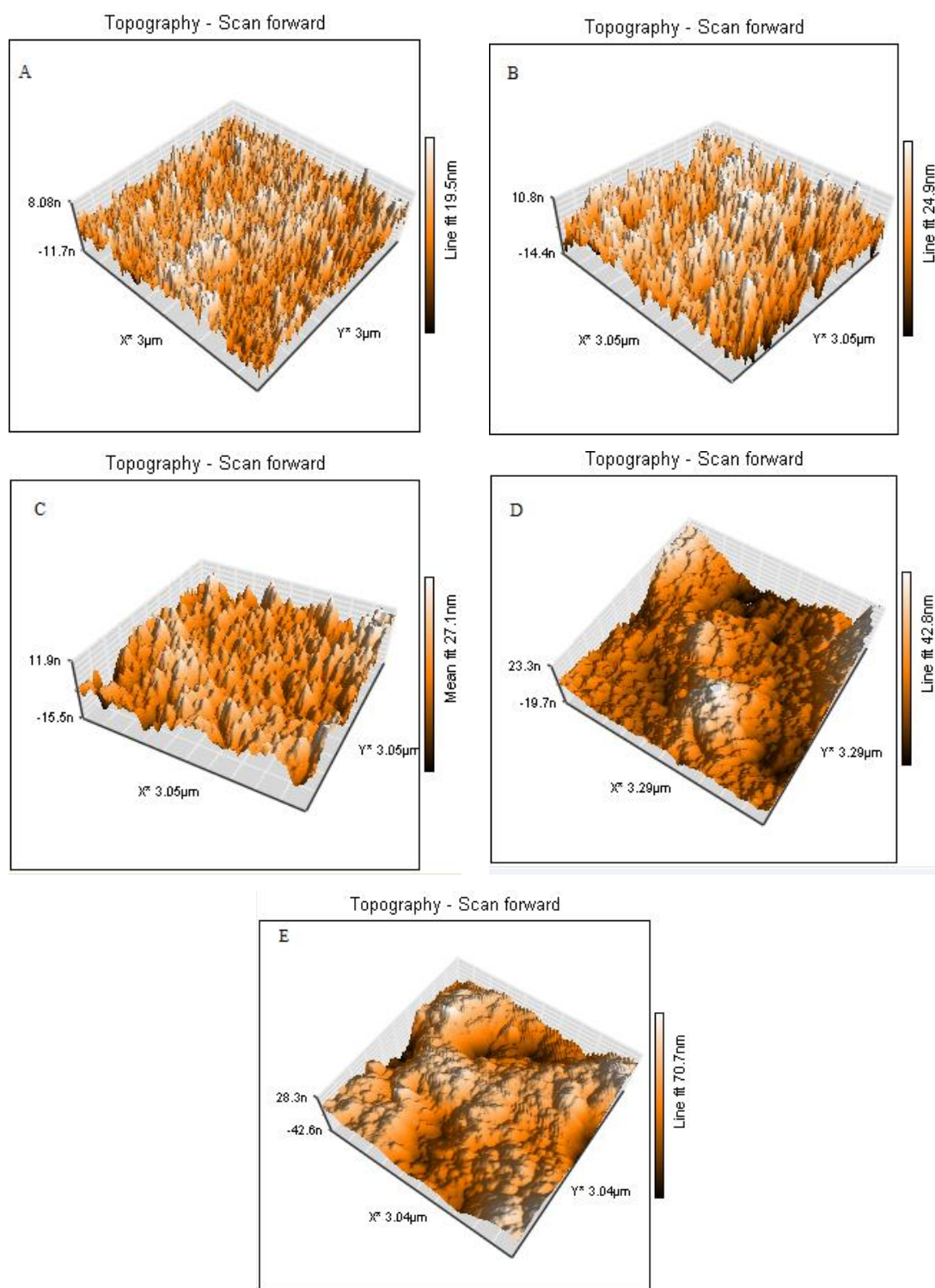


Figure 4.8 Three-dimensional AFM images of the $\text{TiO}_2\text{-SiO}_2$ thin films. (A) Pure TiO_2 (B) 49 wt% SiO_2 (C) 60wt% SiO_2 (D) 92wt% SiO_2 (E) 95wt% SiO_2

4.1.3 XRD results

The XRD patterns of thin films containing different amount of SiO₂ are shown in Figure 4.9. The reference diffraction data of anatase and rutile are presented in Appendix B (Jade Database).

When Figure 4.9(a) is examined, the characteristic peak for anatase (101) plane ($2\Theta = 25.3^\circ$) can be barely seen for 100 wt% TiO₂ thin film. The weak intensity of the peak can be attributed to the smaller film thickness as well as glassy semi-amorphous, semi-crystalline film formation. The addition of 49 wt% SiO₂ and 60 wt% SiO₂ (Figure 4.9(b) and 4.9(c)) improves the crystallinity of TiO₂ as it can be seen by stronger (101) peak and emerging peaks corresponding to (004) and (200) planes of anatase phase ($2\Theta = 37.8^\circ$ and 48°). The broad and weak peaks indicate the presence of small crystallites of TiO₂ and dispersion in SiO₂ matrix. The growth of TiO₂ particles in -Si-O-Si-O- skeleton controlled by diffusion and the formation of larger TiO₂ particles by sintering during the calcination is hindered in the presence of SiO₂ (Sankur and Gunning; 1985; Zhai *et al.*, 1999; Yu and Zhao, 2002). Although the further addition of SiO₂ yields thin films containing less TiO₂, the crystallinity of TiO₂ phase is sustained. The increase on film thickness by the addition of SiO₂ may also contribute to the peak intensity. These results are in good agreement with literature. As it can be seen from Figure 4.9(f) diffraction peak of (101) plane is still apparent for 92% SiO₂ sample.

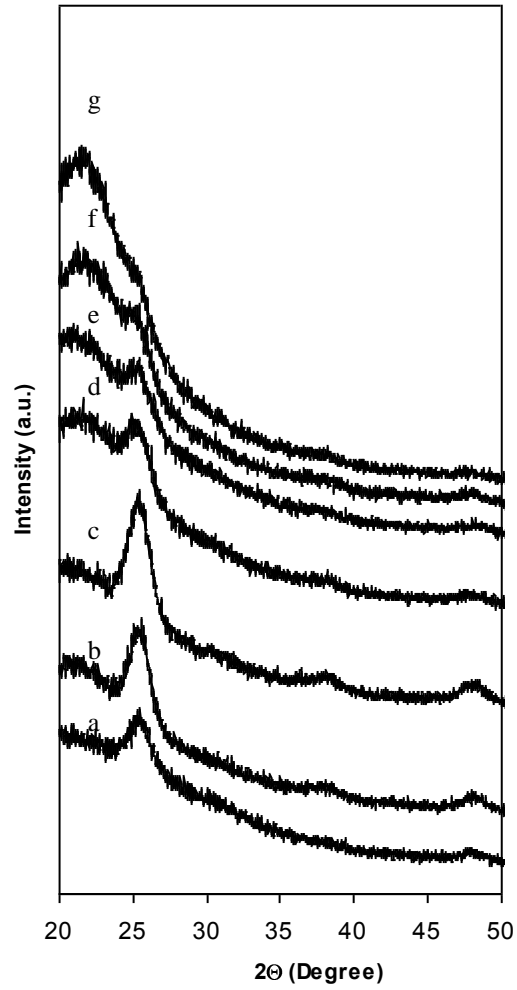


Figure 4.9 XRD patterns of TiO₂-SiO₂ thin films containing different amounts of SiO₂. SiO₂ content: (a) 0 wt% (b) 49 wt% (c) 60 wt% (d) 74 wt% (e) 85 wt% (f) 92 wt% (g) 95 wt%

4.2 Surface Area Measurements of SiO₂-TiO₂ Thin films

The relative surface area of the thin film samples was determined by analyzing methylene blue adsorption data. The MB adsorption equilibrium data was fitted to the Langmuir equation given below (Kipling, 1965; Gregg and Sing, 1982; Inal and Tumsek, 2000).

$$\frac{C_e}{(x/m)} = \frac{1}{k \cdot x_m} + \frac{C_e}{x_m} \quad (4.1)$$

When the thin film sample immersed into MB solution and equilibrium is established, C_e is the equilibrium concentration of MB in the solution (after 72 h), and x/m is the quantity of MB adsorbed per unit glass substrate area. The adsorption capacity (x_m) and binding energy (k) can be determined by data analysis. When the linear plot of $\frac{C_e}{(x/m)}$ versus C_e is performed, the slope of the regression line gives $1/x_m$ where $1/k$ is the intercept. Hence the adsorption capacity value (x_m , mg/cm²) of thin films is obtained. The graphs of adsorption isotherms and Langmuir plots are given in Appendix C. If x_m (mg/cm²) is the amount of MB adsorbed at monolayer per unit area of thin film, A_m (in m²) is the cross-sectional area occupied by the adsorbed MB on the surface and MW is the molecular weight of MB; then the relative surface area of thin film (m²/m²) can be calculated by:

$$RSA = \frac{6.02 \times 10^{23} x_m A_m}{N \cdot MW_{MB} 10^{21}} \quad (4.2)$$

where N is the coverage factor.

In the literature, the size of cross-sectional area of MB molecule which is occupied on the surface, is given in the wide range (İnal and Tümsek, 2000). In this study, A_m value and the coverage factor for MB was taken as 1.2 nm^2 and 2, respectively. The measured relative surface area (RSA) of the thin films is presented in Table 4.2. The RSA of thin film containing pure TiO_2 is lower than the precision limits of the MB adsorption technique because of the glassy, nonporous structure of the surface. The RSA of thin films increases significantly with SiO_2 addition which is in good agreement with the SEM and AFM results.

Table 4.2 Relative surface area of the thin films

SiO ₂ content (wt %)	0	49	60	74	85	92	95
RSA	ND	4±2	6±3	22±3	43±5	83±7	85±4

4.3 Photocatalytic self cleaning activity

Photocatalytic self-cleaning activities of the thin films were characterized through the degradation of MB adsorbed over the thin film surfaces. Photocatalytic self-cleaning activity of the samples were measured quantitatively under 300 W/m^2 ($\lambda = 310\text{-}800 \text{ nm}$) irradiation by using artificial solar irradiation at 35°C as described in section 3.7. Initially the thin films are immersed into MB solution and adsorption equilibrium was achieved in dark. Then the equilibrium concentration of MB over the surface is determined by UV-Vis spectroscopy (Appendix D). The photocatalytic methylene blue degradation under irradiation was followed by analyzing the MB concentration at the same spot by UV-Vis spectroscopy at 663 nm with respect to time (0^{th} , 15^{th} , 30^{th} , 45^{th} , 60^{th} , 90^{th} , 120^{th} , 150^{th} , 230^{th} , 300^{th}

min). The photocatalytic self cleaning activity measurements were compared by control experiments which are carried out in dark and in light conditions in the presence and absence of photocatalytic thin films, respectively. No significant self-cleaning activity was observed in both dark experiments with TiO₂-SiO₂ film and light experiments in the absence of thin film over the glass substrate.

The equilibrium concentrations of MB over the thin film samples are listed in Table 4.3. It can be clearly seen that the MB equilibrium concentration over the thin films increases with the increase of SiO₂. The specific sites of SiO₂ and TiO₂ for methylene blue adsorption data cannot be distinguished from this data. The MB adsorption can take place specifically over the TiO₂ or SiO₂ sites or both. It should be noted that the relative surface area of thin films are also proportional to the equilibrium concentration of MB over the surface.

Table 4.3 Effect of surface composition on MB adsorption over thin films

% wt SiO ₂	Adsorbed MB (mg MB/cm ²)
0	0.066
49	0.075
60	0.076
74	0.072
85	0.085
92	0.091
95	0.062

Figure 4.10 shows effect of irradiation (300 W/m^2) time on the decomposition profiles of MB adsorbed on $\text{TiO}_2\text{-SiO}_2$ thin film samples. No photocatalytic activity was observed for 100 % SiO_2 as expected (Figure 4.10 (h)). Pure TiO_2 has limited photocatalytic activity compared with SiO_2 containing samples. Although the SiO_2 containing samples have higher surface area, pure TiO_2 thin film demonstrates higher activity than the 92 wt% SiO_2 . Thus the addition of SiO_2 improves the photocatalytic activity to certain extent causing smaller catalyst loading. Thin films containing 49 wt% and 60 wt% SiO_2 exhibited stronger self cleaning activities (Figure 4.10(b), 4.10(c)). Complete decolorization was achieved with 60 and 74 wt% SiO_2 samples within 300 min (Figure 4.10(c), 4.10(d)). 92 % $\text{SiO}_2\text{-TiO}_2$ thin film sample completely self cleaned after 700 min. On the other hand, thin film containing 95 wt% and pure SiO_2 did not decompose MB completely under irradiation (Figure 4.10 (g) and 4.10 (h)) indicating the presence of some inaccessible adsorption sites.

Methylene blue degradation over SiO_2 supported TiO_2 follows complex kinetics. The kinetics of methylene blue degradation over pure TiO_2 and $\text{SiO}_2\text{-TiO}_2$ thin films were also analyzed by considering initial reaction rates for first order kinetics. For this purpose, the change in methylene blue concentration over the surface ($C \text{ mg/cm}^2$) with respect to the initial concentration ($C_0, \text{mg/cm}^2$) is analyzed with respect to time by plotting $\ln(C/C_0)$ versus time data (Figure 4.11). The details of the analysis can be found in Appendix E.

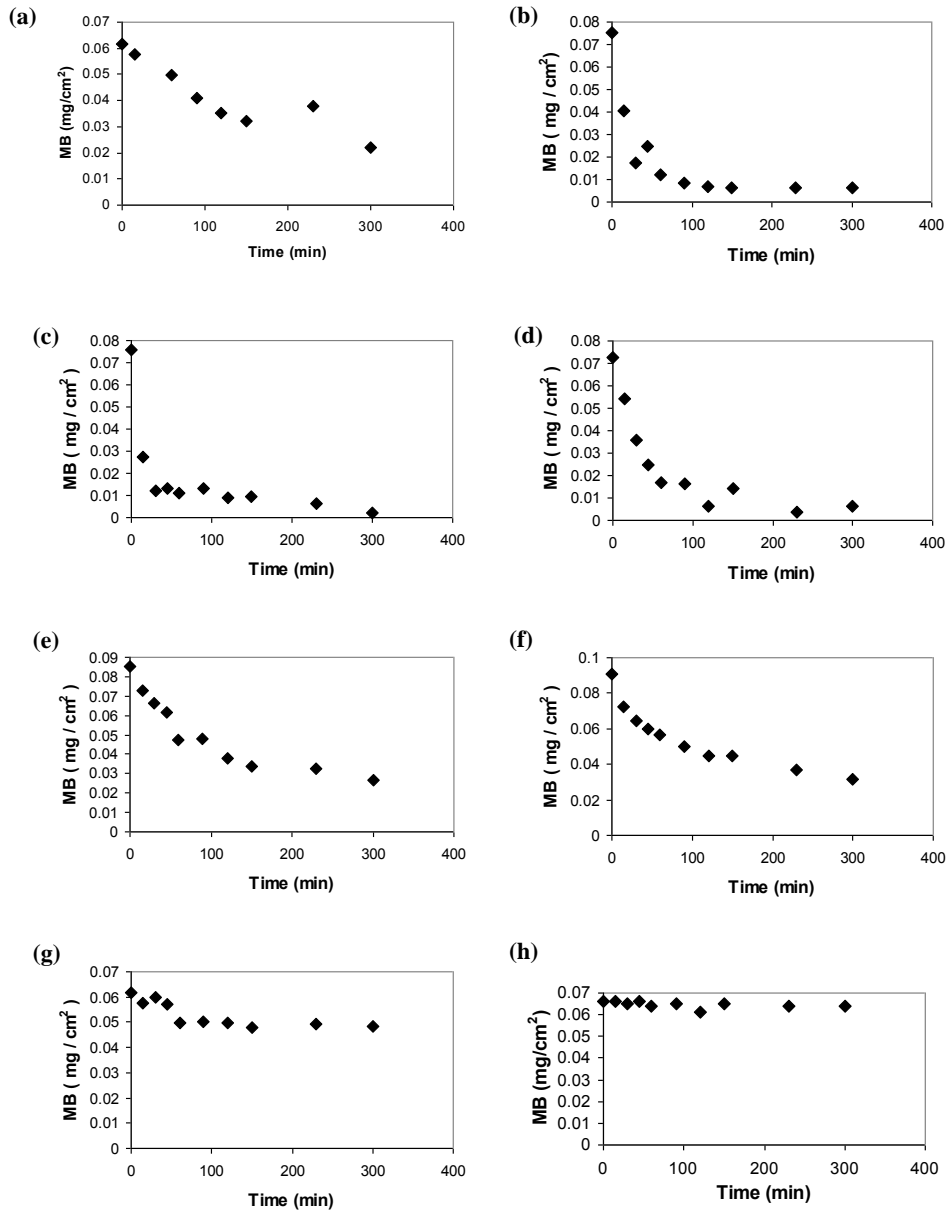


Figure 4.10 Effect of irradiation time ($300 \text{ W}/\text{m}^2$) on the degradation of methylene blue over the TiO_2 - SiO_2 thin films. SiO_2 contents: (a) 0 wt% (b) 49 wt% (c) 60 wt% (d) 74 wt% (e) 85 wt% (f) 92 wt% (g) 95 wt% (h) 100 wt%

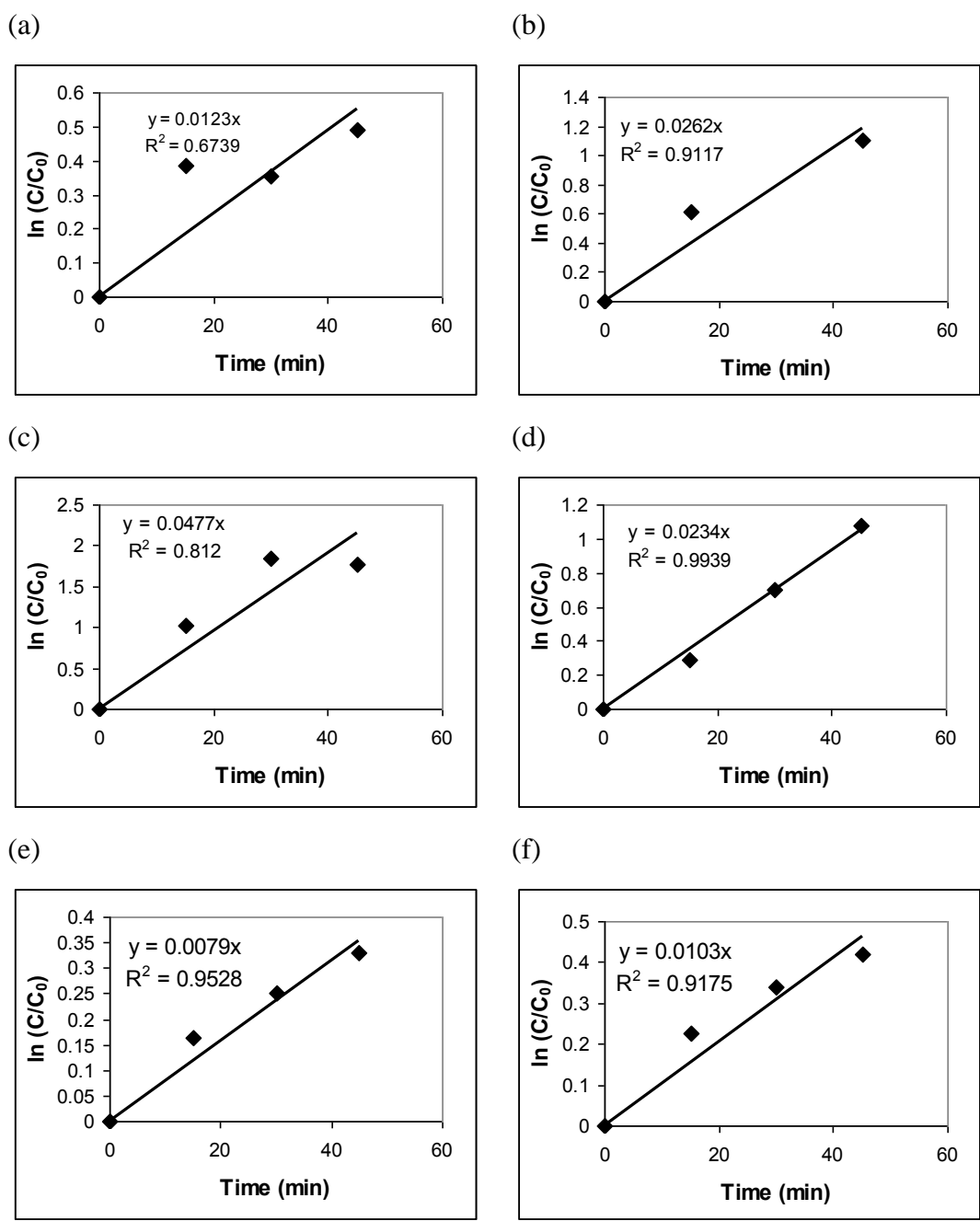


Figure 4.11 $\ln(C/C_0)$ versus reaction time data of TiO_2 - SiO_2 thin films. SiO_2 contents: (a) 0 wt% (b) 49 wt% (c) 60 wt% (d) 74 wt% (e) 85 wt% (f) 92 wt%

Figure 4.12 shows the effect of SiO₂ addition on the initial reaction rate constants obtained for MB degradation. It can be seen that the photocatalytic activity of TiO₂ is enhanced significantly with the addition of SiO₂. The highest initial decomposition rate is obtained for 60 wt% SiO₂ and the activity decreases with further SiO₂ addition. The increase in photocatalytic activity by the SiO₂ addition can be explained by the increase of the amount of MB per unit area of TiO₂-SiO₂ thin films due to porous structure and larger surface area of thin films.

A similar trend was also reported by Suzuki *et al.* (2011) for TiO₂-SiO₂ nanoparticles; in the photocatalytic deposition of MB, the initial reaction rate of silica/titania nano-composite photocatalyst performed faster initial reaction rate than that of nonporous titania up to the amount of silica was 80 wt%. Suzuki *et al.* explained improvement of photocatalytic performance by more effective attack of photogenerated radicals on MB molecules by increase in amount of adsorbed MB. And the decline of photocatalytic performance with addition of 80 wt % SiO₂ was attributed to the increase in distance between neighboring TiO₂ nanoparticles making the radicals generated on the anatase surface unavailable for MB degradation (Yu and Chuang, 2007; Suzuki *et al.*, 2011). These suggestions may explain our results because the complete degradation of MB was also achieved by thin films containing 74 wt% 85 wt% and 92 wt% SiO₂ despite the fact that their initial reaction rates was slower than thin film containing 60 wt % SiO₂. This behavior can be explained by the inclusion of diffusion control with reaction kinetics.

When the XRD results and crystallinity of the samples recalled (Figure 4.9) the higher activity of SiO₂ containing samples could be also related with crystallinity of the samples. When SiO₂ content exceeded 60 wt%, broader and weaker anatase (101) peaks indicate the presence of small isolated and well dispersed TiO₂ crystallites in SiO₂ matrix (Yu and Zhao, 2002; Bui *et al.*, 2011). Based on this observation, it can be concluded that the crystallinity is also important parameter on the photocatalytic activity.

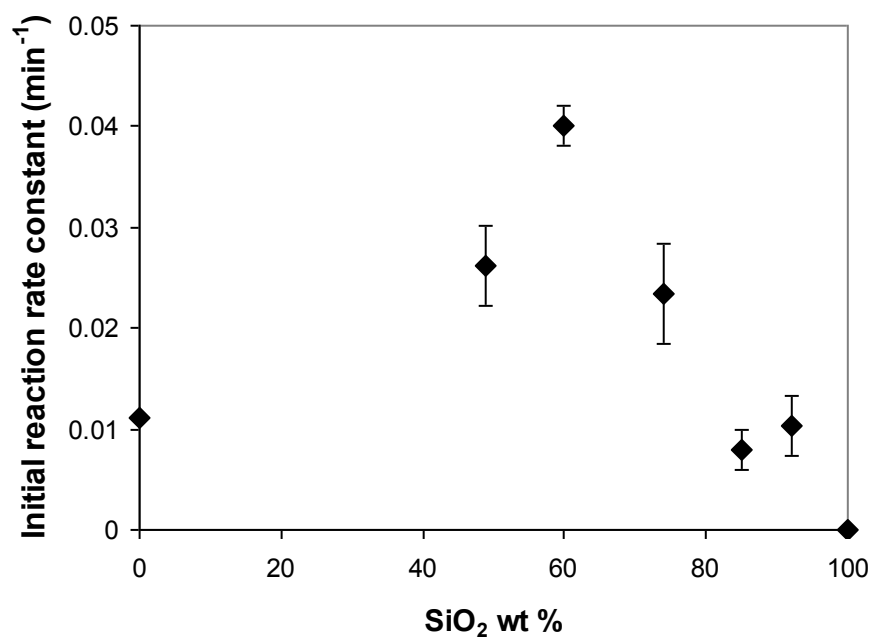


Figure 4.12 Effect of surface composition on the initial reaction rate constants for MB degradation under irradiation (300 W/m²)

4.4 Photocatalytic antibacterial Activity

Escherichiae coli was chosen as a model bacterium to characterize the photocatalytic antibacterial activity of SiO₂-TiO₂ thin films. Photocatalytic antibacterial activity was also examined under the same irradiation rate (300 W/m²) and temperature (35 °C) with the MB decomposition tests.

The photocatalytic inactivation of *E. coli* cells over the TiO₂-SiO₂ thin films was examined by using suspensions containing initial bacterial count of 10⁷-10⁸ cells/ml as described in part 3.6.1. The efficacy of the photocatalytic disinfection was also tested by control experiments in dark and in light in the presence and absence of photocatalytic thin films, respectively. No significant bacterial

inactivation was observed in both dark experiments with TiO₂-SiO₂ film and light experiments in the presence of bare glass substrate. Although complete inactivation was achieved within 2 h irradiation period for majority of the samples, the antibacterial activity at the end of 1 h was chosen to compare the activity of thin films containing different SiO₂ content.

4.4.1 The Effect of Photocatalysis on *E. coli* cells by SEM Analysis

After 1 h irradiation the morphological lesions of *E. coli* cells over the TiO₂-SiO₂ thin film surfaces containing 92 wt% SiO₂ and bare glass was investigated by SEM analysis. As mentioned in part 3.5.3, before fixing the cells on the surfaces by 4% glutaraldehyde solution, 0.2 M sterilized PBS (pH 7.2) was added to *E. coli* suspension over the thin film surfaces and kept at 4 °C for 4h to clearly observe the morphological changes of the cells and minimize the preparation defects.

Figures 4.13, 4.14 and 4.15 illustrate the images of *E. coli* cells over a bare glass under irradiation, 92 wt% SiO₂-TiO₂ sample incubated in the dark, 92 wt% SiO₂-TiO₂ under irradiation, respectively.

As observed clearly from the SEM images, morphological lesions on *E.coli* cells were not observed on the blank experiments with irradiation over bare glass (Figure 4.13) and TiO₂-SiO₂ coated glass samples in the dark (Figure 4.14). On the other hand, the irradiation of the cells over TiO₂-SiO₂ coated samples caused rumples, dents and irregular contours on the cell surface (Figure 4.15) which might be attributed to the cell surface damage by ROS attack under irradiation (Sunada *et al.*, 2003).

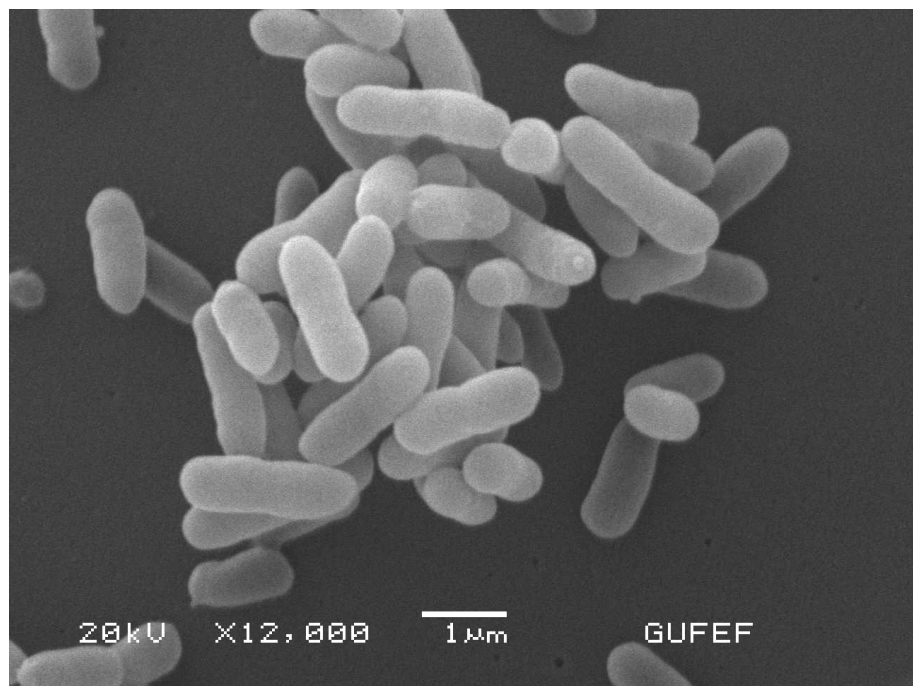
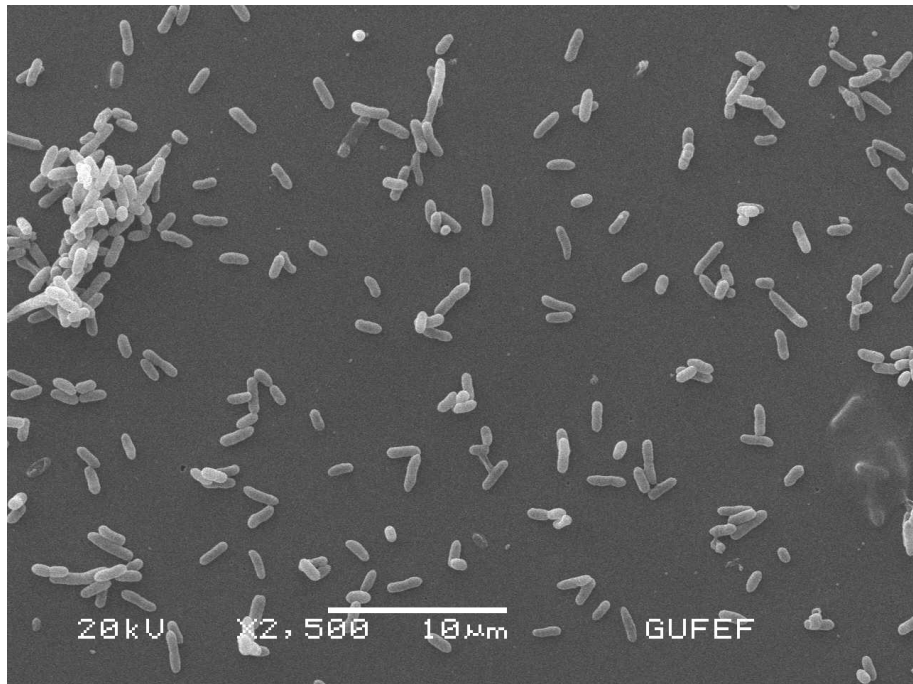


Figure 4.13 SEM images of *E. coli* cell suspensions over the bare glass after 1 h under 300 W/m^2 irradiation.

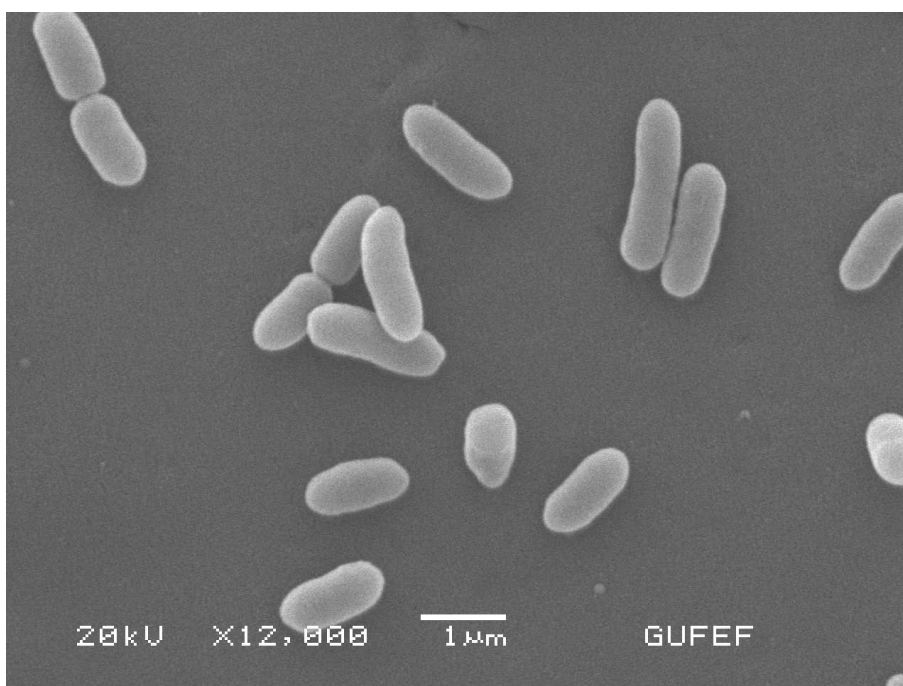
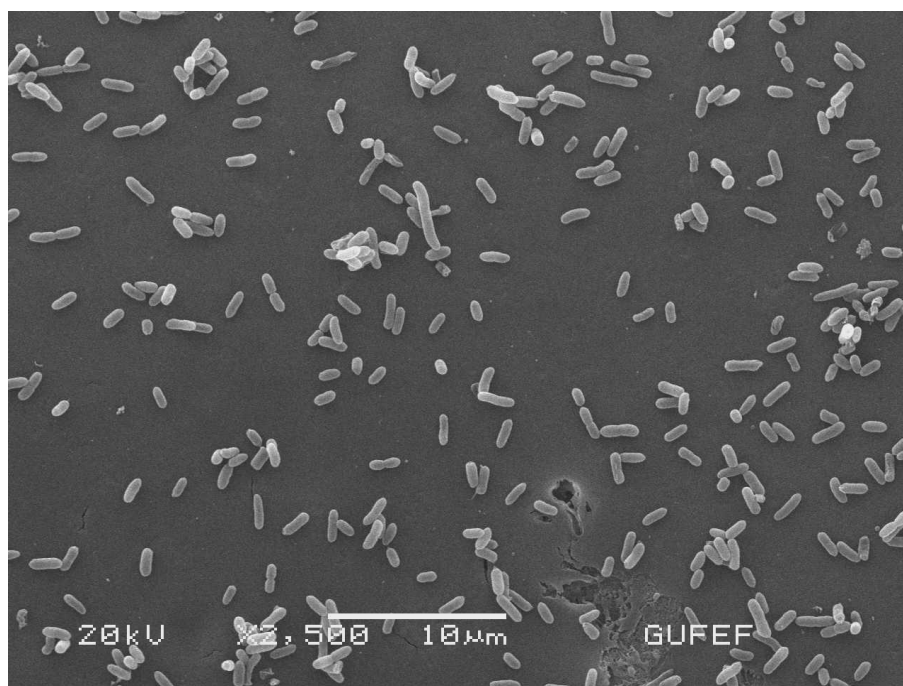


Figure 4.14 SEM images of *E. coli* suspensions over $\text{TiO}_2\text{-SiO}_2$ coated substrate containing 92 wt% SiO_2 after 1h in dark.

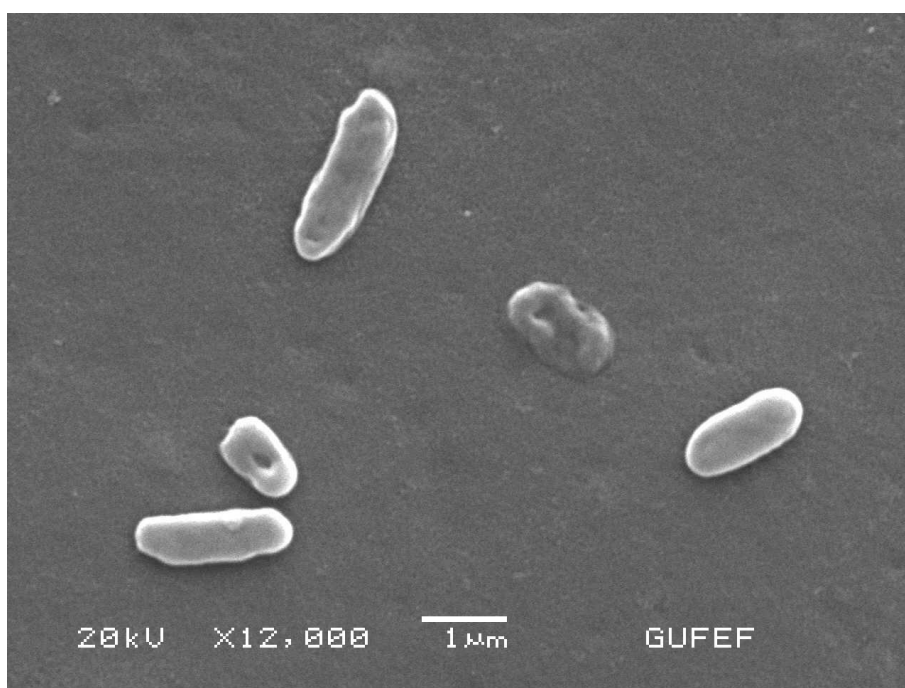
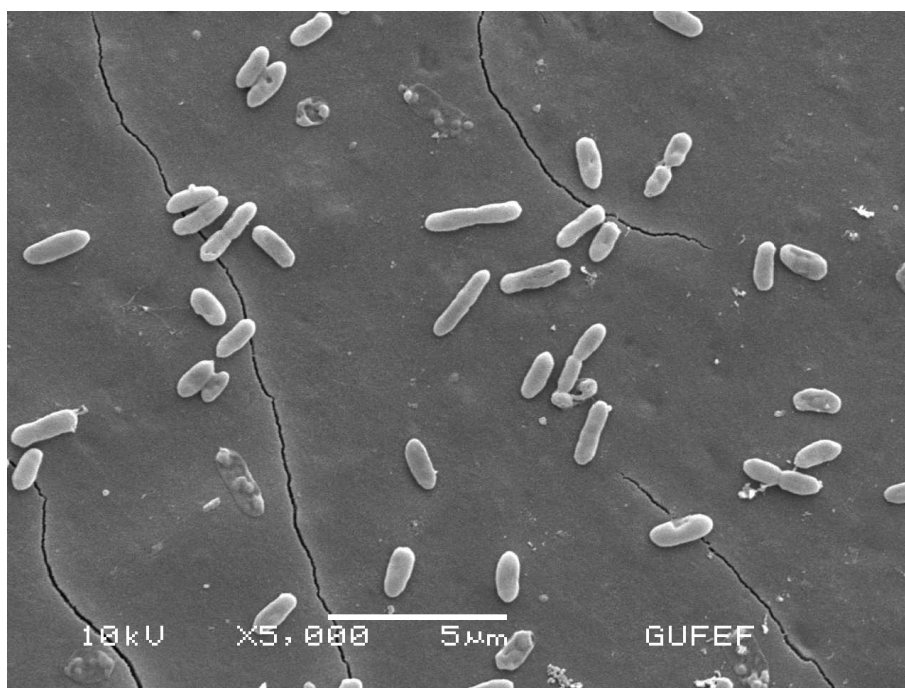


Figure 4.15 SEM images of *E. coli* cell suspensions over the $\text{TiO}_2\text{-SiO}_2$ coated substrate containing 92 wt% SiO_2 after 1h under 300 W/m^2 irradiation.

4.4.2 Photocatalytic inactivation of *E. coli* cells in suspensions

The effect of SiO₂ addition on the photocatalytic antibacterial activity of TiO₂-SiO₂ thin films after 1 h irradiation is given in Figure 4.16. The addition of SiO₂ enhances the photocatalytic antibacterial activity of the composite thin films considerably. The maximum antibacterial activity was achieved as 50 % inactivation over 92 wt% SiO₂ containing thin films at the end of 1 h. Higher SiO₂ loadings caused reduction in the photocatalytic activity most probably because of the dilution of TiO₂ phase and inaccessibility. As observed from Figure 4.16, 20% of *E. coli* cells was inactivated over 95 wt% SiO₂ thin film surface. No antibacterial activity was observed for thin films containing pure SiO₂ as expected.

When the results of antibacterial activity experiments against suspended *E.coli* cells is compared with self cleaning activity tests (MB decomposition), a similar trend could be seen. (Figure 4.17). The major difference between the two different photocatalytic processes is the shift on the composition for maximum antibacterial rate to higher SiO₂ content. Both methylene blue degradation and antibacterial activity are complex processes. The self-cleaning and antibacterial activity contain many complex reaction steps which are controlled by different textural and surface properties.

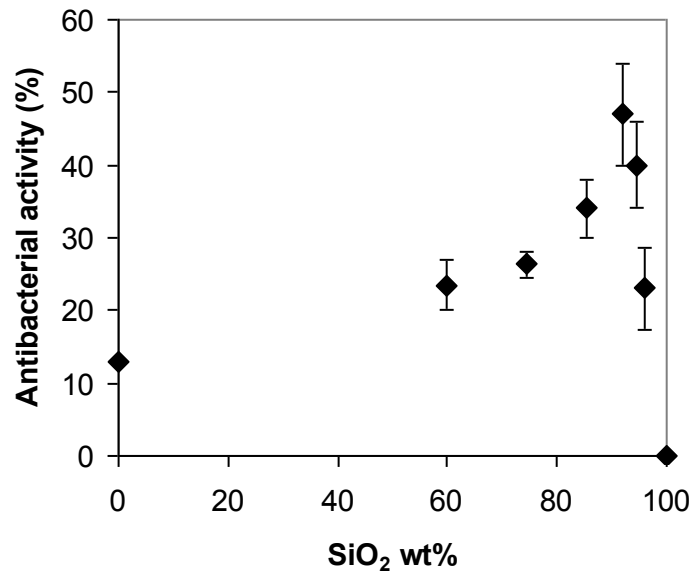


Figure 4.16 Effect of surface composition on the photocatalytic antibacterial activity of TiO₂-SiO₂ thin films at the end of 1 h under 300W/m² irradiation at 35 °C.

When Figure 4.9 is revisited, the crystallinity can be directly related with self-cleaning activity, as mentioned in part 4.3. Although the peak intensity for the anatase phase decreases with the further SiO₂ loading, the increase in antibacterial activity is sustained with further SiO₂ additions which is maximized at 92 wt%. *E. coli* cells are much larger (1.5µm x 0.5µm) (Slonczewski *et al.*, 2009) than MB molecules (1.6 nm x 0.7 nm) (Suzuki *et al.*, 2011). Therefore, the enhancement of photocatalytic antibacterial activity with the addition of SiO₂ can be explained by the improved dispersion of TiO₂ in silica matrix and accessibility of TiO₂ particles. However when the SiO₂ concentration exceeds 92 wt%, photocatalytic antibacterial activity decreases considerably, which can be explained by the dilution effect of TiO₂.

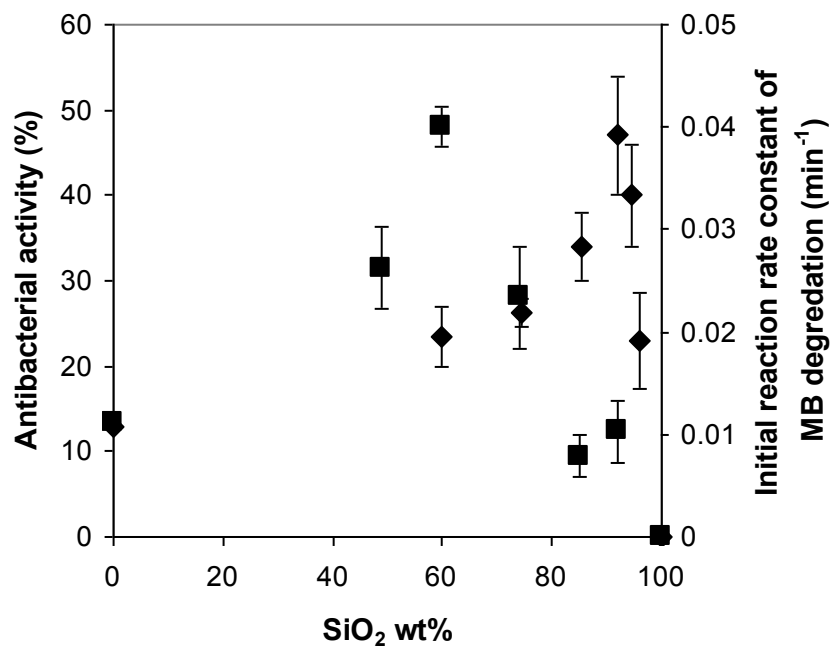


Figure 4.17 Effect of surface composition on initial reaction rate for MB degradation and antibacterial activity of TiO₂-SiO₂ thin films under 300 w/m² irradiation. ■; Initial reaction rate constant (min⁻¹), ◆; Antibacterial activity (%)

The photocatalytic antibacterial activity must be evaluated by considering both the surface composition and the textural properties of surface. The attack of reactive oxygen species (ROS) to cell surface is an essential step for photocatalytic inactivation. ROS are generated over the TiO₂ surface and react with the cell wall of adhered bacteria. On the other hand the reactive oxygen species also diffuse in aqueous phase and may react with the cell walls of suspended bacteria. The inactivation rate of adhered bacteria is supposed to be faster than the diffusion controlled inactivation of suspended bacteria. The proposed mechanism was strengthened by experimental work to examine the relationship between the cell adhesion of *E.coli* over SiO₂-TiO₂ thin films and effect of surface composition on cell adhesion.

The details of proposed mechanism for the photocatalytic inactivation process are illustrated in Figure 4.18. The photo-generated electrons and holes are highly unstable with strong oxidation/reduction power and convert surface adsorbed species such as oxygen and water (surface hydroxyl OH) into ROS such as hydroxyl radicals ($\bullet\text{OH}$), superoxide ion ($\bullet\text{O}_2^-$). The free radicals also react with water and generate hydrogen peroxide H_2O_2 (Hoffmann *et al.*, 1995; Mills and Hunte, 1997; Fujishima *et al.*, 2000). The surface concentration of hydroxy species replenished easily by aqueous phase while the oxygen concentration is rather limited by the low solubility and diffusion step from air to aqueous phase. The hydroxyl ($\bullet\text{OH}$) and super oxygen radicals ($\bullet\text{O}_2^-$) generated over the semiconductor surface can directly interact with the cell surface (Figure 4.18). On the other hand, the interaction of hydroxyl radicals with free bacteria in suspension is limited by the short half-life time of hydroxyl radicals (2-4 μs) and diffusion of active species from the surface to the aqueous phase (diffusion coefficient: $2 \times 10^{-9} \text{ m}^2/\text{s}$), which is suggested as a slow process (Roots and Okada, 1975). In contrast, although superoxide ($\bullet\text{O}_2^-$) ions have longer half-life, they cannot easily penetrate to the cell membrane, because of their negative charge (Banerjee *et al.*, 2006). The formation of H_2O_2 and reaction of H_2O_2 with cell wall are also possible reactions. On the other hand, $\bullet\text{OH}$ radicals are considered to be more effective than other ROS during the photocatalytic inactivation reaction of *E. coli* (Ireland *et al.*, 1993; Cho *et al.*, 2004; Seven *et al.*, 2004; Cho *et al.*, 2005; Hajkova *et al.*, 2007; Văcăroiu *et al.*, 2009). This argument can be plausible, considering higher oxidation potential value of $\bullet\text{OH}$ (2.8 eV) than other strong ROS such as H_2O_2 (1.77 eV) and HO_2^\bullet (1.70 eV) in the water (USAPE, 1998). In addition, Cho *et al.* (2005) hypothesized that both surface-bound hydroxyl radicals on the TiO_2 particles and free hydroxyl radicals in the solution play a major role in the inactivation of *E. coli* rather than ROS such as; $\text{O}_2^{\bullet-}$, H_2O_2 . In Table 4.4, reaction steps of formation of active species and half life of these species are given. As seen from Table 4.4, considering shorter half-life (10 ns) (Carp *et al.*, 2004) and

diffusion coefficient ($2 \times 10^{-9} \text{ m}^2/\text{s}$) (Roots and Okada, 1975) of hydroxyl radicals ($\bullet\text{OH}$) in water, there should be the slow accessibility for free $\bullet\text{OH}$ radicals in aqueous phase to the cell surface by diffusion for suspended *E. coli* cells because of the existence of liquid phase between TiO_2 particle and cells. Therefore, the adhesion of the cells over the thin film surfaces which facilitates the interaction of $\bullet\text{OH}$, $\text{O}_2^{\bullet-}$, and H_2O_2 with cell surface becomes an important issue for antibacterial activity of thin films. These results require detailed analysis of surface structure of $\text{TiO}_2\text{-SiO}_2$ composites, and effect of surface composition on the *E.coli* adhesion must be clarified.

Table 4.4 Reaction steps of formation of active species and their half life values

Reaction	Half life of ROS
$\text{TiO}_2 + h\nu \rightarrow h_{vb}^+ + e_{cb}^-$	
$\text{O}_2 + e_{cb}^- \rightarrow \text{O}_2^{\bullet-}$	Half life of $\text{O}_2^{\bullet-} = 1 \text{ ms}$ (Carp <i>et al.</i> , 2004)
$\text{O}_2^{\bullet-} + e_{cb}^- + 2\text{H}^+ \rightarrow \text{H}_2\text{O}_2$	
$\text{O}_2^{\bullet-} + \text{H}_2\text{O}_2 \rightarrow \bullet\text{OH} + \text{OH}^- + \text{O}_2$ or $e_{cb}^- + \text{H}_2\text{O}_2 \rightarrow \bullet\text{OH} + \text{OH}^-$	Half life of $\bullet\text{OH} = 10 \text{ ns}$ (Carp <i>et al.</i> , 2004)
$h_{vb}^+ + \text{OH}^- \rightarrow \bullet\text{OH}$ or $h_{vb}^+ + \text{H}_2\text{O} \rightarrow \text{H}^+ + \bullet\text{OH}$	Half life of $\bullet\text{OH} = 10 \text{ ns}$ (Carp <i>et al.</i> , 2004)
$2h_{vb}^+ + 2\text{H}_2\text{O} \rightarrow 2\text{H}^+ + \text{H}_2\text{O}_2$	

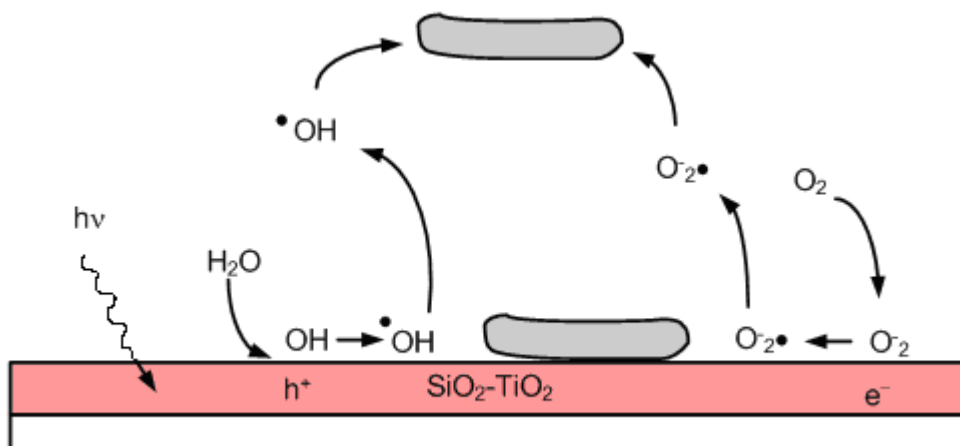


Figure 4.18 Illustration of photocatalytic inactivation of *E. coli* on SiO₂-TiO₂ film process

4.5 Bacterial adhesion test

To clarify the effect of TiO₂-SiO₂ composition of thin films on the cell adhesion, a set of experiments were performed and the number of adhered cells per unit substrate area was determined for all thin film samples experimentally. The details of the experiments can be found in part 3.5.1. As shown in Figure 4.19, the number of adhered bacteria over TiO₂-SiO₂ thin film samples increases consistently with the increase of SiO₂ weight fraction on surface. The number of adhered cells increases from 1.1×10^5 to 3.2×10^5 cells/cm² when SiO₂ content was increased from 0 to 92 wt%. Bacterial adhesion reaches to its maximum value over the same surface composition where the maximum antibacterial activity was determined (Figure 4.20). The results show that the antibacterial activity can be directly related with bacterial adhesion and bacterial adhesion depends on the surface composition. It is well known that, Lifshitz van der Waals (LW) and acid-base (AB) forces affect directly the first phase of bacterial adhesion (Mei *et al.*,

1998). In order to understand the effect of surface thermodynamic properties on the adhesion of bacteria, surface free energy (γ_s) of the TiO₂-SiO₂ thin films were determined and the effect of surface composition of TiO₂-SiO₂ thin films on the surface free energy was investigated.

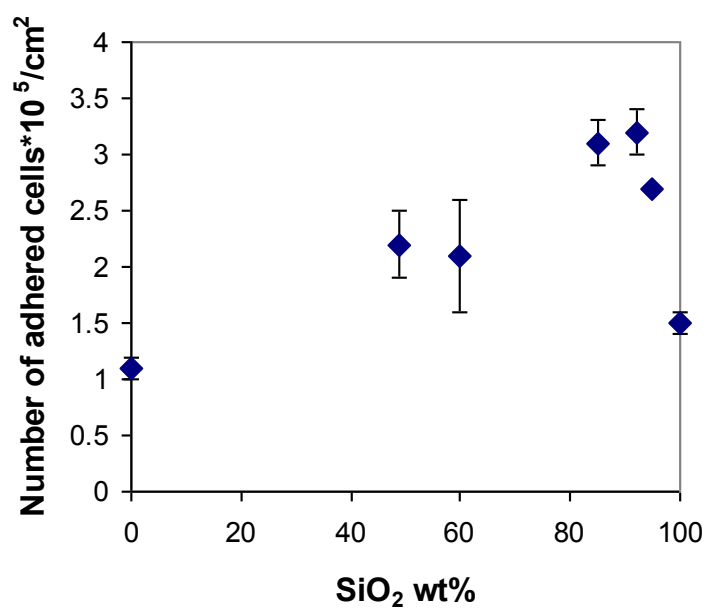


Figure 4.19 Effect of surface composition on the bacterial adhesion over TiO₂-SiO₂ thin films

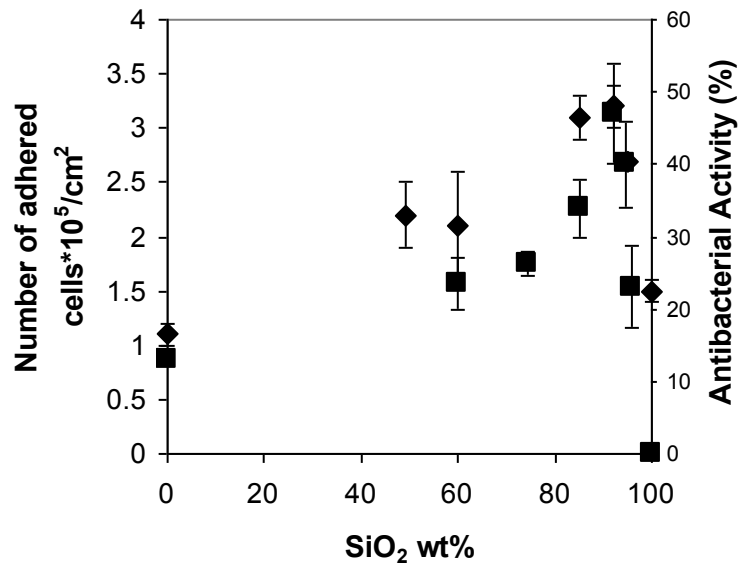


Figure 4.20 Effect surface composition on the bacterial adhesion (♦) and; the photocatalytic antibacterial activity (■) of TiO₂-SiO₂ thin films at the end of 1 h under 300W/m² irradiation at 35 °C.

4.6 The Thermodynamic Properties of SiO₂-TiO₂ Thin Films and *E.coli* Adhesion

4.6.1 Contact angle measurements and surface free energy of SiO₂-TiO₂ Thin Films

The surface energy components of thin films and *E. coli* cell surfaces were determined by using Lifshitz-van der Waals, acid-base (LW-AB) approach and Young-Durpé equation. The details can be found in part 2.8.1.1 (Equation 2.30). Water, glycerol or diiodomethane were chosen as probe liquids with the surface tension components given in Table 4.5 having various polar, acidic and basic

functional groups. The apolar liquid (diiodomethane) was selected to measure non-polar surface tension of surfaces, (γ_s^{LW}) as the acidic (γ_D^+) and basic (γ_D^-) components of diiodometahane equal to zero. Then, as the surface tension components of water and glycerol are given in the literature, the acidic (γ_s^+) and basic (γ_s^-) components of surfaces were also obtained by using Equation 2.30

Table 4.5 Test liquids and their surface tension components (Van Oss, 1993; Li and Logan 2004; Brant and Childress, 2002)

Surface tension data (mN/m)	γ_l^{LW}	γ_l^+	γ_l^-
Water (W)	21.80	25.50	25.50
Glycerol (G)	34.00	3.92	57.40
Di-iodomethane (D)	50.80	0.00	0.00

The contact angle measurements and calculated surface free energy components for TiO₂-SiO₂ thin film samples and *E. coli* cells are presented in Table 4.6. Both TiO₂-SiO₂ coated samples and *E.coli* cells have hydrophilic surface structures. As it is presented in Table 4.6, the contact angle of water decreases significantly with the increasing weight fraction of SiO₂. The lowest water contact angle was measured over 95% SiO₂-TiO₂ surface which is superhydrophilic.

Table 4.6 Contact angles and surface free energy components of the thin film surfaces and bacterial surfaces ((W, water; G, glycerol; D, diiodomethane); T = 25 °C).

Surfaces	Contact angle θ (degrees)			Surface energy components (mN/m)				
	θ^w	θ^p	θ^g	γ^{LW}	γ^+	γ^-	$\gamma_{AB} = 2\sqrt{\gamma^+ \gamma^-}$	γ^{TOT}
SiO ₂ content (wt%)								
0	26.0±0.7	46.2±1.5	31.0±4.2	44.0	<0.1	56.3	1.3	45.3
49	24.0±2.0	39.6±9.0	16.5±3.3	49.0	0.1	50.1	3.6	52.4
60	27.0±3.7	40.1±7.0	20.5±7.0	48.0	0.1	48.0	4.6	52.2
74	13.0±9.0	33.7±12.0	19.3±8.3	48.0	0.2	54.2	7.1	55.1
85	11.5±2.0	33.0±6.0	20.0±2.0	48.0	0.3	53.9	7.8	55.7
92	9.2±3.0	23.0±5.0	13.2±2.5	49.5	0.8	48.0	12.4	62.0
95	5.4±3.0	18.4±6.0	12.2±4.5	49.1	1.0	47.0	16.6	63.0
100	8.2±2.0	36.6±3.0	11.0±2.0	50.0	<0.1	58.2	2.8	53.0
<i>E. coli</i> XL1-blue cell surface	15.0±1.0	49.0± 5.0	32.7± 3.0	35.0	1.7	55.1	19.5	54.1

The surface free energies of 14 different stains of *E. coli* cells were reported in literature (ven der Mei and Busscher, 1998) by using the same LW-AB approach. The surface free energy of different strains of *E. coli* cell varied between the range of 47 -56 mN/m (van der Mei and Busscher, 1998). In this study, the surface free energy of *E. coli* XL1-blue cell surface is found 54.1 mN/m (Table 4.6) which is consistent with the values given in literature.

Although, the contribution of dispersive (γ^{LW}) component (ranging from 44 to 50 mN/m) in surface free energy is more significant than the polar (acid-base) (γ^{AB}) component (ranging from 1.3 to 16.6), there is no significant difference for the dispersive (γ^{LW}) component of surface free energy with SiO₂ addition as much as the polar (acid-base) (γ^{AB}) component. The acid base component (γ^{AB}) is generally established by carboxyl (-COOH), hydroxyl (OH⁻) and hydroperoxyl

(HO₂[•]) groups over the surface (Van Oss *et al.*, 1988; Marciano *et al.*, 2009; Roy *et al.*, 2009; Kinnari *et al.*, 2010). Therefore the increase in polar component (γ^{AB}) with silica loading can be associated by the increase in surface hydroxyl OH groups associated with silica surface. The total surface free energy (γ^{TOT}) of the samples increases with SiO₂ loading which is in good agreement with surface roughness and surface area.

The repulsive forces between the particles are caused by electron donor components over the solid surfaces (Schneider, 1996). In Figure 4.21, the electron donor components of the surface free energy of the SiO₂-TiO₂ samples are plotted with respect to the number of adhered cells. As the electron donor component of thin films increases, the number of adhered *E.coli* cells decreases indicating the repulsive forces between the thin film surface and *E.coli* cells which is parallel with the literature (Schneider, 1996). As seen from Table 4.6, for pure SiO₂, the electron donor component (γ^-) reaches its maximum value. Therefore reduction of number of bacterial adhesion at that point can be explained by the increase of repulsive force.

The contribution of surface free energy by polar component (γ^{AB}) is dominated by electron donor component (γ^-) for both thin film samples and *E.coli* surface rather than the electron acceptor component (γ^+). Thus, the *E.coli* cells and thin film surfaces are negatively charged (Su *et al.*, 2009) under the applied experimental conditions. Therefore, the *E.coli* adhesion should be determined by hydrophobic interactions significantly rather than the electrostatic interactions. In addition, higher value of the electron donor component than the electron acceptor component is another evidence of hydrophilic character of the SiO₂-TiO₂ sample surfaces (Busscher *et al.*, 1984; Ong *et al.*, 1999; Mafu *et al.*, 2011).

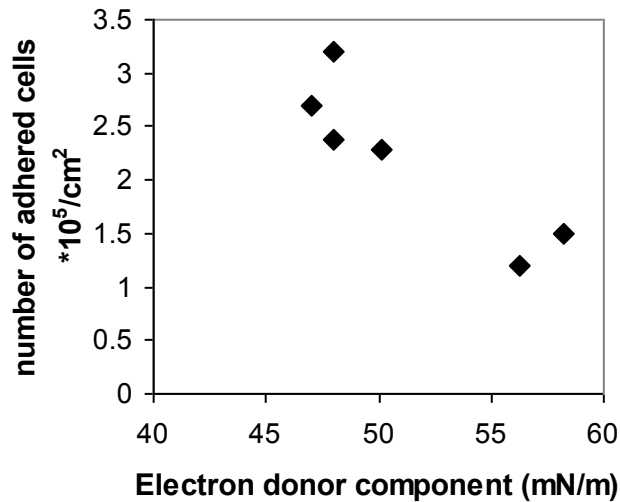


Figure 4.21 *E. coli* adhesion over the TiO₂-SiO₂ thin surface vs the electron donor component of thin films

In this study thermodynamic theory which describes bacterial adhesion considering attractive and repulsive interactions and expresses them in terms of surface free energy (SFE) was used to explain the change of bacterial adhesion change with SiO₂ addition.

4.6.2 Interfacial free energy of adhesion of *E.coli* on SiO₂-TiO₂ Thin Films

In order to understand the bacterial adhesion mechanism and relate the surface free energy of the thin film samples with *E.coli* adhesion, total interaction energy of adhesion was also calculated. As mentioned in part 2.8.1.2, mechanism of bacterial adhesion can be explained by work of adhesion (ΔF_{Adh}) or Gibbs free energy owing to bacterial adhesion (interfacial energy) (ΔG_{adh}) (Busscher *et al.*, 1984; ; Harnett *et al.*, 2007; Marciano *et al.*, 2010). Dupré equation relates the work of adhesion with interfacial surface tension (Absolom *et al.*, 1983).

$$\Delta F_{Adh} = \gamma_{SB} - \gamma_{SL} - \gamma_{BL} \quad (4.3)$$

where γ_{SB} , γ_{SL} and γ_{BL} are the solid -*E.coli* cell surface, the solid -aqueous solution and *E.coli* cell surface-aqueous solution interfacial free energies, respectively. γ_s and γ_B can not be measured directly. However the contact angle data with probe liquids can be utilized by using LW-AB approach by van Oss method (Van Oss *et al.*, 1988) to calculate γ_s and γ_B . The work of bacterial adhesion can be determined by equation 4.4.

$$\Delta F_{Adh} = 2 \left(\begin{array}{l} \sqrt{\gamma_s^{LW} \gamma_L^{LW}} + \sqrt{\gamma_s^+ \gamma_L^-} + \sqrt{\gamma_s^- \gamma_L^+} \\ + \sqrt{\gamma_B^{LW} \gamma_L^{LW}} + \sqrt{\gamma_B^+ \gamma_L^-} + \sqrt{\gamma_B^- \gamma_L^+} \\ - \sqrt{\gamma_s^{LW} \gamma_B^{LW}} - \sqrt{\gamma_s^+ \gamma_B^-} - \sqrt{\gamma_s^- \gamma_B^+} - \gamma_L \end{array} \right) \quad (4.4)$$

The solid-liquid (γ_{SL}), solid-bacteria (γ_{SB}) and bacteria-liquid (γ_{BL}) interfacial energy values and the work of adhesion of the thin film samples are shown in Table 4.7.

In order to account the difference between water and suspending medium (0.2 M PHS, pH=7.2), the solid-suspending liquid and bacteria-suspending liquid interfacial energies and surface tension of suspending medium were also measured. The surface tension of the suspending liquid media was obtained from contact angle measurements on the thin film surfaces with known surface free energy properties (Table 4.6) and was found as $\gamma_{PHS}^{Tot} = 65$ mN/m ($\gamma_{PHS}^{LW} = 44.30$ mN/m, $\gamma_{PHS}^+ = 4.64$ mN/m, and $\gamma_{PHS}^- = 23.05$ mN/m). Table 4.7 shows the results of the solid-suspending medium (γ_{SL}), solid-bacteria (γ_{SB}) and bacteria-suspending

medium (γ_{BL}) interfacial energy values and work of adhesion of the thin film surfaces.

Table 4.7 The solid-liquid (γ_{SL}), solid-bacteria (γ_{SB}) and work of adhesion of the thin film surfaces

SiO ₂ content (wt%)	0	49	60	74	85	92	95	100
γ_{SL} (mN/m)	-11.1	-8.5	-7.7	-8.5	-8.2	-5.2	-4.5	-11.0
γ_{SB} (mN/m)	0.3	2.0	2.00	1.2	1.2	1.7	1.7	0.9
ΔF_{Adh} (mN/m)	15.3	14.3	13.5	13.5	13.2	10.8	10.0	15.7

The interfacial energy between the bacteria and suspending liquid medium was determined as -3.8 mN/m. As seen from Table 4.7, the work of adhesion of TiO₂-SiO₂ thin film surfaces varies within the range of 15.7-10.0 mN/m². The interfacial energy between the thin film surfaces and suspending liquid media (γ_{SL}) and work of adhesion (ΔF_{Adh}) decreases significantly with the increase of SiO₂ weight fraction on SiO₂-TiO₂ thin films. As it is reported in the literature, the reduction of the absolute value of solid-liquid interfacial free energy (γ_{SL}) is the significant driving force for adhesion of any organic substance to surface from colloidal solution (Schneider, 1996). The solid-liquid interfacial free energy (γ_{SL}) of pure SiO₂ and pure TiO₂ was found higher (-11 mN/m) than all SiO₂-TiO₂ containing samples which indicates the synergy contributed by the addition of SiO₂ to TiO₂.

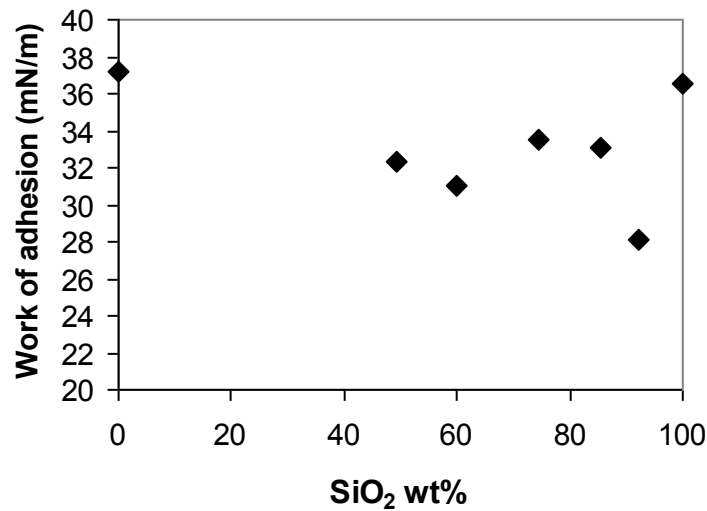


Figure 4.22 The effect of surface composition on work of adhesion (mN/m).

The relationship between the work of adhesion of *E.coli* cells to the composition of TiO₂-SiO₂ thin film surfaces (ΔF_{Adh}) are depicted in Figure 4.22. And the relationship between the work of adhesion and number of adhered cells are shown in Figure 4.23. As it can be seen from the Figure, thin film surfaces containing pure TiO₂ and pure SiO₂ perform very similar work of adhesion values. There is strong correlation between the work of adhesion and number of adhered cells ($R^2 = 0.7714$). Bacterial adhesion is favored by decreasing work of adhesion thermodynamically. Therefore, the number of adhered cells increases with increasing SiO₂ content. SiO₂-TiO₂ thin films become thermodynamically more favorable to bacterial adhesion with increasing SiO₂ loading and direct contact between TiO₂ and *E. coli* cells increases.

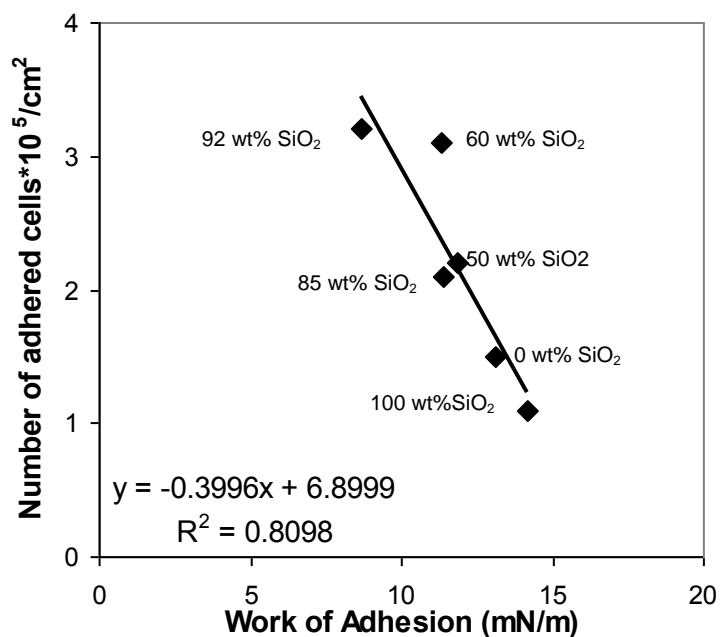


Figure 4.23 Effect of work of adhesion on number of adhered cells

The relationship between the work of adhesion of *E.coli* cells to TiO₂-SiO₂ thin film surfaces (ΔF_{Adh}) and antibacterial activity of thin films are shown on the Figure 4.24. As seen from the Figure, linear correlation was observed between the work of adhesion and antibacterial activity. Thus the increase in the photocatalytic antibacterial activity of TiO₂-SiO₂ thin films with the increase of SiO₂ loading, can be explained by the favored bacterial adhesion which enhances direct contact of bacteria with TiO₂ particles and surface ROS. These results and the proposed mechanism were strengthened by the additional control experiments. The photocatalytic antibacterial activity tests were also repeated with both adhered *E. coli* cells and suspending bacteria separately by isolating the each from the other.

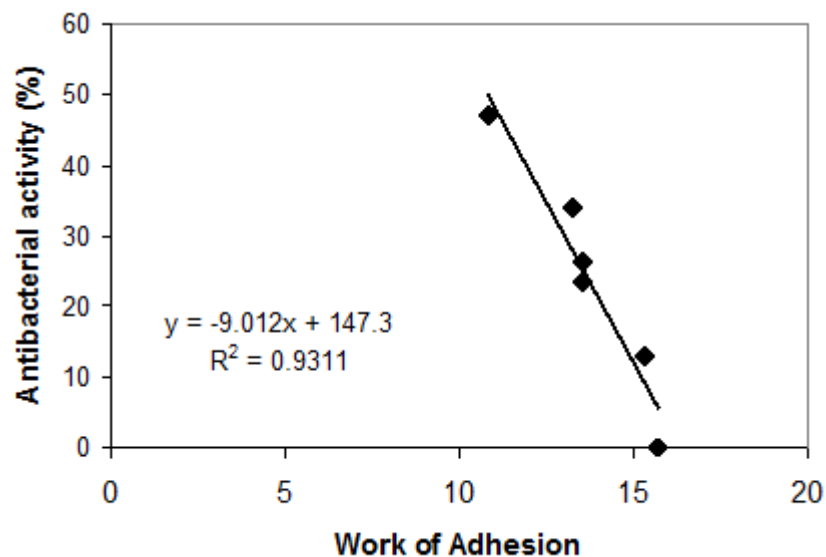


Figure 4.24 The effect of work of adhesion on antibacterial activity.

4.7 Antibacterial activity measurements of suspended *E.coli* cells and adhered *E.coli* cells

The survival ratio of *E.coli* in suspension over the 92 wt% SiO₂-TiO₂ sample surface was determined by removing adhered cells from the surface. Similarly the photocatalytic inactivation of adhered cells was measured with respect to time by removing suspended bacteria. Both experiments were performed under the same conditions (300 W/m²). The results are shown in Figure 4.25. The photocatalytic inactivation against suspended *E. coli* cells over 92% SiO₂-TiO₂ surface (♦), demonstrated two different kinetic regimes. The bacterial inactivation rate is very low during the first 15 min of irradiation which can be named as shoulder. The inactivation rate increases after this lag. On the other hand, when the inactivation performance of the substrate containing 92 wt% SiO₂ was examined against

adhered *E. coli* cells (■), almost constant inactivation rate was observed starting immediately after the irradiation was turned on.

In the former case, formation of the shoulder period can be explained by two reasons. The first reason can be the insufficient bacterial adhesion to the substrate surface. According to relevant literature, once bacteria are attracted to the surface which is performed by physicochemical interactions (such as; van der Waals forces, electrostatic attractions and hydrophobic interactions) (Busscher *et al.*, 1984; Bos&Busscher, 1999; Wang *et al.*, 2004; Bayoudh *et al.*, 2006) the formation of second phase of bacterial adhesion which is irreversible, molecular or cellular phase takes at least several hours (Marshall *et al.*, 1971; Hermansson *et al.*, 1999). Therefore, within the initial 15 min of the photocatalytic inactivation reaction, suspended *E. coli* cells may be attracted to surface and after this period the reaction rate can be increase. In addition the second reason of the time lag can be insufficient concentration of reactive oxygen species ROS in aqueous phase.

Considering the short life time period of free radicals, the probability of diffusion of reactive radicals from thin film surface to the cell wall of suspended bacteria without decay is very low. However, the formation of H₂O₂ and other ROS species might be produced by the interaction of H₂O and O₂ with •OH radicals is more probable.

In addition, the faster inactivation rate of substrate containing 92 wt% SiO₂ against adhered *E. coli* cells (■) which followed by shoulder can be explained by the initial stage of bacterial inactivation which is facilitated by direct attack of •OH species to the cell surface. Therefore the mass transfer resistance between the liquid phase and the cell surface is eliminated during the inactivation of adhered cells. As a result survival ratio of adhered cells starts to decrease with respect to time with irradiation without any time lag. In this case, higher concentration of ROS can attack to the cell surface and adhered cells are more readily inactivated by direct contact with the surface with higher rate. However,

after 20 min the inactivation reaction proceeds with a slower rate. This behavior has been attributed to the competition of free radicals such as $\cdot\text{OH}$ between remaining alive bacteria and organic species released from inactivated bacteria. These results are in good agreement with literature (Rincón and Pulgarin, 2004; Marugán *et al.*, 2008).

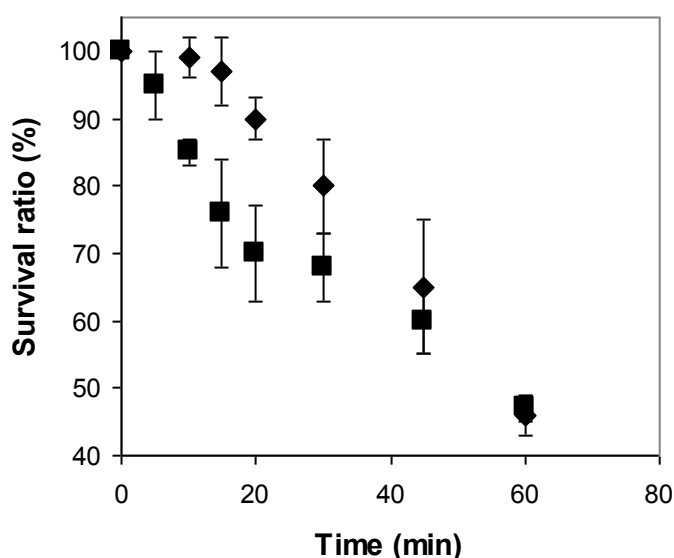


Figure 4.25 Effect of irradiation time on the survival ratio of suspended (◆) and adhered *E. coli* cells over the $\text{TiO}_2\text{-SiO}_2$ thin film surface containing 92 wt% SiO_2 (■). (Under 300 W/m^2 irradiation at $35 \text{ }^\circ\text{C}$).

4.8 Reusability Test of Thin Films

To check the life time and stability of the thin films the reusability tests were performed. For this purpose, the photocatalytic inactivation of *E. coli* cells over 92 wt% $\text{SiO}_2\text{-TiO}_2$ sample was examined by using suspensions containing initial

bacterial count of 10^7 - 10^8 cells/ml in phosphate buffer as described in part 3.6.1. Photocatalytic inactivation was examined under 300 W/m^2 irradiation in the Suntest solar simulator cabin at $35 \text{ }^\circ\text{C}$. After each use, thin film was cleaned with deionized water, and dried at $45 \text{ }^\circ\text{C}$ in dark for 24 h. As seen from the Figure 4.26 after second use, the photocatalytic activity of thin films begins to decrease.

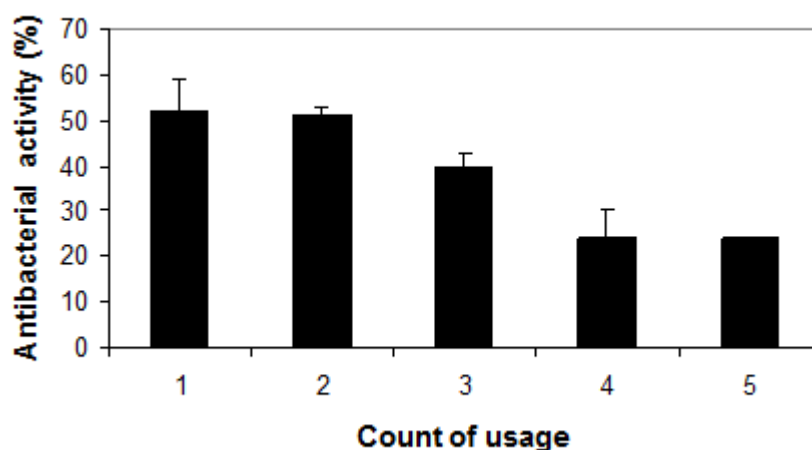


Figure 4.26 Effect of multiple use on the photocatalytic antibacterial activity of thin films under 1 h irradiation (300 W/m^2). Dilutions were done by using phosphate buffer.

There might be several reasons for the activity loss. Photo-erosion, surface contamination, poisoning, surface re-structuring, aging are the most common deactivation causes reported in literature (Sakai *et al.*, 1998; Wang *et al.*, 1998; Carp *et al.*, 2004). First the contamination and poisoning effect of phosphate buffer used during the antibacterial tests were tested by control experiments by using de-

ionized water instead of buffer solution. The experimental results showed similar activity loss after 3rd cycle as shown on Figure 4.27.

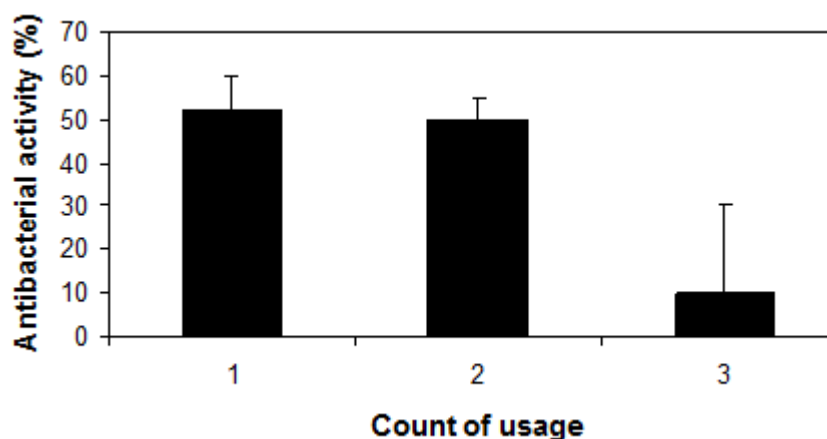


Figure 4.27 Effect of use on the photocatalytic antibacterial activity of thin films under 1 h irradiation (300 W/m^2). Dilutions were done by using de-ionized water.

The surface thermodynamic properties were also tested between the resubility cycles. It was realized that, after each reusability cycle, not only photocatalytic activity but also the wettability of the thin films decreases significantly. In this case, the decrease in photocatalytic performance can be attributed to reconversion of thin film surfaces from hydrophilic to hydrophobic form during the incubation of $\text{TiO}_2\text{-SiO}_2$ thin films in dark.

As mentioned in part 2.5, under irradiation, TiO_2 films became hydrophilic by the reaction of sensitized electrons and holes with surface ad-species. This phenomena is called as photo-induced hydrophilicity. In this process, trapped electrons reduced Ti^{4+} cations to Ti^{3+} and the holes oxidize the O_2^- anions and generated

the oxygen vacancies. Then the vacancies could be filled by adsorbed water. The surface decorated with more adsorbed OH species becomes more hydrophilic. On the other hand, in the dark, the reduced sites can be reoxidized by oxygen and hydroxyl groups desorbed from the surface which is called reversion process. The reversion process is slower than the photoinduced hydrophilicity phenomenon (Sakai *et al.*, 1998; Wang *et al.*, 1998; Wang *et al.*, 1999; Sakai *et al.*, 2001; Sun *et al.*, 2001; Yu *et al.*, 2003; Carp *et al.*, 2004).

In order to test the possibility of reversion is being a cause of activity loss during reusability cycles, the 92 wt% SiO₂-TiO₂ sample taken from the first antibacterial cycle was incubated in the dark for ten days instead of 24 h and photocatalytic inactivation performance test repeated. Another control experiment was performed by using UV irradiation to improve surface hydrophilicity. As it is shown in Figure 4.28, bacterial inactivation performance of thin film decreased 50 % when incubated in dark for ten days. However, when the sample was induced by UV light irradiation for 24h, the photocatalytic antibacterial performance replenished. These results indicated that, the cause of the reduction of the antibacterial activity of the thin films can be related with the reversion process of the surfaces in the dark which causes reduction of hydroxyl groups adsorbed on the surface.

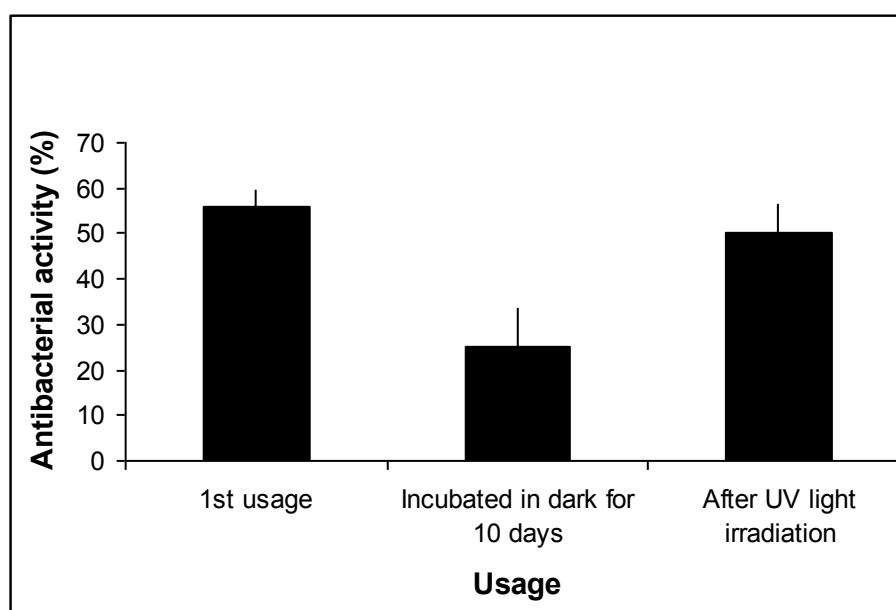


Figure 4.28 Effect of incubation in the dark and UV light irradiation on antibacterial activity of thin film containing 92 wt% SiO₂. 1 h irradiation at 300 W/m² was used.

4.9 Photo-induced hydrophilicity

The photo-induced hydrophilicity of TiO₂/SiO₂ thin films were characterized by measuring water contact angle over the thin films subjected to UV light irradiation for 4 h and incubated in dark for 24 h. The results are shown in Figure 4.29. No change was observed for the pure SiO₂ thin film indicating the lack of photoactivity. For pure TiO₂ sample, the contact angle was determined as 7 and 30 degrees for irradiation under UV light and incubated in dark, respectively. The effect of UV light irradiation on the water contact angle values is more pronounced on the samples containing higher SiO₂. The water contact angle values of thin films containing 85 wt% and 92 wt% SiO₂, approaches almost zero indicating superhydrophilicity.

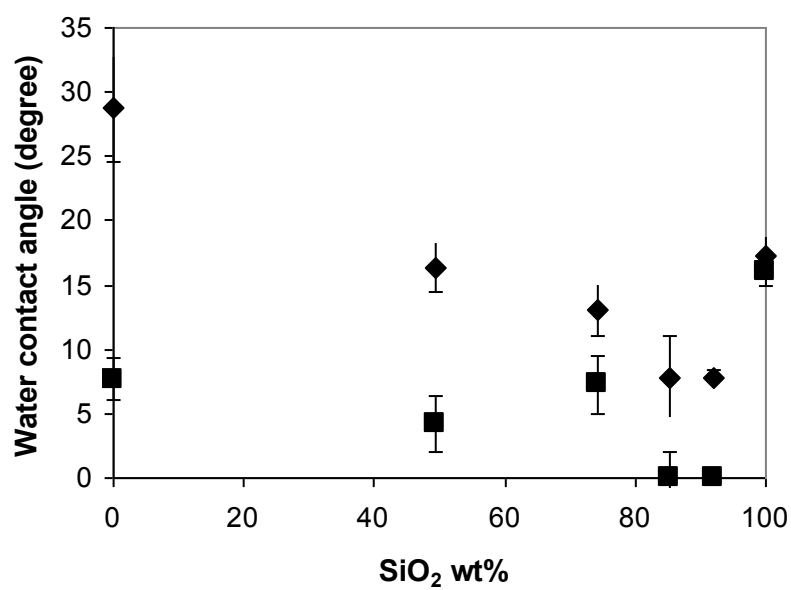


Figure 4.29 Effect of surface composition on the photo-induced change in water contact angle of TiO₂/SiO₂ thin films. (♦; after 4 h UV lamp irradiation, ■; after incubation in dark for 24 h)

CHAPTER 5

CONCLUSIONS

In this study, TiO₂-SiO₂ mixed oxides were synthesized by sol-gel method and coated over soda-lime glass plates as thin films by dip coating technique. The effect of SiO₂ addition on photocatalytic self-cleaning activity, photocatalytic antibacterial activity and the surface characteristics of TiO₂-SiO₂ thin films were investigated. Photocatalytic self-cleaning activity of the thin films was characterized through the degradation of MB molecules adsorbed over the thin film surfaces. *Escherichia coli* was chosen as a model bacterium to characterize the photocatalytic antibacterial activity of SiO₂-TiO₂ thin films. XRD, AFM, SEM, contact angle measurements, the relative surface area measurements by methylene blue (MB) adsorption technique were used for characterization of SiO₂-TiO₂ thin films. Based on the experimental results the following arguments can be put forward:

- Thin films containing pure TiO₂ show limited photocatalytic activity due to having glassy and smooth surfaces without roughness and pores.
- The addition of silica increased the surface roughness, porosity, thickness and relative surface area of thin films. It was understood that the increase in consistency of sol-gel solutions with SiO₂ addition affected the film thickness.
- When XRD analysis of thin films containing TiO₂-SiO₂ and pure TiO₂ samples were examined, it was seen that all samples have anatase structure. The crystallinity of thin film samples increased up to the degree where SiO₂ addition became 60 wt%. With the further addition of SiO₂, broader and weaker peaks were observed which indicated the presence of small crystallites of TiO₂ and dispersion of TiO₂ in SiO₂ matrix.

- Considering the increase in polar component (γ^{AB}) of surface free energy of thin films and decrease in water contact angle values of thin films with silica loading, addition of SiO₂ should increase surface OH⁻ groups and hydrophilic character of surfaces, respectively.
- The addition of SiO₂ enhanced the photocatalytic antibacterial and self-cleaning activity of TiO₂-SiO₂ thin films to a certain extent. However, the antibacterial and self-cleaning activities reached their maximum values on thin films having different SiO₂ contents.
- Antibacterial and self-cleaning activities reached their maximum values at different SiO₂/TiO₂ ratios. Because self-cleaning and antibacterial activities are controlled by different textural and surface properties.
- The relative surface area of thin films was proportional to the total amounts of MB molecules adsorbed over the surface.
- The maximum initial reaction rate constant of photocatalytic degradation of MB of TiO₂-SiO₂ thin film was obtained as the result of the increase in crystallinity but independent of the total amounts of MB molecules adsorbed over the surface. Therefore, it can be concluded that initial reaction rate of photocatalytic degradation of MB is directly proportional with crystallite size and crystallinity.
- The maximum antibacterial activity is observed over the same surface composition where bacterial adhesion reaches to its maximum value. Hence, the enhancement of photocatalytic antibacterial activity with the addition of SiO₂ can be attributed to improving dispersion and accessibility of TiO₂ particles.
- Inactivation reaction of *E. coli* cell is mainly through the surface bounded ROS produced by TiO₂ rather than free bulk phase ROS.
- Thermodynamic calculations showed that thin films became thermodynamically more favorable to bacterial adhesion with increasing SiO₂ loading and at the same time, direct contact between TiO₂ and *E. coli* cells increased. Direct contact between TiO₂ and *E. coli* cells

facilitated the interaction of surface ROS such as, $\bullet\text{OH}$, $\text{O}_2^{\bullet-}$, and H_2O_2 with cell surface during the photocatalytic reaction. In this case, during the diffusion of ROS from liquid phase to the cell wall, mass transfer limitation reduced and more ROS could attack the cell wall.

- Through the quantitative understanding of adhesion degree of *E. coli* cell to the thin film surfaces and inactivation rate of *E. coli* cells over the thin film surfaces containing different amount of SiO_2 , the importance of the formation of direct contact between the *E. coli* cell and thin film surface for photocatalytic antibacterial activity of $\text{TiO}_2\text{-SiO}_2$ thin films was clarified for the first time. It was understood that with the increasing weight ratio of SiO_2 , the amount of adsorbed *E. coli* cells per TiO_2 particles also increased due to the larger surface area and by this way photocatalytic antibacterial activity of $\text{TiO}_2\text{-SiO}_2$ thin films also increased.
- The cause of the reduction of the antibacterial activity of the thin films after second usage can be related with the reconversion process of the surfaces in the dark which causes reduction of hydroxyl groups adsorbed on the surface.
- The present study shows the significance of the use of porous silica nanoparticles to realize high photocatalytic performance which increases surface OH^- groups, hydrophilic character, surface area and adsorption capacity of surfaces.

REFERENCES

Abdullah H. A., Gaya I. U., “Heterogeneous photocatalytic degradation of organic contaminants over titanium dioxide: A review of fundamentals, progress, and problems” *Journal of Photochemistry and Photobiology C: Photochemistry Reviews* 9 (2008) 1

Absolom, D. R., Lamberti F. V., Policova Z., Zingg W., Van Oss C. J, and Neumann A. W., “Surface thermodynamics of bacterial adhesion” *Applied Environmental Microbiology* 46 (1983) 90

Adamson W. A., Gast P. A., “*Physical Chemistry of Surfaces* 6th Edition, Wiley, New York, 1997 (Chapter X)

Ahn H. B., Ahn J. S., Lee S. J., Kim T. W., Nahm D. S., “Analysis of surface roughness and surface free energy characteristics of various orthodontic materials” *American Journal of Orthodontics and Dentofacial orthopedics* 136 (5) (2009) 668

Al-Salim NY, Abagshaw S, Bittar A, Kemmett T, McQuilla AJ, Mills AM, “Characterization and activity of sol-gel prepared TiO₂ photocatalysts modified with Ca, Sr or Ba additives” *Journal of Materials Chemistry* 10 (2000), 2358.

An Y. H., Friedman R. J., “Concise review of mechanisms of bacterial adhesion to biomaterial surfaces” *Journal of biomedical materials research* 43 (1998) 338

Anderson, C., and Bard, J. A., “An Improved Photocatalyst of TiO₂/SiO₂ Prepared by a Sol-Gel Synthesis” *Journal of Physical Chemistry* 99 (1995) 9882

Anderson C., and Bard J. A., “Improved Photocatalytic Activity and Characterization of Mixed $\text{TiO}_2/\text{SiO}_2$ and $\text{TiO}_2/\text{Al}_2\text{O}_3$ Materials” *Journal of Physical Chemistry B* 101 (1997) 2611

Anpo M., Nakaya H., Kodama S., Kubokawa Y., Domen K., and Onishi T., “Photocatalysis over binary metal oxides. Enhancement of the photocatalytic activity of titanium dioxide in titanium-silicon oxides” *Journal of Physical Chemistry* 90 (1986) 1633

Anpo, M., “Use of visible light. Second-generation titanium oxide photocatalysts prepared by the application of an advanced metal ion-implantation method” *Pure Applied Chemistry*, 72 (9), (2000) 1787

Anpo, M., and Takeuchi, M., “The design and development of highly reactive titanium oxide photocatalysts operating under visible light irradiation” *Journal of Catalysis* 216 (2003) 505

Asadinezhad A., Novák I., Lehoccky M., Sedlarak V, Vesel A., Junkar I., Sába P. , Chodák I., “A Physicochemical Approach to Render Antibacterial Surfaces on Plasma-Treated Medical-Grade PVC: Irgasan Coating” *Plasma and Processes Polymers* 7 (2010) 504

Brant, J.A., Childress, A.E. “Assessing short-range membrane–colloid interactions using surface energetics” *Journal of Membrane Science* 203 (2002) 25

Banerjee, S., Gopal, J., Muraleedharan, P., Tyagi, K. A., Roj, B., “Physics and chemistry of photocatalytic titanium dioxide: Visualization of bactericidal activity using atomic force microscopy” *Current Science* 90 (2006) 1378

Bayouhd S., Othmane A., Bettaieb F., Bakhrouf A., Ben Ouada H., Ponsonnet L., “Quantification of the adhesion free energy between bacteria and hydrophobic and hydrophilic substrata” *Material Science and Engineering* 26 (2006) 300

Benabbou A. K., Derriche Z., Felix C., Lejeune P., Guillard C., “Photocatalytic inactivation of *Escherichia coli* Effect of concentration of TiO₂ and microorganism, nature and intensity of UV irradiation” *Applied Catalyst B: Environmental* 76 (2007) 257

Bendavid A., Martin P. J., Randeniya L., Amin M. S., “The properties of fluorine containing diamond-like carbon films prepared by plasma enhanced chemical vapor deposition.” *Diamond Related Material* 18 (2009) 66

Bickley R. I., Gonzales-Carreno T., Lees J. L., Palmisano L., Tilley RDJ. “A structural investigation of titanium dioxide photocatalysts” *Journal of Solid State Chemistry* 92 (1991) 178

Blanco J., Avila P., Bahamonde A., Alvarez E., Sanchez B., Romero M., “Photocatalytic destruction of toluene and xylene at gas phase on a titanium based monolithic catalyst” *Catalyst Today* 29 (1996) 437

Boland T, Latour RA, Stutzenberger FJ. “Molecular basis of bacterial adhesion. In: An YH, Friedman RJ, eds. Handbook of bacterial adhesion.” Totowa, NJ: Humana Press, 2000; 29.

Bos R., Busscher H. J., “ Role of acid–base interactions on the adhesion of oral streptococci and actinomyces to hexadecane and chloroform—influence of divalent cations and comparison between free energies of partitioning and free energies obtained by extended DLVO analysis ” *Colloids and Surfaces B: Biointerfaces* 14 (1999) 169

Brinker C.J. and Scherer G.W., *Sol-Gel Science: The Physics and Chemistry of Sol-Gel Processing*, Academic Press, New York, (1990).

Brinker C.J., Hurd A.J., Schunk P.R., Frye G.C. and Ashley C. S., “Review of Sol-Gel Thin Film Formation”, *Journal of Non-Crystalline Solids*, 147 (1992) 424

Bui D. C., Kang S. Z., Li X., Mu J., “Effect of Si doping on the photocatalytic activity and photoelectrochemical property of TiO₂ nanoparticles” *Catalysis Communications* 13 (2011) 14

Burks, G. A., Velegol, S. B., Watson, E. U., Lindenmuth, B. E., Feick, J. D., Logan B. E. “Macroscopic and Nanoscale Measurements of the Adhesion of Bacteria with Varying Outer Layer Surface Composition” *Langmuir* 19 (6) (2003) 2366.

Busscher HJ, van Pelt AWJ, de Boer P, de Jong HP, Arends J. “The effect of surface roughening of polymers on measured contact angles of liquids.” *Colloids Surfaces* 9 (1984) 319

Busscher HJ., Weerkamp AH., ven der Mei HC., van Pelt AW, de Jong HP., Arends J., “Measurement of the surface free energy of bacterial cell surfaces and its relevance for adhesion” *Applied Environmental Microbiology* 48 (1984) 980

Camera-Roda G., Santarelli F., “Optimization of the thickness of a photocatalytic film on the basis of the effectiveness factor” *Catalysis Today* 129 (2007) 161

Carp O., Huisman L. C., Reler A. “Photoinduced reactivity of titanium dioxide” *Progress in Solid State Chemistry* 32 (2004) 33

Černigoj U., Štangař L. U., Trebše P., Krašovec O. U., Gross S., “Photocatalytically active TiO₂ thin films produced by surfactant-assisted sol-gel processing” *Thin Solid Films* 495 (2006) 327

Chandrasekharan, N., Kamat, P. V. “Improving the Photoelectrochemical Performance of Nanostructured TiO₂ Films by Adsorption of Gold Nanoparticles” *Journal of Physical Chemistry B* 104 (2000) 10851

Chen D., Li F., Ray K. A., “External and internal mass transfer effect on photocatalytic degradation” *Catalysis Today* 66 (2001) 475

Chen G., Zhu H., “Bacterial adhesion to silica sand as related to Gibbs energy variations” *Colloids and Surfaces B: Biointerfaces* 44 (2005) 41

Chen, F., Yang, X., Wu, Q., “Antifungal capability of TiO₂ coated film on moist wood” *Building and Environment* 44 (2009) 1088

Chien M. D., Viet N.N., Van K.T.N., Phong P.T.N.,” Characteristics modification of TiO₂ thin films by doping with silica and alumina for self-cleaning application” *Journal of Experimental Nanoscience* 4 (2009) 15

Cho, M., Chung, H., Yoon, J., “Disinfection of Water Containing Natural Organic Matter by Using Ozone-Initiated Radical Reactions” *Applied Environmental Microbiology* 69 (2003) 2284

Cho M., Chung H., Choi W., Yoon J., “Linear correlation between inactivation of E. coli and OH radical concentration in TiO₂ photocatalytic disinfection” *Water Research* 38 (2004) 1069

Cho M., Chung H., Choi W., Yoon J., “Different Inactivation Behaviors of MS-2 Phage and Escherichia coli in TiO₂ Photocatalytic Disinfection” *Applied And Environmental Microbiology* 71 (2005) 270

Chong N. M., Jin B., Chow C., “Recent developments in photocatalytic water treatment technology: A review” *Water Research* 44 (2010) 2997

Chun M., Shim E., Kho E., Park K., Jung J., Kim J., Kim B., Ki-Heon L. “Surface Modification of Orthodontic Wires with Photocatalytic Titanium Oxide for its Antiadherent and Antibacterial Properties” *Angle Orthodontist*, 77 (2007) 483

Dagan, G., Sampath, S., Lev, O., “Preparation and Utilization of Organically Modified Silica-Titania Photocatalysts for Decontamination of Aquatic Environments” *American Chemical Society* 7 (1995) 446

Daoud A. W., Xin H. J., “Nucleation and growth of anatase crystallites on cotton fabrics at low temperatures” *Communications of American Ceramic Society* 87(5) (2004) 953-955

Deng X., Yue Y. Gao Z., “Gas-phase photo-oxidation of organic compounds over nanosized TiO₂ photocatalysts various preparation” *Applied Catalysis B: Environmental* 39 (2002) 135

Desai, S. V., Kowshik, M. “Antimicrobial activity of titanium dioxide nanoparticles synthesized by sol-gel technique” *Research Journal of Microbiology* 4(3) (2009) 97

Diebold U., “The surface science of titanium dioxide” *Surface Science Reports* 48 (2003) 53-22

- Ding, Z., Lu, G.Q., Greenfield, P. F., "Role of the Crystallite Phase of TiO₂ in Heterogeneous Photocatalysis for Phenol Oxidation in Water" *Journal of Physical Chemistry B* 104 (2000) 4815
- Ding H., Sun H., Shan Y., "Preparation and characterization of mesoporous SBA-15 supported dye-sensitized TiO₂ photocatalyst" *Journal of Photochemistry and Photobiology A* 169 (2005) 101
- Djambazov S., Ivanova Y., Yoleva A., "Ceramic Pigments on the Base of the CoO-ZnO-SiO₂ System Obtained by a Sol-Gel Method" *Ceramics Internationals* 24 (1998) 281
- Dobosz, A., Sobczykński, A. "The influence of silver additives on titania photoactivity in the photooxidation of phenol" *Water Research* 37 (2003) 1489
- Doshi S., Takeuchi M., Anpo M., "Effect of the local structure of Ti-oxide species on the photocatalytic reactivity and photo-induced super-hydrophilic properties of Ti/Si and Ti/B binary oxide thin films" *Catalysis Today* 85 (2003) 19
- Erdural B.K., Yurum A., Bakir U., Karakas G., Hydrothermal Synthesis of Nanostructured TiO₂ Particles and Characterization of Their Photocatalytic Antimicrobial Activity, *Journal of Nanoscience and Nanotechnology*, 8(2), (2008) 878-886.
- Erkan A., Bakir U., Karakas G., "Photocatalytic microbial inactivation over Pd doped SnO₂ and TiO₂ thin films" *Journal of Photochemistry and Photobiology A: Chemistry* 184 (2006) 313-321

Faille C., Jullien C., Fontaine F., Bellon-Fontaine M., Slomianny C “Adhesion of *Bacillus* spores and *Escherichia coli* cells to inert surfaces: role of surface hydrophobicity” *Canadian Journal of Microbiology* 28 (2002) 728

Feng L., Li S., Li Y., Li H., Zhang L., Zhai J., Zhu D., “Super-hydrophobic surfaces: From natural to artificial” *Advanced Materials* 14 (2002) 1857

Fletcher M., “The Effects of Methanol, Ethanol, Propanol and Butanol on Bacterial Attachment to Surfaces”, *Journal of General Microbiology* 129 (1983) 633

Fox, M. A., Dulay, M. T. “Heterogeneous photocatalysis” *Chemical Reviews* 93 (1993) 341

Fu X., Louis A., Clark A., Yang Q., Anderson A., “Enhanced photocatalytic performance of Titania-based binary metal oxides: $\text{TiO}_2/\text{SiO}_2$ and $\text{TiO}_2/\text{ZrO}_2$ ” *Environmental Science and Technology* 30 (1996) 647

Fujishima A., Rao N.T., Tryk A.D, “Titanium dioxide photocatalysis”, *Journal of Photochemistry and Photobiology C*, 1 (2000) 1

Gallardo-Moreno A. M., Gonzalez-Martin M.L., Bruque J.M., Perez-Giraldo C., “The adhesion strength of *Candida parapsilosis* to glass and silicone as a function of hydrophobicity, roughness and cell morphology” *Colloids and Surfaces A: Physicochem. Eng. Aspects* 249 (2004) 99

Gao X., Bare R. S., Fierro G. L. J., Banares A. M., Wachs E. I. “Preparation and in-situ spectroscopic characterization of molecularly dispersed titanium oxide on silica” *Journal of Physical Chemistry* 102 (1998) 5653

Gao, X., Wachs, E. I., “Titania-silica as catalysts: molecular structural characteristics and physico-chemical properties” *Catalysis Today* 51 (1999) 233

Gao L, McCarthy TJ., "Contact angle hysteresis explained." *Langmuir* 22 (2006) 6234

Genzer, J., Efimenko, K., "Recent developments in superhydrophobic surfaces and their relevance to marine fouling: a review" *Biofouling* 22 (2006) 339

Gregg, S. J. and Sing, K. S. W. "Adsorption, Surface Area and Porosity", 2nd ed., 61-84, Academic Press, London, 1982

Giese R., van Oss J. C. "Colloid and surface properties of clays and related minerals" Surfactant science series Volume 105, Marcel Dekker Inc, New York, (2002)

Gottenbos B, Busscher HJ, Van Der Mei HC, Nieuwenhuis P "Pathogenesis and prevention of biomaterial centered infections." *Journal of Material Science: Materials in Medicine* 13 (2002) 717.

Grela M.A., Coronel M.E.J. and Colussi A.J., "Quantitative Spin-Trapping Studies of Weakly Illuminated Titanium Dioxide Solutions: Implications for the Mechanism of Photocatalysis" *Journal of Physical Chemistry* 100 (1996) 16940

Grieken van R., Marugán J., Sordo C., Pablos C., "Comparison of the photocatalytic disinfection of *E. coli* suspensions in slurry, wall and fixed-bed reactors" *Catalysis Today* 144 (2009) 48

Guan K., Lu B., Yin Y., "Enhanced effect and mechanism of SiO₂ addition in super-hydrophilic property of TiO₂ films" *Surface and Coatings Technology* 173 (2003) 219

- Guan K., “Relationship between photocatalytic activity, hydrophilicity and self-cleaning effect of TiO₂/SiO₂ films” *Surface and Coatings Technology* 191 (2005) 155
- Guan KS., Yin YS., “Effect of rare earth addition on super-hydrophilic property of TiO₂/SiO₂ composite film” *Materials Chemistry and Physics* 92 (2005) 10
- Hadnadjev M., Ranogajec J., Petrovic S., Markova S., Ducmanb V., Neducina M. R., “Design of self-cleaning TiO₂ coating on clay roofing tiles” *Philosophical Magazine* 90 (2010) 2988
- Hague D. C., Mayo M. J., “Controlling crystallinity during processing of nanocrystalline titania” *Journal of American Ceramic Society* 77 (1994) 1957
- Hajkova, P., Spatenka, P., Horsky, J., Horska, I., Kolouch, A., “Photocatalytic Effect of TiO₂ Films on Viruses and Bacteria” *Plasma Processes and Polymers* 4 (2007) 397
- Hamadi F., Latrache H., Zekraoui M., Ellouali M., Bengourramb J. “Effect of pH on surface energy of glass and Teflon and theoretical prediction of *Staphylococcus aureus* adhesion” *Materials Science and Engineering C* 29 (2009) 1302
- Hannay B. N. “Semiconductors” American Chemical Society, London, 1959
- Harnett E. M., Alderman J., Wood T., “The surface energy of various biomaterials coated with adhesion molecules used in cell culture” *Colloids and Surfaces B: Biointerfaces* 55 (2007) 90

Hattori A., Kawahara T., Uemoto T., Suzuki F., Tada H., Ito S., "Ultra thin SiO_x Film Coating Effect on the Wettability Change of TiO₂ Surfaces in the Presence and Absence of UV Light Illumination" *Journal of Colloid and Interface Science* 232 (2000) 410

Hermansson M., "The DLVO theory in microbial adhesion" *Colloids and Surfaces B: Biointerfaces* 14 (1999) 105

Hewitt J., "Formulating water-resistant TiO₂ sunscreens" *Cosmetics and Toiletries* 114 (1999) 59

Hoffman M.R., Martin S.T., Choi W. and Bahnemann D.W., Environmental Applications of Semiconductor Photocatalysis, *Chemistry Reviews*, 95(1), 69-96, (1995).

Hogt, A. H.; Dankert, J.; de Vries, J. A.; Feijen, J., "Adhesion of coagulase-negative staphylococci to biomaterials." *Journal of General Microbiology* 129 (1983) 129-139

Huang N., Xiao Z., Huang D., Yuan C., "Photochemical disinfection of *Escherichia coli* with a TiO₂ colloid solution and a self assembled TiO₂ thin film", *Supramolecular Science* 5 (5-6) (1998) 559

Huang Z., Maness C. P., Blake M. D., Wolfrum J. E., Smolinski L. S., Jacoby A. W., "Bacterial mode of titanium dioxide photocatalysis" *Journal of Photochemistry and Photobiology A* 130 (2000) 163

Gartner M.; Trapalis C.; Todorova N.; "Doped sol-gel TiO₂ films for biological applications" *Bulletin of the Korean Chemical Society* 29 (5) (2008) 1038

İnel O., Tümsek F., “The measurement of surface areas of some silicate bu solution adsorption” *Turkish Journal of Chemistry* 24 (2000) 9

Ireland C. J., Klostermann P., Rice W. E., Clark M. R. “Inactivation of *Escherichia coli* by Titanium Dioxide photocatalytic oxidation” *Applied and Environmental Microbiology* 59 (1993) 1668

Itoh M., Hattori H., Tanabe K., “The acidic properties of TiO₂-SiO₂ and its catalytic activities for the amination of phenol, the hydration of ethylene and the isomerization of butane” *Journal of Catalysis* 35 (1974) 225

Jade Database

Jafry, H. R., Liga, V. M., Li, Q., Barron, R. A., “Simple Route to Enhanced Photocatalytic Activity of P25 Titanium Dioxide Nanoparticles by Silica Addition” *Environmental Science and Technology* 45 (2011) 156

Jucker, A. B., Harms, H., Zehnder, A., “Adhesion of the Positively Charged Bacterium *Stenotrophomonas (Xanthomonas) maltophilia* 70401 to Glass and Teflon” *Journal of Bacteriology* 178 (1997) 5472

Jung Y. K., Park B. S., “Anatase-phase titania: preparation by embedding silica and photocatalytic activity for the decomposition of trichloroethylene“ *Journal of Photochemistry and Photobiology A*. 127 (1999) 117

Kang, X., Chen, S., “Photocatalytic reduction of methylene blue by TiO₂ nanotube arrays: effects of TiO₂ crystalline phase” *Journal of Material Science* (45) 2010 2696

Kajihara K., Nakanishi K., Tanaka K., Hirao K., Soga N., "Preparation of macroporous titania thin films by a sol-gel dip-coating method from a system containing Poly(ethylene glycol)" *Journal of American Ceramic Society* 81 (1998) 2670

Kamat V. P. "Photoinduced transformations in semiconductor-metal nanocomposite assemblies" *Pure Applied Chemistry* 74 (9) (2002) 1693

Kaneco, S., Shimizu, Y., Ohta, K., Mizuno, T., "Photocatalytic reduction of high pressure carbon dioxide using TiO₂ powders with a positive hole scavenger" *Journal of Photochemistry and Photobiology A: Chemistry* 115 (1998) 223

Kato K., Tsuzuki A., Taoda H., Torii Y., Kato T., Butsugan Y., "Crystal structures of TiO₂ thin coatings prepared from the alkoxide solution via the dip-coating technique affecting the photocatalytic decomposition of aqueous acetic acid", *Journal of Material Science* 29 (1994) 5911

Katsikogianni M., and Missirlis Y.F., "Concise review of mechanisms of bacterial adhesion to biomaterials and of techniques used in estimating bacteria material interactions" *European Cells and Materials* 8 (2004) 37

Kikuchi Y., Sunada K., Iyoda T., Hashimoto K., Fujishima A., "Photocatalytic bactericidal effect of TiO₂ thin films: dynamic view of the active oxygen species responsible for the effect" *Journal of Photochemistry and Photobiology A* 106 (1997) 51

Kim, D. H., Hong, H. S., Kim, S.J., Song, S. J., Lee, K. S. "Photocatalytic behaviors and structural characterization of nano-crystalline Fe-doped TiO₂ synthesized by mechanical alloying" *Journal of Alloys and Compounds* 375 (2004), 259

Kinnari T. J., Esteban J., Zamora N., Fernandez R., López-Santos C., Yubero F., Mariscal D., Puertolas J. A., Gomez-Barrena E., “Effect of surface roughness and sterilization on bacterial adherence to ultra-high molecular weight polyethylene” *Clinical Microbiology and Infection* 16 (7) (2010) 1036

Kipling, J. J. “Adsorption from Solutions of Non-electrolytes”, Academic Press, London, 1965.

Kiwi, J. and Nadtochenko, V. “New Evidence for TiO₂ Photocatalysis during Bilayer Lipid Peroxidation” *Journal of Physical Chemistry B* 108 (2004) 17675

Kumar S.R., Suresh C., Vasudevan K.A., Suja N.R., Mukundan P., Warriar K.G.K., “Phase transformation in sol–gel titania containing silica” *Materials Letters* 38 (1999) 161

Kühn P. K., Chaberny F. I., Massholder K., Stickler M., Benz W. V., Sonntag G. H., Erdinger L., “Disinfection of surfaces by photocatalytic oxidation with titanium dioxide and UVA light” *Chemosphere* 53 (2003) 7

Kwon H. C., Kim H. J., Jung S. I., Shin H., Yoon H. K., “Preparation and characterization of TiO₂-SiO₂ nano-composite thin films” *Ceramics International* 29 (2003) 851

Lan Y., Hu C., Hu X., Qu J., “Efficient destruction of pathogenic bacteria with AgBr/TiO₂ under visible light irradiation”, *Applied Catalysis B: Environmental* 73 (2007) 354

Lasa de H., Serrano B., Salaices M., “Photocatalytic Reaction Engineering” Springer, New York, 2005

Lee D., Choi Y. "Preparation of photocatalytic TiO₂-SiO₂ thin films by sol-gel coating" *Metal and Materials* 10 (2004) 357

Li, X. Z., Li, F. B., Fanc, C. M., Sunc, Y. P., "Photoelectrocatalytic degradation of humic acid in aqueous solution using a Ti/TiO₂ mesh photoelectrode" *Water Research* 36 (2002) 2215

Li B., Logan E. B., "Bacterial adhesion to glass and metal-oxide surfaces" *Colloids and Surfaces B: Biointerfaces* 36 (2004) 81

Lichter, J. A., Vliet, K. J. V., Rubner, M. F., "Design of Antibacterial Surfaces and Interfaces: Polyelectrolyte Multilayers as a Multifunctional Platform" *Macromolecules* 42 (2009) 8573

Lin J., Yu C. J., Lo D., Lamy S. K. "Photocatalytic Activity of Rutile Ti_{1-x}Sn_xO₂ Solid Solutions" *Journal of Catalysis* 183 (1999) 368

Lin HX, Xu ZT, Wang XX, Long JL, Su WY, Fu XZ, Lin Q, "Photocatalytic and Antibacterial Properties of Medical-Grade PVC Material Coated With TiO₂ Film" *Journal of Biomedical Materials Research B* 87B (2008) 42

Linsebigler, L. A., Lu, G., and Yates, J. T., "Photocatalysis on TiO₂ Surfaces: Principles, Mechanisms and Selected Results" *Chemical Reviews* 95 (1995) 735

Liu, Z., and Davis, R. J., "Investigation of the Structure of Microporous Ti-Si Mixed Oxides by X-ray, UV Reflectance, FT-Raman, and FT-IR Spectroscopies," *Journal of Physical Chemistry* 98 (1994) 1253.

Liu Y., Yang S. F., Li Y., Xu H., Qin L., Tay J. H., “The influence of cell and substratum surface hydrophobicities on microbial attachment” *Journal of Biotechnology* 110 (2004) 251

Liu C., Zhao Q., Liu Y., Wang S., Abel E. W., “Reduction of bacterial adhesion on modified DLC coatings” *Colloids and Surfaces B: Biointerfaces* 61 (2008) 182

Livage, J.; Henry, M.; Sanchez, C., “ Sol-gel chemistry of transition metal oxides” *Progress in Solid State Chemistry* 18 (1988) 259

Lonnena, J., Kilvingtona S., Kehoe, S.C., Al-Touati, F., McGuigan, K.G. “Solar and photocatalytic disinfection of protozoan, fungal and bacterial microbes in drinking water” *Water Research* 39 (2005) 877

Ma, C., Lee, Y. L., Hong, G. H., Su, T., Shie, J., Chang, C., “Effect of platinum on the photocatalytic degradation of chlorinated organic compound” *Journal of Environmental Sciences* 23 (2011) 687

Machida M., Norimoto K., Watanabe T., Hashimoto K., Fujishima A., “The effect of SiO₂ addition in super-hydrophilic property of TiO₂ photocatalyst” *Journal of Material Science* 34 (1999) 2569

Macwan, D. P., Dave, P. N. “A review on nano-TiO₂ sol-gel type syntheses and its applications” *Journal of Material Science* 46 (2011) 3669

Mafu, A. A.; Roy, D.; Goulet, J.; Savoie, L. “Characterization of physicochemical forces involved in adhesion of *Listeria monocytogenes* to surfaces.” *Applied Environmental Microbiology* 57 (1991) 1969

Mafu, A. A., Plumety, C., Deschenes, L., and Goulet J., "Adhesion of Pathogenic Bacteria to Food Contact Surfaces Influence of pH of Culture" *International Journal of Microbiology* (2011) 1

Mahanty, S., Roy, S., Sen S., "Effect of Sn doping on the structural and optical properties of sol-gel TiO₂ thin films" *Journal of Crystal Growth* 261 (2004) 77

Mandelbaum P., Regazzoni A., Belsa M., Bilmes S., "Photo-electro-oxidation of alcohols on titanium dioxide thin film electrodes" *Journal of Physical Chemistry B* 103 (1999) 5505

Maneerat, C., Hayata, Y., "Antifungal activity of TiO₂ photocatalysis against *Penicillium expansum* in vitro and in fruit tests" *International Journal of Food Microbiology* 107 (2006) 99

Maness C. P., Smolinski S., Blake M. D., Huang Z., Wolfrum E. J., Jacoby A. W., "Bacterial activity of photocatalytic TiO₂ reaction: toward an understanding of its killing mechanism" *Applied Environmental Microbiology* 65 (1999) 4094

Marciano F. R., Lima-Oliveira D. A., Da-Silva N. S., Diniz A. V., Corat E.J, Trava-Airoldi V. J. "Antibacterial activity of DLC films containing TiO₂ nanoparticles" *Journal of Colloid and Interface Science* 340 (2009) 87

Marciano F. R., Lima-Oliveira D. A., Da-Silva N. S., Corat E. J., Trava-Airoldi V. J., "Antibacterial activity of fluorinated diamond-like carbon films produced by PECVD" *Surface and Coating Technology* 204 (2010) 2986

Markowska-Szczupaka, A., Ulfigb, K., Morawski, A.W., "The application of titanium dioxide for deactivation of bioparticulates: An overview" *Catalysis Today* 169 (2011) 249

Marugán J., Grieken R., Sordo C., Cruz C., “Kinetics of the photocatalytic disinfection of *Escherichia coli* suspensions” *Applied Catalysis B: Environmental* 82 (2008) 27

Marshall, K.C., Stout, R., Mitchell, R. “Mechanism of the initial events in the sorption of marine bacteria to surfaces” *Journal of General Microbiology* 68 (1971) 337

Matsunaga T., Tomoda R., Nakajima T., Wake H., “Photoelectrochemical sterilization of microbial cells by semiconductor powders”, *Fems Microbiology Letters* 29 (1985) 211

Matsunaga T., Tomoda R., Nakajima T., Nakamura N., Komine T., “Continuous-sterilization system that uses photosemiconductor powders” *Applied and Environmental Microbiology* 54 (1988) 1330

Mccullagh C., Robertson C. J., Bahnemann W. D., Robertson J. K., “The application of TiO₂ photocatalysis for disinfection of water contaminated with pathogenic micro-organisms: a review” *Research on Chemical Intermediates* 33 (2007) 359

Meacock G., Taylor K. D. A. , Knowles M, Himonides A., “The improved whitening of minced cod flesh using dispersed titanium dioxide” *Journal of the Science of Food Agriculture* 73 (1997) 221

Mills A., Hunte Le S., “An overview of semiconductor photocatalysis” *Journal of Photochemistry and Photobiology A* 108 (1997) 1

Mills A., Lee S. K., Lepre A. “Photodecomposition of ozone sensitized by a film of titanium dioxide on glass” *Journal of Photochemistry and Photobiology A: Chemistry* 155 (2003) 199

Moser J, Gratzel M. "Photosensitised electron injection in colloidal semi-conductors." *Journal of American Chemical Society* 106 (1984) 6557

Mozes, N., Rouxhet, P.G. "Methods for measuring hydrophobicity of microorganisms." *Journal of Microbiological Methods* 57 (1987) 99

Naeem K., and Ouyang F., "Preparation of Fe³⁺ doped TiO₂ nanoparticles and its photocatalytic activity under UV light" *Physica: B Condensed Matter* 405 (2010) 221

Nag,M., Guin, D., Basak, P., Manorama, S. V. "Influence of morphology and surface characteristics on the photocatalytic activity of rutile titania nanocrystals" *Materials Research Bulletin* 43 (2008) 3270

Negishi N., Takeuchi K., "Structural changes of transparent TiO₂ thin films with heat treatment" *Materials Letters* 38 (1999) 150

Nonami T., Hase H., Funakoshi K., "Apatite-coated titanium dioxide photocatalyst for air purification" *Catalysis Today* 96 (2004) 113-118

Novotná P., Zita J., Krysa J., Kalousek V., Rathousky J., "Two component TiO₂/SiO₂ and TiO₂/PDMS films as efficient photocatalysts for environmental cleaning" *Applied Catalysis B* 79 (2007) 179

Ong L. Y., Razatos A., Georgiou G., Sharma M. M., "Adhesion forces between *E. coli* bacteria and biomaterial surfaces" *Langmuir* 15 (1999) 2719

Ou, H., Lo, S., "Effect of Pt/Pd-doped TiO₂ on the photocatalytic degradation of trichloroethylene" *Journal of Molecular Catalysis A: Chemical* 275 (2007) 200

Pereni C. I., Zhao Q., Liu Y., Abel E., “Surface free energy effect on bacterial retention” *Colloids and Surfaces B: Biointerfaces* 48 (2006) 143

Periyat, P., Baiju, K. V., Mukundan, P., Pillai, P. K., Warriar, K.G.K. “High temperature stable mesoporous anatase TiO₂ photocatalyst achieved by silica addition” *Applied Catalysis A: General* 349 (2008) 13

Periyathamby U., Ray A.K. “Computer Simulation of a Novel Photocatalytic Reactor Using Distributive Computing Environment” *Chemical Engineering and Technology* 22 (1999) 881

Permpoon, S., Houmard, M., Riassetto, D., Rapenne, L., Berthomé, G., Baroux, B., Joud, J.C., Langlet M. “Natural and persistent superhydrophilicity of SiO₂/TiO₂ and TiO₂/SiO₂ bi-layer films” *Thin Solid Films* 516 (2008) 957

Pigeot-Rémy S., Simoneta F., Errazuriz-Cerdad E., Lazzaroni J. C., Atlane D., Guillarda C., “Photocatalysis and disinfection of water: Identification of potential bacterial targets” *Applied Catalysis B: Environmental* 104 (2011) 390

Poortinga A. T., Bos R., Norde W., Busscher J. H., “Electric double layer interactions in bacterial adhesion to surfaces” *Surface Science Reports* 47 (2002) 1

Qi K., Daoud A. W., Xin H. J., Mak L. C., Tang W., Cheung P. W., “Self-cleaning cotton” *Journal of Materials Chemistry* 16 (2006) 4567-4574

Quan X., Liu Z., Fu H., Li X., Yang K., “Effect of embedded-silica on microstructure and photocatalytic activity of titania prepared by ultrasound-assisted hydrolysis” *Applied Catalysis B: Environmental* 52 (2004) 33

Rahaman, M.N. “Ceramic Processing”, Boca Raton: CRC Press. (2007) 242

Ramamurthy V., Schanze S. K. "Semiconductor photochemistry and photophysics"
Marcel Dekker Inc., New York, 2003

Reddy K.M., Manorama S.V. and Reddy A.R., Bandgap Studies on Anatase Titanium Dioxide Nanoparticles, *Materials Chemistry and Physics*, 78(1), (2002) 239

Ren D., Cui X., Shen J., Zhang Q., Yang X., Zhang Z., Ming L., "Study on the Superhydrophilicity of the SiO₂-TiO₂ Thin Films Prepared by Sol-Gel Method at Room Temperature" *Journal of Sol-Gel Science and Technology* 29 (2004) 131

Rincón G. A., Pulgarin C., "Effect of pH, inorganic ions, organic matter and H₂O₂ on *E. coli* K12 photocatalytic inactivation by TiO₂ implications in solar water disinfection" *Applied Catalysis B* 51 (2004) 283

Rizzo P. Baril A., S. Galvagno Neri G. "Sol-Gel Glass from Organic Modified Silicates for Optics Applications" *Journal of Sol-Gel Science and Technology* 26, (2003) 1017

Roy P.K., Choi W. H., Yi M. W., Moon K. R., Lee D. K., Han J. H., Shin A., Kamijo T., "Hemocompatibility of surface-modified, silicon-incorporated, diamond-like carbon films" *Acta Biomaterialia* 5 (2009) 249

Saito T., Iwase T., Horie J., Morioka T., "Mode of photocatalytic bacterial action of powdered semiconductor TiO₂ on mutants streptococci" *Journal of Photochemistry and Photobiology B* 14 (1992) 369

Sakai N., Fujishima A., Watanabe T., Hashimoto K., "Enhancement of the Photoinduced Hydrophilic Conversion Rate of TiO₂ Film Electrode Surface by Anodic Polarization", *Journal of Physical Chemistry B* 105 (2001) 3023

Sakai N., Wang R., Fujishima A., Watanabe T., Hashimoto K., “Effect of ultrasonic treatment on highly hydrophilic TiO₂ surfaces” *Langmuir* 14 (1998) 591

Sakthivel, S., Shankar, M. V., Palanichamy M, Arabindoob B, Bahnemanna D M, Murugesan V., “Enhancement of photocatalytic activity by metal deposition: characterization and photonic efficiency of Pt, Au and Pd deposited on TiO₂ catalyst” *Water Research*, 38(13) (2004) 3001

Sankur H. and Gunning W., “Crystallization and diffusion in composite TiO₂-SiO₂ thin films” *Journal of Applied Physics* 66 (10) (1985) 4747

Sato S, Susa K., Matsuyama I., “Sol-gel preparation and optical properties of SiO₂-Ta₂O₅ glass” *Journal of Non-Crystalline Solids* 306 (2002) 300

Satou, N., Satou, J., Shintani, H., Okuda, K. “Adherence of streptococci to surface-modified glass.” *Journal of General Microbiology* 134 (1988) 1299

Schiavello, M., (1997) “Heterogeneous photocatalysis” Wiley, New York, USA

Schmidt D. L., Brady R.F., Lam K., Schmidt D. C., Chaudhury M. K. “Contact angle hysteresis, adhesion, and marine biofouling.” *Langmuir* 20 (2004) 2830

Schneider P. R., “Conditioning Film-Induced Modification of Substratum Physicochemistry—Analysis by Contact Angles” *Journal of Colloid and Interface Science* 182(1) (1996) 204

Serpone N., Terzian R., Lawless D., Kennepohl P. and Sauve G., “On the Usage of Turnover Numbers and Quantum Yields in Heterogeneous Photocatalysis” *Journal of Photochemistry and Photobiology A: Chemistry* 11 (1993) 73

Seven O., Dindar B., Aydemir S., Metin D., Ozinel A. M., Icli S., "Solar photocatalytic disinfection of a group of bacteria and fungi aqueous suspensions with TiO₂, ZnO and Sahara desert dust" *Journal of Photochemistry and Photobiology A* 165 (2004) 103

Sharma P. K., Rao H. K. "Analysis of different approaches for evaluation of surface energy of microbial cells by contact angle goniometry" *Advances in Colloid and Interface Science* 98 (2002) 341

Shellenberger K., Logan B. E., "Effect of molecular scale roughness of glass beads on colloidal and bacterial deposition" *Environmental Science and Technology* 36 (2002) 184

Sjogren, J. C., and Sierka R. A." Inactivation of phage MS2 by iron-aided titanium dioxide photocatalysis. *Applied and Environmental Microbiology* 60 (1994) 344

Slonczewski, L. J., Foster, W. J., Gillen, M. K., "Microbiology An Evolving Science" W. W. Norton & Company, Inc., New York, 2009

Soumya, E., Mohamed, M., Fatimazahra, B., Hassan, L., Abdellah, H., Fatima, H., Saad, I., "Study of Microbial Adhesion on Some Wood Species: Theoretical Prediction" *Microbiology* 80 (2011) 43

Sökmen M., Candan F., Sümer Z., "Disinfection of *E. coli* by the Ag-TiO₂/UV system: lipidperoxidation" *Journal of Photochemistry and Photobiology A: Chemistry* 143 (2001) 241

Su C., Hong Y. B., Tseng C. M., "Sol-gel preparation and photocatalysis of titanium dioxide" *Catalysis Today* 96 (2004) 119

Su W., Wang S., Wu L., Wang X., Liu P., Fu X. "Surface Anti-bacterial Adhesion Characteristics of TiO₂-coated PMMA" *Journal of Structural Chemistry* 28 (2009) 1497

Su, Y., Wu, J., Quan X., Chen, S., "Electrochemically assisted photocatalytic degradation of phenol using silicon-doped TiO₂ nanofilm electrode" *Desalination* 252 (2010) 143

Sumita T., Otsuka H., Kubota H., Nagota M., Honda Y., Miyagawa R., Trurushima T., Sadoh T., "Ion-beam modification of TiO₂ film to multilayered photocatalyst" *Nuclear Instrument and Methods in Physics Research B* 148 (1999) 758

Sun R., Nakajima A., Sakai N., Fujishima A., Watanabe T., Hashimoto K., "Photoinduced Surface Wettability Conversion of ZnO and TiO₂ Thin Films" *Journal of Physical Chemistry B* 105 (2001) 1984

Sun B., Sun S., Li T., "Preparation and antibacterial activities of Ag-doped SiO₂-TiO₂ composite films by liquid phase deposition (LPD) method" *Journal of Materials Science* 42 (2007) 10085

Sunada K., Kikuchi Y., Hashimoto K., Fujishima A., "Bactericidal and detoxification effects of TiO₂ thin film photocatalysts" *Environmental Science and Technology* 32 (1998) 726

Sunada K., Watanabe T., Hashimoto K., "Studies on photokilling of bacteria on TiO₂ thin film" *Journal of Photochemistry and Photobiology A* 156 (2003) 227

Suzuki, N., Jiang, X., Radhakrishnan, L., *et al.*, "Hybridization of Photoactive Titania Nanoparticles with Mesoporous Silica Nanoparticles and Investigation of Their Photocatalytic Activity" *Bulletin of Chemical Society Japan* 84 (7) (2011) 812

Stakheev, A. Y., Shpiro, E. S., Apijok, J., "XPS and XAES Study of TiO₂-SiO₂ Mixed Oxide System" *Journal of Physical Chemistry* 97 (1993) 5668.

Tanaka K., Capule M.F.V., Hisanaga T., "Effect of crystallinity of TiO₂ on its photocatalytic action" *Chemical Physics Letters* 187 (1991) 73

Teixeira P., Trindade C. Godinho H., Azeredo J., Oliveira R., Fonseca G., "Staphylococcus epidermidis adhesion on modified urea/urethane elastomers." *Journal of Biomaterial Science Polymer* 17 (2006) 239

Teoh W. Y., Mädler, L., Amal R., "Inter-relationship between Pt oxidation states on TiO₂ and the photocatalytic mineralisation of organic matters" *Journal of Catalysis* 251 (2007) 271

Testino, A., Bellobono, I. R., Buscagila, V., Canevali, C., Arienzo, M. D., Polizzi, S., Scotti, R., Morazzoni, F., "Optimizing the Photocatalytic Properties of Hydrothermal TiO₂ by the Control of Phase Composition and Particle Morphology. A Systematic Approach" *Journal of American Chemical Society* 129 (2007) 3564

Thompson L. T., Yates T. J., "Surface Science Studies of the Photoactivation of TiO₂ New Photochemical Processes" *Chemical Reviews* 106 (2006) 4428

Trapalis, C. C., Keivanidis, P., Kordas, G., Zaharescu, M., Crisan, M., Szatvanyi, A., Gartner, M. "TiO₂(Fe³⁺) nanostructured thin films with antibacterial properties" *Thin Solid Films* 433 (2003) 186

Turchi, C. S., Ollis D. F. "Photocatalytic degradation of organic water contaminants: Mechanisms involving hydroxyl radical attack" *Journal of Catalysis* 122 (1990) 178

Ubonchonlakate, K., Sikong, L., Saito, F. “Photocatalytic disinfection of *P.aeruginosa* bacterial Ag-doped TiO₂ film” *Procedia Engineering* 32 (2012) 656

U.S. Environmental Protection Agency “Handbook On Advanced Photochemical Oxidation Processes” Washington DC (1998)

van der Mei, H. C., Bos, R. and Busscher, H. J. “A reference guide to microbial cell surface hydrophobicity based on contact angles.” *Colloids and Surfaces B: Biointerfaces* 11 (1998) 213

Van Oss J. C., Good J. R., Chaundhury M. K., “The role of van der Waals forces and hydrogen bonds in “hydrophobic interactions” between biopolymers and low energy surfaces” *Journal Colloid Interface Science* 111 (1986) 378

Van Oss J. C., Chaudhury K. M., Good J. R., “Interfacial Lifshitz-van der Waals and Polar interactions in macroscopic systems” *Chemical Review.* 88. (1988) 927

Van Oss, C.J. “Acid-base interfacial interactions in aqueous media” *Colloids and Surfaces A: Physicochemical and Engineering Aspects* 78 (1993) 1

Van Oss, J. C., “Use of the combined Lifshitz–van der Waals and Lewis acid–base approaches in determining the apolar and polar contributions to surface and interfacial tensions and free energies” *Adhesion Science and Technology* 16 (2002) 669

Văcăroiu, C., Enache, M., Gartner, M., Popescu, G., Anastasescu, M., Brezeanu A. *et al.*, “The effect of thermal treatment on antibacterial properties of nanostructured TiO₂(N) films illuminated with visible light” *World Journal of Microbiology and Biotechnology* 25 (2009) 27

Viswananth N. R., Ramasamy S. "Study of nanocrystallites in TiO₂-SiO₂ composites" *Colloids and Surfaces A* 133 (1998) 49

Volpe D. C., Siboni S., "Acid-base surface free energies of solids and the definition of scales in the God-van oss-Chaudhury theory" *Journal of Adhesion Science Technology* 14 (2) (2000) 235

Wang, C. M., Heller, A., Gerischer, H., "Palladium catalysis of O₂ reduction by electrons accumulated on TiO₂ particles during photoassisted oxidation of organic compounds." *Journal of American Chemical Society* 114 (1992) 5230

Wang C. C., Ying j. Y., "Sol-gel synthesis and hydrothermal processing of anatase and rutile titania nanocrystals" *Chemistry of Materials* 11 (1999) 3113

Wang J., Huang N., Pan J. C., Kwok H. C. S., Yong P., Leng X. Y., Chen Y. J., Sun H., Wan J. G., Liu Y. Z., Chu K. P., "Bacterial repellence from polyethylene terephthalate surface modified by acetylene plasma immersion ion implantation-deposition" *Surface & Coatings Technology* 186 (2004) 299

Wang R., Hashimoto K., Fujishima A., Chikuni M., Kojima E., Kitamura A., Shimohigoshi M., Watanabe T., "Photogeneration of Highly Amphiphilic TiO₂ Surfaces" *Advanced Materials* 10 (1998) 135

Wang R., Sakai N., Fujishima A., Watanabe T., Hashimoto K., "Studies of Surface Wettability Conversion on TiO₂ Single-crystal Surfaces" *Journal of Physical Chemistry B* 103 (1999) 2188

Wang, H., Sodagari, M., Chen, Y., He, X., Newby, Z. B., Ju, L., "Initial bacterial attachment in slow flowing systems: Effects of cell and substrate surface properties" *Colloids and Surfaces B: Biointerfaces* 87 (2011) 415

Wardle B. "Principles and applications of photochemistry" Wiley, UK, 2009

Watanabe T, Nakajimaa A., Wanga R., Minabea M., Koizumi S., Fujishimab A., Hashimotoa K., "Photocatalytic activity and photoinduced hydrophilicity of titanium dioxide coated glass" *Thin Solid Films* 351 (1999) 260

Watts, R. J., Kong, S., Orr, M. P. G., Miller, C., Henry, B. E. " Photocatalytic inactivation of coliform bacteria and viruses in secondary wastewater effluent" *Water Research* 29 (1995) 95

Wei C., Lin Y. W., Zainal Z., Willams E. N., Zhu K., Kruzic P. A., Smith L. R., Rajeshwar K "Bacterial activity of TiO₂ photocatalyst in aqueous media: Toward a solar-assisted water disinfection system" *Environmental Science and Technology* 28 (1994) 934

Wiencek KM, Fletcher M. "Bacterial adhesion to hydroxyl and methyl-terminated alkanethiol self-assembled monolayers." *Journal of Bacteriology* 177 (1995) 1959

Wist, J., Dierolf, C., Torres, W., Pulgarin, C., "Evaluation of photocatalytic disinfection of crude water for drinking-water production" *Journal of Photochemistry and Photobiology A: Chemistry* 147 (2002) 241

Wright D. J., Sommerdijk N. "Sol-gel Materials Chemist and Applications" Taylor & Francis, Netherlands (2003)

Wolfrum, J. E., Huang, J., Blake, M.D., Maness, P., Huang, Z., and Fiest, J., "Photocatalytic oxidation of bacteria, bacterial and fungal spores, and model biofilm components to carbon dioxide on titanium dioxide-coated surfaces" *Environmental Science and Technology* 36 (2002) 3412

Wu, D., Long M., “Enhancing visible-light activity of the self-cleaning TiO₂-coated cotton fabrics by loading AgI particles” *Surface & Coatings Technology* 206 (2011) 1175

Wu C G, Chao C C, Kuo F T, “Enhancement of the photocatalytic performance of TiO₂ catalysts via transition metal modification.” *Catalysis Today*, 97 (2004) 103

Xu AW, Gao Y, Xu HQ. “The preparation, characterization and their photocatalytic Activities of Rare-Earth-Doped TiO₂ Nanoparticles” *Journal of Catalysis* 207 (2002) 151.

Xu P., Liu X., Wang W., Chen S., “Improving the antibacterial and UV-resistant properties of cotton by the titanium hydrosol treatment” *Journal of Applied Polymer Science* 102 (2006) 1478

Yin H., Wada Y., Kitamura T., Kambe S., Murasawa S., Moni H., Sakata T., Yanagida S., “ Hydrothermal Synthesis of nanosized anatase and rutile using amorphous phase TiO₂” *Journal of Material Chemistry* 11 (2001) 1694

Yoldas, B. E., Partlow, D. P., “Formation of broad band antireflective coatings on fused silica for high power laser applications” *Thin Solid Films* 129 (1985) 1

Yu J. G. and Zhao X. J. “Effect of surface treatment on the photocatalytic activity and hydrophilic property of the sol-gel derived TiO₂ thin films” *Material Research Bulletin* 36 (2001) 97

Yu C. J., Yu J., Wingkei H., Zhao J., “Light-induced super-hydrophilicity and photocatalytic activity of mesoporous TiO₂ thin films” *Journal of Photochemistry and Photobiology A: Chemistry* 148 (2002) 33

Yu J., Zhao X., “The Effect of SiO₂ Addition on the Grain Size and Photocatalytic Activity of TiO₂ Thin Films” *Journal of Sol-Gel Science and Technology* 24 (2002) 93

Yu C. J., Ho W., Lin J., Yip H., Wong K. P., “Photocatalytic Activity, Antibacterial Effect, and Photoinduced Hydrophilicity of TiO₂ Films Coated on a Stainless Steel Substrate” *Environmental Science and Technology*. 37 (2003) 2296

Yu H., Zhang, Z., Hu, F. “Phase stabilities and photocatalytic activities of P/Zn–TiO₂ nanoparticles able to operate under UV–vis light irradiation” *Journal of Alloys and Compounds* 465 (2008) 484

Zhai J., Zhang L., Yao X., “Effects of composition and temperature on gel-formed TiO₂/SiO₂ films” *Journal of Non-Crystalline Solids* 260 (1999) 160

Zhang ZB, Wang CC, Zakaria R, Ying JY.” Role of Particle Size in Nanocrystalline TiO₂-Based Photocatalysts” *Journal of Physical Chemistry B* 102 (1998) 10871

Zhang, J., Ayusawa, T., Minagawa, M., *et al.*, “Investigations of TiO₂ Photocatalysts for the Decomposition of NO in the Flow System” *Journal of Catalysis* 198 (2001) 1

Zhang T. X., Sato O., Taguchi M., Einaga Y., Murakami T., Fujishima A., “Self-cleaning particle coating with antireflection properties” *Chemistry of Materials* 17 (2005) 696

Zhang M., Shi L., Yuan S., Zhao Y., Fang J., “Synthesis and photocatalytic properties of highly stable and neutral TiO₂/SiO₂ hydrosol” *Journal of Colloid and Interface Science* 330 (2009) 113

Zhao X., Yu C. J., Zhong G., Zhao Q., “The grain size and surface hydroxyl content of super-hydrophilic TiO₂/SiO₂ composite nanometer thin films” *Journal of Material Science Letters* 20 (2001) 1745

Zhao Q., Wang H. Müller-Steinhagen “Tailored surface free energy of membrane diffusers to minimize microbial adhesion” *Applied Surface Science* 230 (2004) 371

Zhao Q., Liu Y., Wang C., Wang S., Müller-Steinhagen H. “Effect of surface free energy on the adhesion of biofouling and crystalline fouling” *Chemical Engineering Science* 60 (2005) 4858

Zhou L. J., Yan S. S., Tian B. Z., “Preparation of TiO₂-SiO₂ film with high photocatalytic activity on PET substrate”, *Materials Letters* 60 (2006) 396

Zhao Q., Wang C., Liu Y., Wang S., “Bacterial adhesion on the metal polymer composite coatings” *International Journal of Adhesion and Adhesives* 27 (2007) 85

Zhao B. X., Mele, G., Pio, I., Li, J., Palmisano L., Vasapollo, G. “Degradation of 4-nitrophenol (4-NP) using Fe-TiO₂ as a heterogeneous photo-Fenton catalyst” *Journal of Hazardous Materials* 176 (2010) 569

APPENDIX A

LIGHT SPECTRUM OF THE UV SIMULATOR

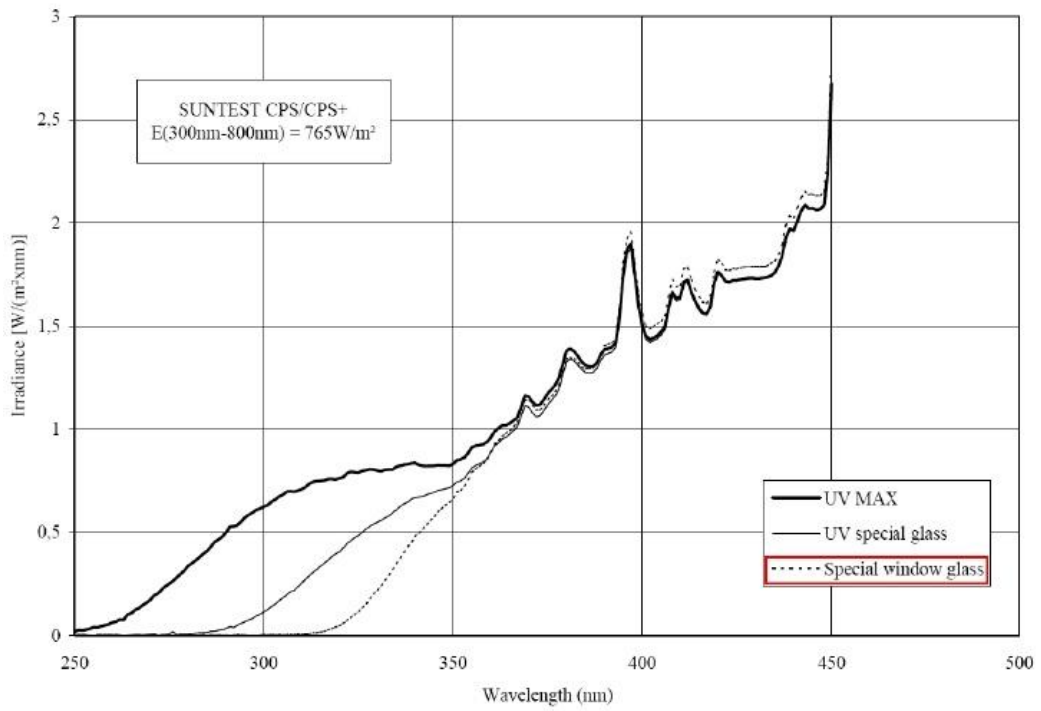


Figure A.1 Light spectrum of the UV simulator used in the experiments

APPENDIX B

XRD RESOURCES

Table B1. XRD Diffractogram of Anatase

2 θ	d(A ^o)	Intensity (%)	hkl
25.281	3.5200	100	101
36.947	2.4310	10	103
37.801	2.3780	20	004
38.576	2.3320	10	112
48.050	1.8920	35	200
53.891	1.6999	20	105
55.062	1.6665	20	211
62.121	1.4930	4	213
62.690	1.4808	14	204
68.762	1.3641	6	116
70.311	1.3378	6	220
74.031	1.2795	2	107
75.032	1.2649	10	215
76.020	1.2509	4	301
80.727	1.1894	2	008
82.139	1.1725	2	303
82.662	1.1664	6	224
83.149	1.1608	4	312
93.220	1.0600	2	217
94.181	1.0517	4	305
95.143	1.0436	4	321
98.318	1.0182	2	109
99.804	1.0070	2	208
101.221	0.9967	2	323
107.448	0.9555	4	316
108.962	0.9464	4	400
112.840	0.9246	2	307
113.861	0.9192	2	325
114.909	0.9138	2	411
118.439	0.8966	4	219
120.104	0.8890	2	228
121.725	0.8819	2	413
122.336	0.8793	2	404
131.035	0.8464	2	420
135.998	0.8308	2	327
137.391	0.8268	4	415
143.887	0.8102	2	309
150.039	0.7974	4	424
152.633	0.7928	2	0012

Table B2. XRD Diffractogram of Rutile

2θ	$d(\text{\AA}^0)$	Intensity (%)	hkl
27.447	3.2470	100	110
36.086	2.4870	50	101
39.188	2.2970	8	200
41.226	2.1880	25	111
44.052	2.0540	10	210
54.323	1.6874	60	211
56.642	1.6237	20	220
62.742	1.4797	10	002
64.040	1.4528	10	310
65.480	1.4243	2	221
69.010	1.3598	20	301
69.790	1.3465	12	112
72.410	1.3041	2	311
74.411	1.2739	1	320
76.510	1.2441	4	202
79.822	1.2006	2	212
82.335	1.1702	6	321
84.260	1.1483	4	400
87.464	1.1143	2	410
89.557	1.0936	8	222

2θ	$d(\text{\AA}^0)$	Intensity (%)	hkl
90.708	1.0827	4	330
95.275	1.0425	6	411
96.017	1.0364	6	312
97.176	1.0271	4	420
98.514	1.0167	1	331
105.099	0.9703	2	421
106.019	0.9644	2	103
109.406	0.9438	2	113
116.227	0.9072	4	402
117.527	0.9009	4	510
120.059	0.8892	8	213
122.788	0.8774	8	431
123.660	0.8738	8	332
131.847	0.8437	6	422
136.549	0.8292	8	303
140.052	0.8196	12	521
143.116	0.8120	2	440
155.869	0.7877	2	530

APPENDIX C

SURFACE AREA MEASUREMENTS OF SiO₂-TiO₂ THIN FILMS

The surface area measurements of thin films were calculated by using MB solution adsorption technique. Experiments were performed in the dark. The MB solution concentration was 2 ppm. The initial absorbance value (A_0) of feed stock solution was analyzed by UV-Visible spectrometer at 663 nm. Coated glasses with areas of 1.04 cm², 2.88 cm², 5.25 cm², 9.13 cm² put into the 25 ml of feed stock solution for 72 h in the dark. The final absorbance value of MB solution after adsorption was performed by UV-Visible spectrometer at 663 nm (A).

- At the end of 72 h the equilibrium concentration of was calculated as;

$$C_e = \frac{A}{A_0} * C_{int}$$

C_e : Equilibrium concentration of MB remaining in the solution after adsorption (ppm)

C_{int} : Initial concentration of MB solution (ppm)

C_e (mg/l)	Area of coated glass (cm ²)
1.9958	1.04
1.9835	3.20
1.9670	6.63
1.9444	8.25

- The adsorbed MB quantity (in mg) by thin films was calculated by using the final and initial solute amount in the water.

$$x = \frac{25ml}{1000ml} * (C_{int} - C_e)$$

x: Adsorbed MB by thin films (mg)

x (mg)	Area of coated glass (cm ²)
0.000102881	1.04
0.000411523	3.20
0.000823045	6.63
0.001388889	8.25

- The adsorption data were analyzed according to the Langmiur equation.

$$\frac{C_e}{(x/m)} = \frac{1}{k.x_m} + \frac{C_e}{x_m}$$

- Define as $y = b + mx$ where $y = \frac{C_e}{(x/m)}$ and $b = \frac{1}{kx_m}$

where C_e is the equilibrium concentration of solute remaining in the solution, x/m is the quantity of solute adsorbed per unit thin film area, x_m and k are Langmiur constants. These constants are called adsorption capacity and bonding energy constant, respectively.

Straight lines were fitted to the points by the method of least squares, where the slope of the regression line is $1/x_m$ and the intercept is $1/k.x_m$. The Langmiur constant are given in Table C.7 for all samples.

Table C.1 Surface area measurement of thin film ($\text{SiO}_2/\text{TiO}_2 = 0$)

Area (cm^2)	Ce (mg/l)	x (mg)	x/m (mg/cm^2)	Ce/(x/m)
1,04	1,9958848	0,000102881	$9,89237 \cdot 10^{-5}$	20176
3,2	1,9835391	0,000411523	0,000128601	15424
6,625	1,9670782	0,000823045	0,000124233	15833
8,25	1,9444444	0,001388889	0,00016835	11550

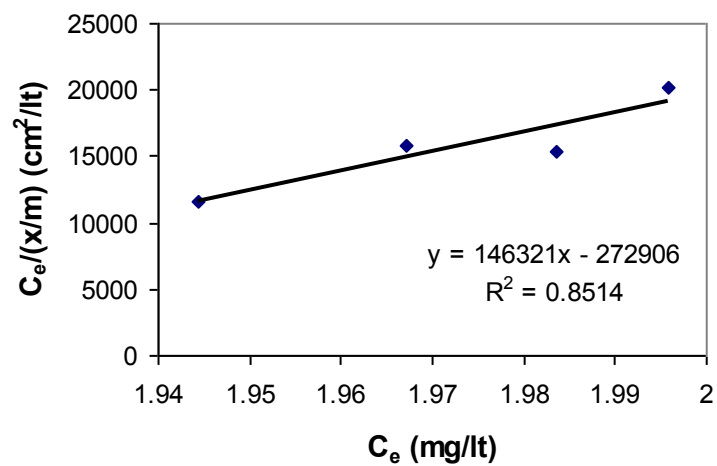


Figure C.1 Adsorption isotherm of thin film contain pure TiO_2

Table C.2 Surface area measurement of thin film (49 wt % SiO₂)

Area (cm ²)	Ce (mg/l)	x (mg)	x/m (mg/cm ²)	Ce/(x/m)
2	1.9670782	0.000823045	0.000411523	4780
3.5	1.9403292	0.00149177	0.00042622	4552
7	1.8436214	0.003909465	0.000558495	3301

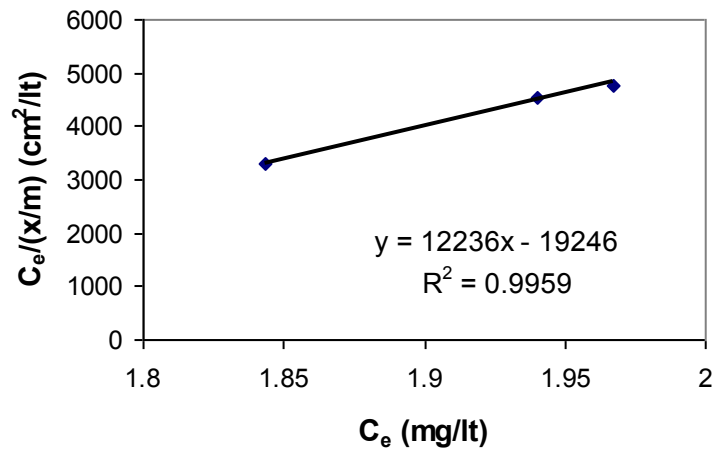


Figure C.2 Adsorption isotherm of thin film contain SiO₂ and TiO₂ (49 wt % SiO₂)

Table C.3 Surface area measurement of thin film (60wt % SiO₂)

Area (cm ²)	Ce (mg/l)	x (mg)	x/m (mg/cm ²)	Ce/(x/m)
2	1.9588477	0.001028807	0.000514403	3808
3.6	1.9012346	0.002469136	0.000685871	2772
5.59	1.8518519	0.003703704	0.000662559	2795
7.75	1.6584362	0.008539095	0.001101819	1505

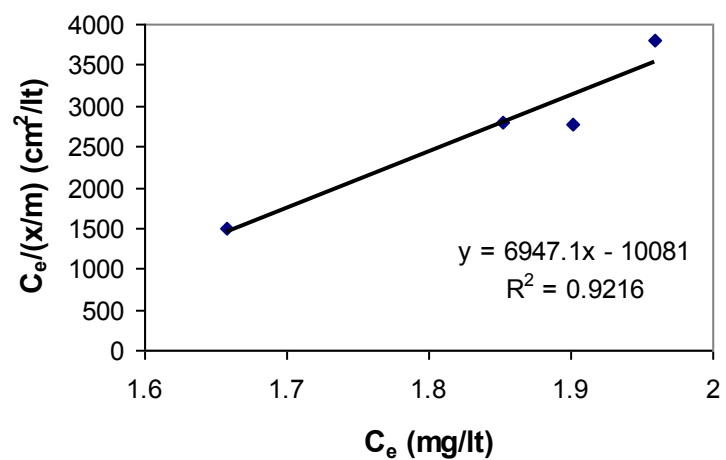


Figure C.3 Adsorption isotherm of thin film contain SiO_2 and TiO_2 (60wt % SiO_2)

Table C.4 Surface area measurement of thin film (74 wt % SiO_2)

Area (cm^2)	C_e (mg/lit)	x (mg)	x/m (mg/cm^2)	$C_e/(x/m)$
7.25	1.7391304	0.0078261	0.00107946	1611
20.5	1.2147826	0.0235565	0.001149099	1057
29.5	1.0226087	0.0293217	0.000993957	1029

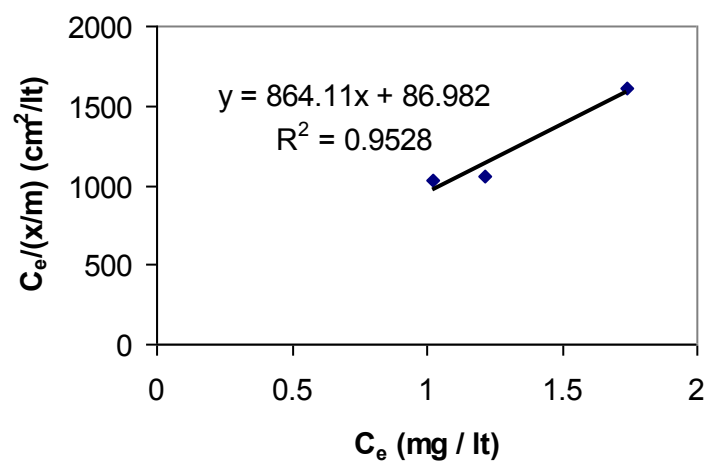


Figure C.4 Adsorption isotherm of thin film contain SiO_2 and TiO_2 (74 wt % SiO_2)

Table C.5 Surface area measurement of thin film (85 wt % SiO_2)

Area (cm^2)	C_e (mg/lit)	x (mg)	x/m (mg/cm^2)	$C_e/(x/m)$
8	1.4909597	0.0152712	0.001908901	781.05647
21	0.9401947	0.0317942	0.001514008	620.99738
30	0.4979138	0.0450626	0.001502086	331.48148

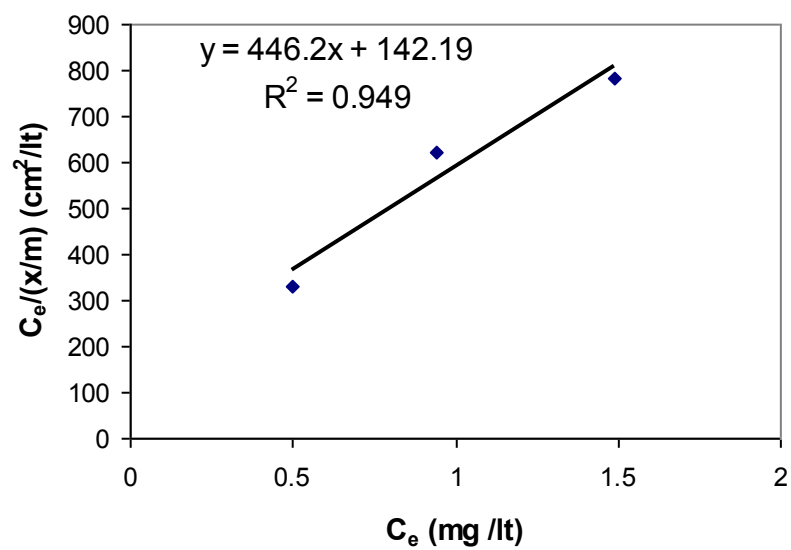


Figure C.5 Adsorption isotherm of thin film contain SiO_2 and TiO_2 (85 wt % SiO_2)

Table C.6 Surface area measurement of thin film (92 wt % SiO_2)

Area (cm^2)	C_e (mg/lt)	x (mg)	x/m (mg/cm^2)	$C_e/(x/m)$
9.125	0.9043478	0.0328696	0.003602144	251
22	0.3095652	0.050713	0.002305138	134
30	0.1113043	0.0566609	0.001888696	59

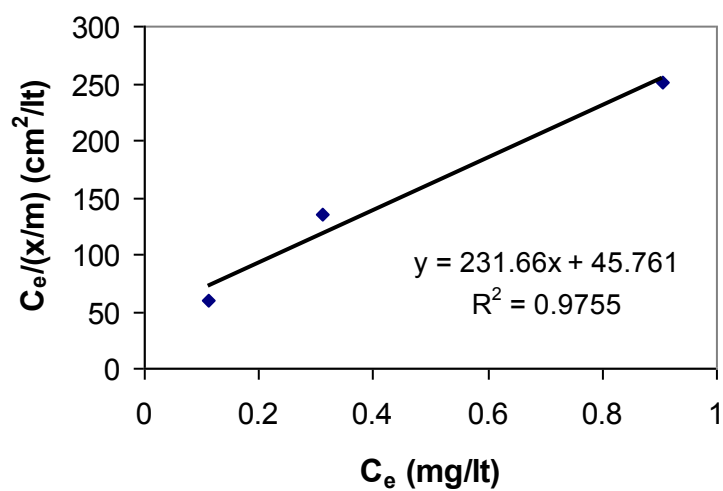


Figure C.6 Adsorption isotherm of thin film contain SiO_2 and TiO_2 (92 wt % SiO_2)

Table C.7 Langmiur constants and correlation coefficients of linear regression lines

% wt SiO_2	0	49	60	75	85	92
R^2	0.8514	0.9959	0.9216	0.9528	0.949	0.9755
k	-0.54	-0.63	-0.07	0.01	0.03	0.01
x_m	$6.8 \cdot 10^{-6}$	$8.2 \cdot 10^{-5}$	$1.4 \cdot 10^{-4}$	$1.2 \cdot 10^{-3}$	$2.2 \cdot 10^{-3}$	$4.3 \cdot 10^{-3}$

APPENDIX D

PHOTOCATALYTIC METHYLENE BLUE DEGRADATION REACTIONS

The initial adsorbed MB concentration per unit area of thin film was calculated by feed stock analysis. Experiments were performed in the dark. The MB solution concentration was 100 ppm. The initial absorbance value (A_0) of feed stock solution was analyzed by UV-Visible spectrometer at 657 nm. Thin films containing different amount of SiO_2 with areas of 10 cm^2 immersed in the 20 ml of feed stock solution for 24 h in the dark. The final absorbance value of MB solution after adsorption was performed by UV-Visible spectrometer at 657 nm (A).

- At the end of 24 h the equilibrium concentration of was calculated as;

$$C_e = \frac{A}{A_0} * C_{\text{int}}$$

C_e : Equilibrium concentration of MB remaining in the solution after adsorption (ppm)

C_{int} : Initial concentration of MB solution (ppm)

Table D.1 Equilibrium concentration of MB remaining in the solution after adsorption (ppm)

SiO ₂ content (wt%)	C _e (ppm)
0	66.70
49	62.39
60	56.17
74	63.80
85	57.33
92	62.10
95	69.15
100	67.32

- The adsorbed MB quantity (mg) by thin films was calculated by using the final and initial solute amount in the water.

$$x = \frac{20ml}{1000ml} * (C_{int} - C_e)$$

x: Adsorbed MB by thin films (mg)

Table D.2 The adsorbed MB quantity (mg) by thin films

SiO ₂ content (wt%)	x (mg/cm ²)
0	0.066
49	0.075
60	0.076
74	0.072
85	0.085
92	0.091
95	0.062
100	0.065

- Table D.3 shows the changes in the absorbance values of methylene blue adsorbed over thin films with respect to irradiation time.
- The absorbance values of methylene blue adsorbed over thin film convert to concentration of MB per unit area of thin film surface by using calibration curves which are given in Figure D.1, D.2, D.3, D.4, D.5, D.6, D.7.

Table D.3 Changes in the absorbance values of methylene blue adsorbed over thin film containing pure TiO₂

0wt% SiO ₂		49 wt% SiO ₂		60 wt% SiO ₂		74 wt% SiO ₂		85 wt% SiO ₂		92 wt% SiO ₂		95 wt% SiO ₂		100 wt% SiO ₂	
t (min)	Abs	t (min)	Abs	t (min)	Abs	t (min)	Abs	t (min)	Abs	t (min)	Abs	t (min)	Abs	t (min)	Abs
0	0.049	0	0.233	0	0.237	0	0.201	0	0.345	0	0.496	0	0.168	0	0.106
15	0.033	15	0.126	15	0.100	15	0.150	15	0.293	15	0.395	15	0.157	15	0.094
30	0.034	30	0.053	30	0.077	30	0.100	30	0.268	30	0.353	30	0.163	30	0.0925
45	0.030	45	0.077	45	0.067	45	0.068	45	0.248	45	0.326	45	0.156	45	0.088
60	0.025	60	0.038	60	0.076	60	0.047	60	0.191	60	0.307	60	0.136	60	0.098
90	0.026	90	0.025	90	0.048	90	0.046	90	0.194	90	0.272	90	0.137	90	0.111
120	0.027	120	0.022	120	0.033	120	0.018	120	0.152	120	0.243	120	0.136	120	0.098
150	0.019	150	0.020	150	0.034	150	0.040	150	0.137	150	0.243	150	0.13	150	0.096
230	0.022	230	0.020	230	0.024	230	0.010	230	0.132	230	0.202	230	0.134	230	0.093
300	0.018	300	0.020	300	0.007	300	0.017	300	0.108	300	0.172	300	0.132	300	0.101

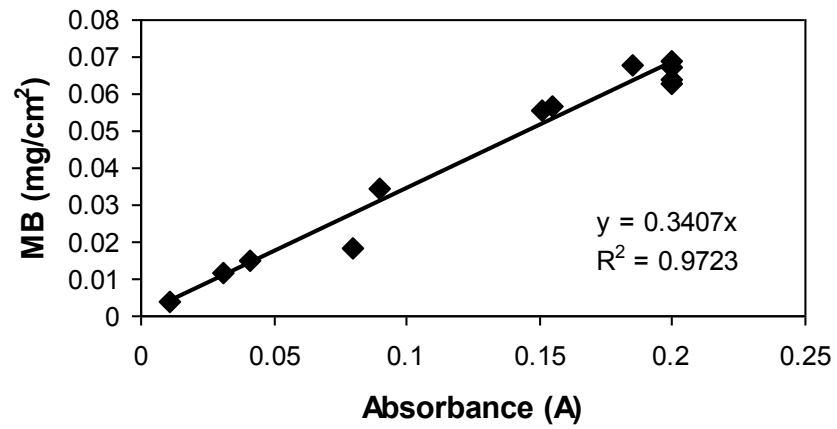


Figure D.1 Adsorbed MB over per unit area of thin film vs changes in the absorbance values of MB over thin film surface containing pure TiO₂

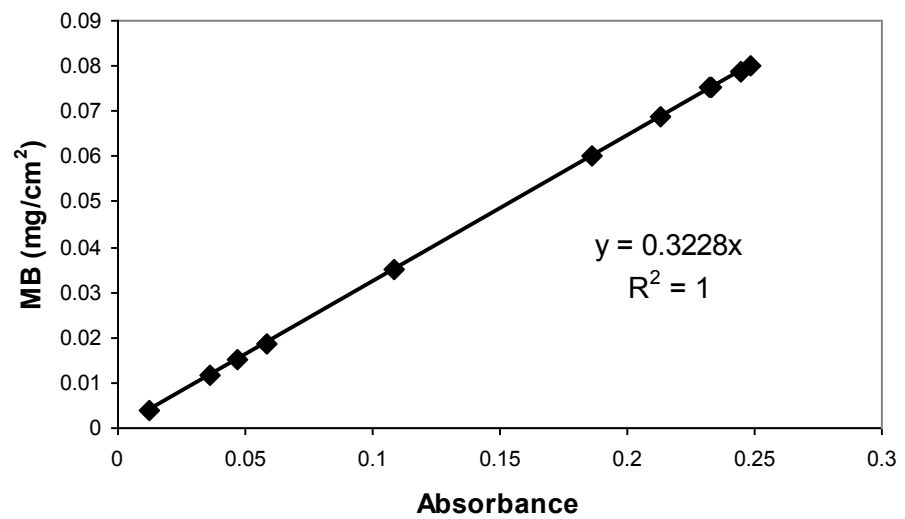


Figure D.2 Adsorbed MB over per unit area of thin film vs changes in the absorbance values of MB over thin film surface containing 49 wt% SiO₂

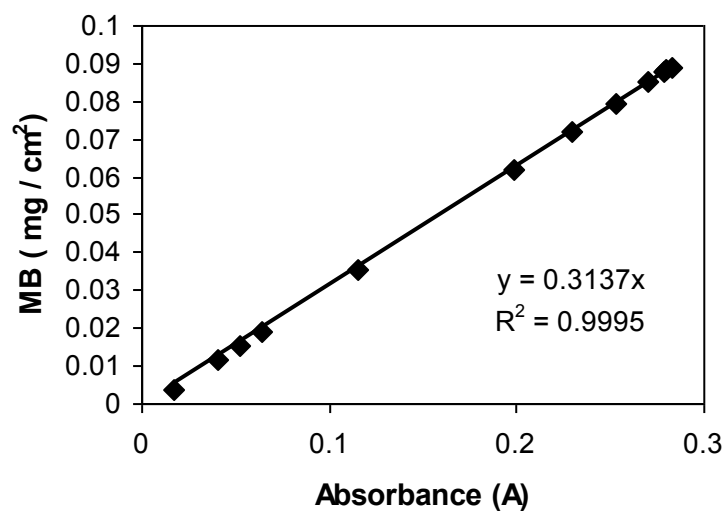


Figure D.3 Adsorbed MB over per unit area of thin film vs changes in the absorbance values of MB over thin film surface containing 60 wt% SiO₂

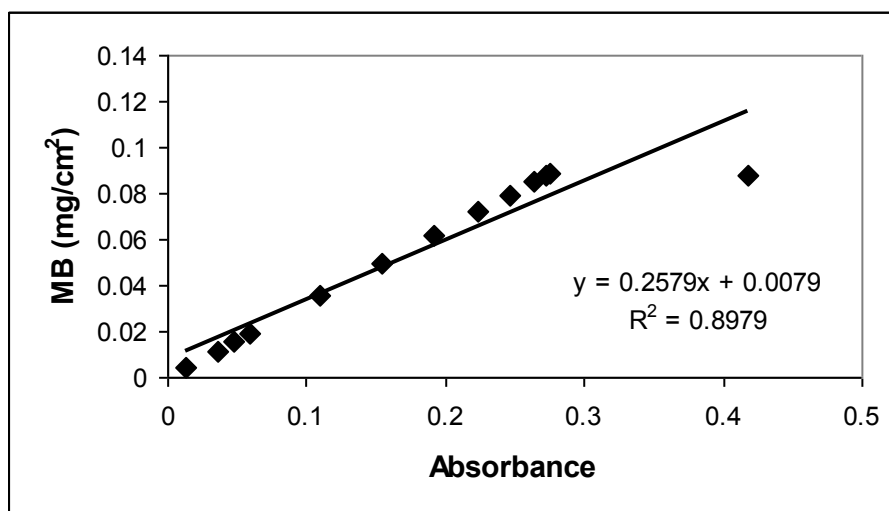


Figure D.4 Adsorbed MB over per unit area of thin film vs changes in the absorbance values of MB over thin film surface containing 74 wt% SiO₂

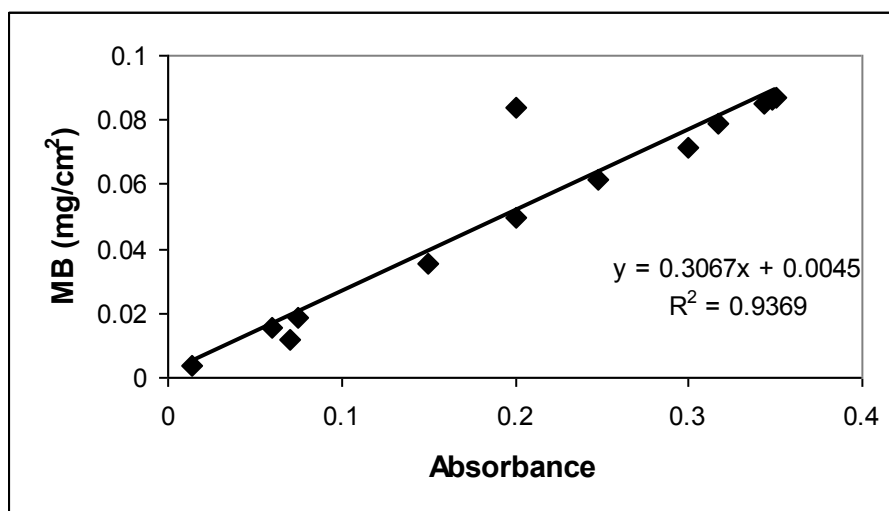


Figure D.5 Adsorbed MB over per unit area of thin film vs changes in the absorbance values of MB over thin film surface containing 85 wt% SiO₂

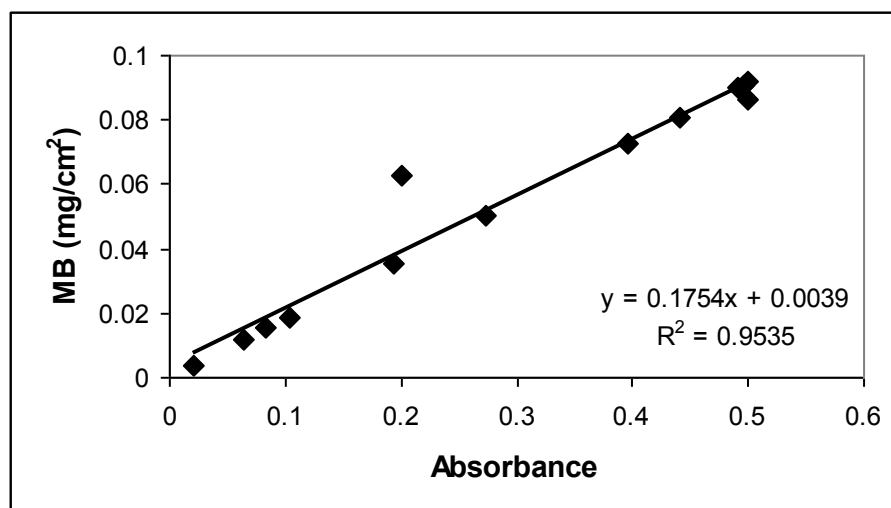


Figure D.6 Adsorbed MB over per unit area of thin film vs changes in the absorbance values of MB over thin film surface containing 92 wt% SiO₂

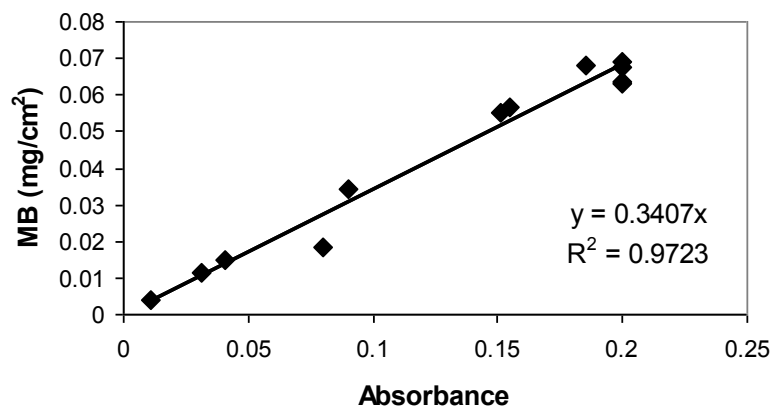


Figure D.7 Adsorbed MB over per unit area of thin film vs changes in the absorbance values of MB over thin film surface containing 95 wt% SiO₂

APPENDIX E

CALCULATION OF INITIAL REACTION RATE CONSTANTS FOR PHOTOCATALYTIC DEGRADATION OF METHYLENE BLUE

From the results obtained in the MB degradation tests, the kinetic analysis of the data was carried out. Because of the complexity of the inactivation kinetics, the initial rate constants were estimated by analyzing the data which corresponds to the first 0-45 minutes period of experiments. For this purpose, the behavior of the photocatalytic oxidation of MB over titanium dioxide was fitted to pseudo - first order kinetic model (Lasa *et al.*, 2005)

$$-\frac{dc}{dt} = kC \quad (\text{E.1})$$

It can be integrated with boundary conditions as follows:

$$C = C_0 \exp(-kt) \quad (\text{E.2})$$

where C_0 (mg/cm^2) is the initial concentration of MB adsorbed on the unit area of thin film and k is the initial reaction rate constant ($\text{mg MB}/\text{cm}^2 \cdot \text{min}$).

As seen from following figures, data which corresponds to the first 0-45 minutes period of experiments yielded linear $\ln(C/C_0)$ versus time plots..

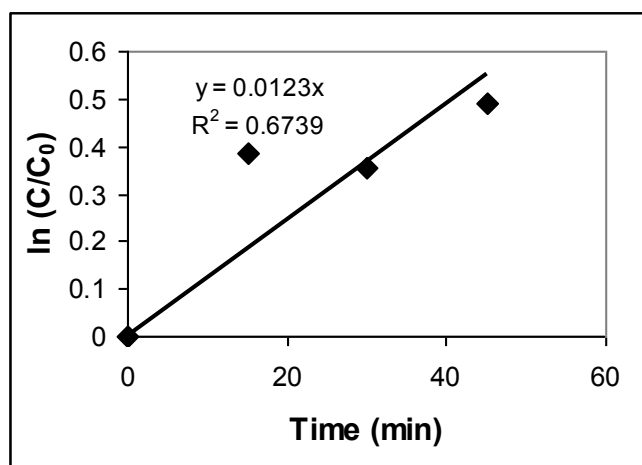


Figure E.1 $\ln(C/C_0)$ versus reaction time data of thin film containing pure TiO_2

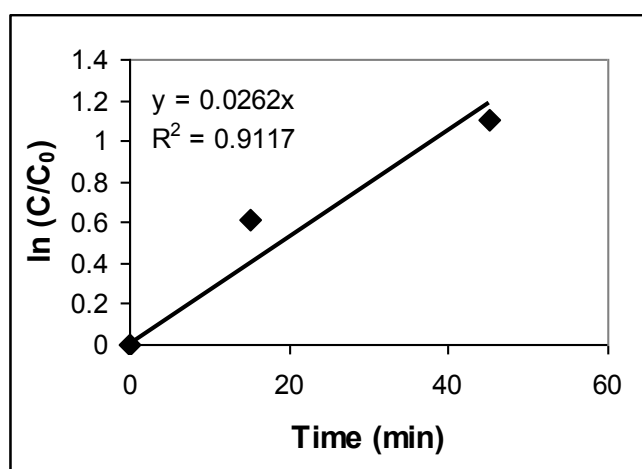


Figure E.2 $\ln(C/C_0)$ versus reaction time data of thin film 49 wt% SiO_2

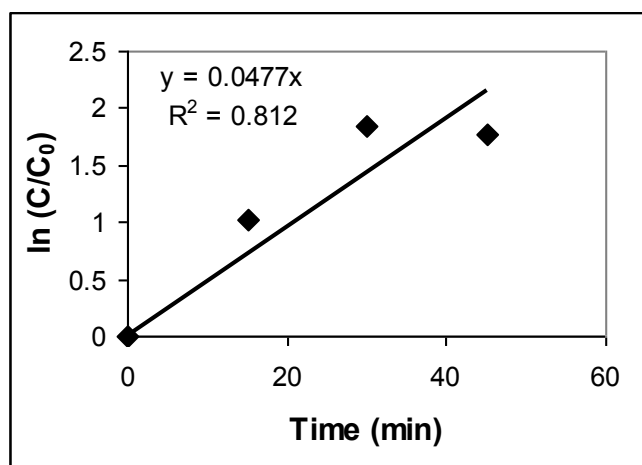


Figure E.3 $\ln(C/C_0)$ versus reaction time data of thin film 60 wt% SiO_2

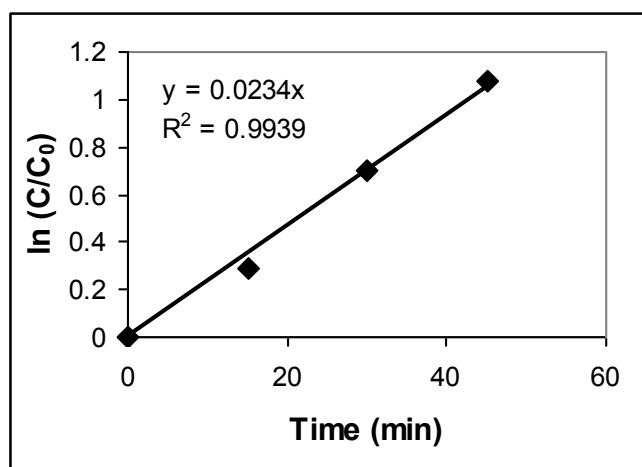


Figure E.4 $\ln(C/C_0)$ versus reaction time data of thin film containing 74 wt% SiO_2

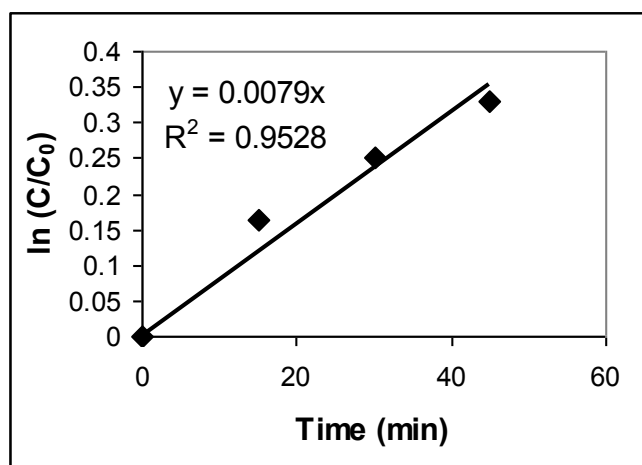


Figure E.5 $\ln(C/C_0)$ versus reaction time data of thin film containing 85 wt% SiO_2

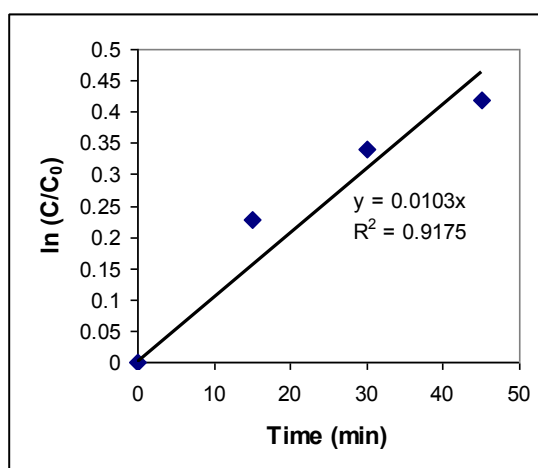


Figure E.6 $\ln(C/C_0)$ versus reaction time data of thin film containing 92 wt% SiO_2

CURRICULUM VITAE

PERSONAL INFORMATION

Surname, Name: Korkmaz Erdural, Beril
Nationality: Turkish (TC)
Date and Place of Birth: 5 October 1980, Diyarbakır
Marital Status: Married with 1 child
Phone: +90 312 284 52 11
E-mail: berilkorkmaz@gmail.com

EDUCATION

Degree	Institution	Year of Graduation
MS	METU Chemical Engineering	2006
BS	Gazi University Chemical Engineering	2003
High School	Konya Ataturk High School	1998

WORK EXPERIENCE

Year	Place	Enrollment
2010- Present	M.T.A.	Chemical Engineer
2004 – 2010	METU Chemical Engineering	Teaching Assistant
2002 July	T.P.A.O.	Intern Engineering Student
2001 July	Konya Cimento	Intern Engineering Student

FOREIGN LANGUAGES

Advanced English

PUBLICATIONS

1. Research Articles

Erdural, K. B., Yurum A., Bakır U., Karakas G. "Hydrothermal Synthesis Nanostructured TiO₂ Particles and Characterization of Their Photocatalytic Antimicrobial Activity" *Journal of Nanoscience and Nanotechnology* Vol: X, pp:1-9 (2007)

2. Book Chapters

Erdural, K. B., Yurum A., Bakır U., Karakas G., “Antimicrobial Properties of Titanium Nanoparticles” Ed., A. Vaseashta, and I. N. Mihailescu “Functionalized Nanoscale Materials, Devices, and Systems” Springer, 2008, 409

3. International Conference Publications

Erdural K. B., Bakır U., Karakas G., Cetin D., Suludere Z.” Antimicrobial Properties of TiO₂-SiO₂ Thin Films” 14th European Congress on Biotechnology September 13-16, 2009, Barcelona, Spain

Erdural, K. B., Yurum A., Bakır U., Karakas G., “Antimicrobial Properties of Titanium Nanoparticles” NATO-Advanced Study Institute June 4-15, 2007, Sinaia, Romania

Erdural, K. B., Yurum, A., Bakır, U., Karakas, G., “Preparation, Characterization and Antimicrobial Properties of Titanium Nanoparticles” International Workshop on Nanostructured Nanomaterials (NANOMAT 2006). June 2006, Antalya, Turkey

Erdural, K. B., Bakır, U., Ogel, B. Z., Demir, A. S. “Biotransformation of Morphine to Pseudo-morphine by Microbial Phenol Oxidases” 6th European Symposium on Biochemical Engineering (ESBES-2006). August 27-30, 2006, Salzburg, Austria

4. National Conference Publications

Erdural K. B., Bakır Ufuk, Karakaş G., “TiO₂-SiO₂ İnce Filmlerin Fotokatalitik Özellikleri” Dokuzuncu Ulusal Kimya Mühendisliği Kongresi 22-25 Haziran 2010, Ankara

Erdural K. B., Yurum A., Karakas G., Bakır U., “TiO₂ Parçacıklarının Fotokatalitik Özellikleri Üzerine Hidrotermal İşlemlerin Etkisi” Sekizinci Ulusal Kimya Mühendisliği Kongresi, 26-29 Ağustos 2008, Malatya

Erdural K. B., Doğu D., Karakaş G. “Improving the Photocatalytic Activity of TiO₂ by Photon Up Conversion” İkinci Ulusal Kataliz Kongresi 18-21 Haziran 2008, Erzurum

Erdural K. B., Bakır U., Demir A. S., “Mikrobiyal Fenol Oksidazlardan Yararlanılarak Morfinden Pseudo-Morfin Eldesi” Yedinci Ulusal Kimya Mühendisliği Kongresi 5-8 Eylül 2006, Eskişehir